DISSERTATION ZUR ERLANGUNG DES DOKTORGRADES

DER FAKULTÄT FÜR CHEMIE UND PHARMAZIE
DER LUDWIG-MAXIMILIANS-UNIVERSITÄT

The myxobacterial acetyl-CoA carboxylase inhibitor Soraphen A as a novel anti-metastatic and anti-proliferative agent

Katharina Stoiber (geb. Ferkaljuk)
aus Karaganda, Kasachstan

2015

ERKLÄRUNG

Diese Dissertation wurde im Sinne von § 7 der Promotionsordnung vom 28. November 2011 von Frau Prof. Dr. Angelika M. Vollmar betreut.

EIDESSTATTLICHE VERSICHERUNG

Diese Dissertation wurde eigenständig und ohne unerlaubte Hilfsmittel erarbeitet.

München, den _____

_____

(Katharina Stoiber, geb. Ferkaljuk)

Dissertation eingereicht am:	04.12.2015
1. Gutachter	Prof. Dr. Angelika M. Vollmar
2. Gutachter	Prof. Dr. Stefan Zahler
Mündliche Prüfung am:	03.02.2016

MEINEN ELTERN

Table of Contents

1 Introduction

1.1 Increased *de novo* lipogenesis - a hallmark of cancer

1.1.1 Fundamentals of lipogenesis

Lipogenesis is defined as the conversion of carbohydrates into fatty acids, which are one of the most abundant molecules in living organisms and the main building blocks for cellular lipids. Fatty acids can either be synthesized *de novo* or obtained from diet (Rui 2014). Most human tissues are supplied with lipids from circulation except the liver, lactating breast and cycling endometrium, where *de novo* fatty acid synthesis is active (Swinnen et al. 2006). In the postprandial state, when an excess of carbohydrates prevails, glucose is converted into fatty acids in lipogenic tissues (Rui 2014). The transport of pyruvate, the product of glycolysis into mitochondria from the cytosol can be defined as the starting point of *de novo* fatty acid synthesis. There its decarboxylation and conversion to acetyl-CoA by the pyruvate dehydrogenase (PDH) takes place. Next the condensation of acetyl-CoA with oxaloacetate to form citrate is catalysed by citrate synthase (CS). Citrate can either be oxidized in the tricarboxylic acid (TCA) cycle and the oxidative phosphorylation (OXPHOS) to produce ATP, or be translocated from the mitochondria to the cytosol and converted back to oxaloacetate and acetyl-CoA by ATP-citrate lyase (ACLY) in the fed state. Acetyl-CoA is irreversibly carboxylated to malonyl-CoA by the acetyl-CoA carboxylase (ACC) in the cytosol (Abramson 2011, Rui 2014). The next step comprises the generation of palmitic acid from malonyl-CoA and acetyl-CoA, catalysed by the fatty acid synthase (FAS). Subsequently, palmitate the ester of palmitic acid is further processed by elongases to long chain fatty acids. Desaturation, which gives rise to unsaturated fatty acids is accomplished by desaturases (Tong & Harwood 2006). Fatty acids or their activated CoA-esters are utilized for the synthesis of triglycerides, sphingolipids, glycolipids and phospholipids, which are secreted as very low density lipoproteins (VLDLs) for transport to extrahepatic tissues (Abramson 2011). An overview of the fatty acid metabolism is given in **Fig. 1**.

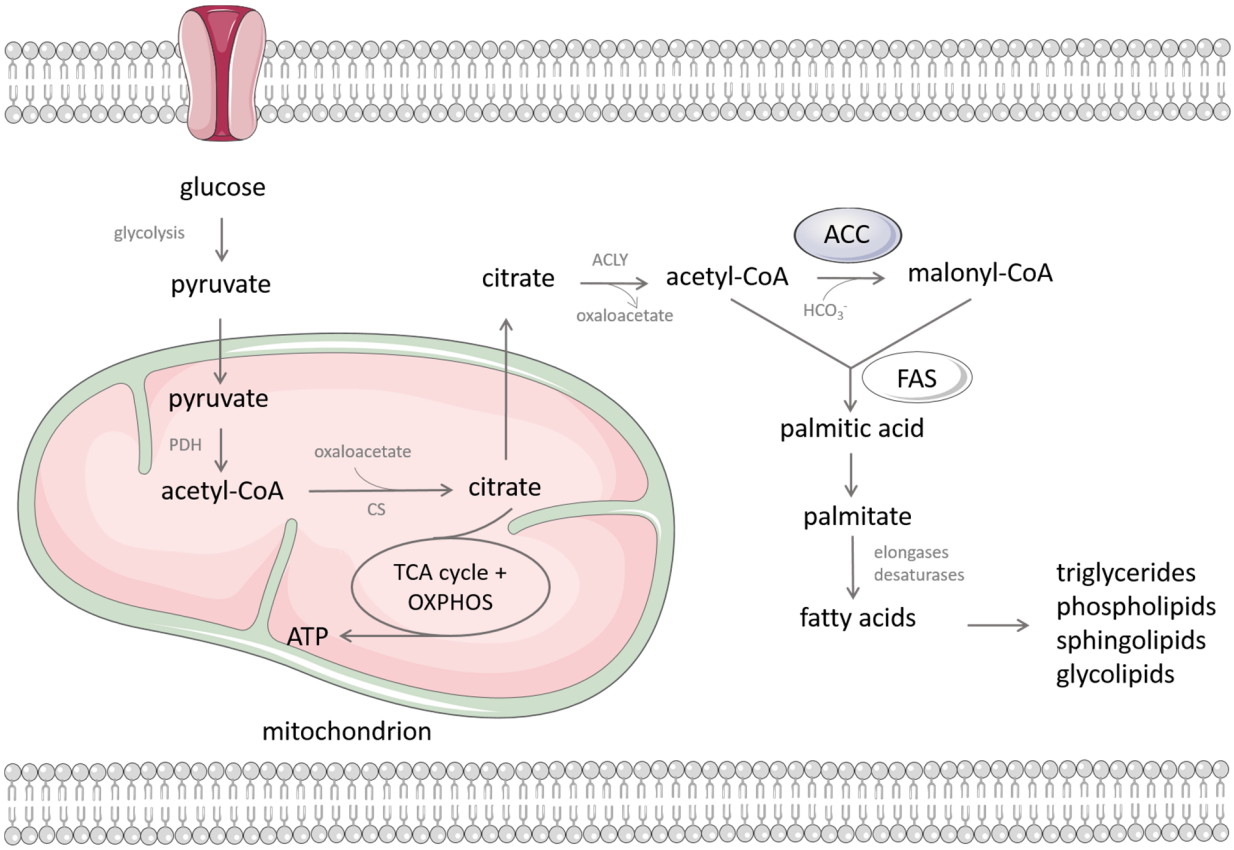

Fig. 1 Overview of lipogenesis and its connection to the glucose metabolism. Pyruvate derived from glycolysis is transported to mitochondria and converted to acetyl-CoA by pyruvate dehydrogenase (PDH). Citrate synthase (CS) catalyses the condensation of acetyl-CoA with oxaloacetate to form citrate, which is converted back to acetyl-CoA by the ATP-citrate lyase (ACLY) in the cytosol. Alternatively, citrate can be utilized in the tricarboxylic acid (TCA) cycle and the oxidative phosphorylation (OXPHOS) to generate ATP. The carboxylation of acetyl-CoA to malonyl-CoA is accomplished by the acetyl-CoA carboxylase (ACC). Next, palmitic acid synthesis is catalysed by the fatty acid synthase (FAS). Elongation or desaturation of fatty acids is performed by elongases and desaturases. The generated fatty acids or their CoA-ester are used for triglyceride, phospholipid, sphingolipid or glycolipid synthesis. Figure adapted from Abramson 2011 and Tong & Harwood 2006.

Lipids are involved in a number of cellular processes. As triglycerides, the fatty acid triesters of glycerol, lipids function as the major reservoir of energy. As phospholipids, which are composed of two fatty acids and a glycerol or sphingosine unit that is attached to a phosphate group, they act as the main constituents of cellular membranes. According to the alcohol backbone, phospholipids can be divided in two classes: glycerophospholipids, that have a glycerol backbone and phosphosphingolipids, which are derived from sphingosines. The most abundant phospholipids found in membranes are the glycerophospholipids phosphatidylcholine (PC), phosphatidylserine (PS), phosphatidylinositol (PI) and phosphatidylethanolamine (PE). Beyond phospholipids, glycolipids and cholesterol can also be

found in cellular membranes and belong to the group of membrane lipids (Berg et al. 2007). Phospholipids and glycolipids anchor target proteins to membranes and can act as precursors of second messengers, e.g. diacylglycerols, ceramides, eicosanoids or lysophosphatidic acid (Abramson 2011), whereas cholesterol functions as an important modulator of cellular membrane organization and signaling (Maxfield & Tabas 2005). A schematic overview of the membrane constitution is pictured in **Fig. 2**.

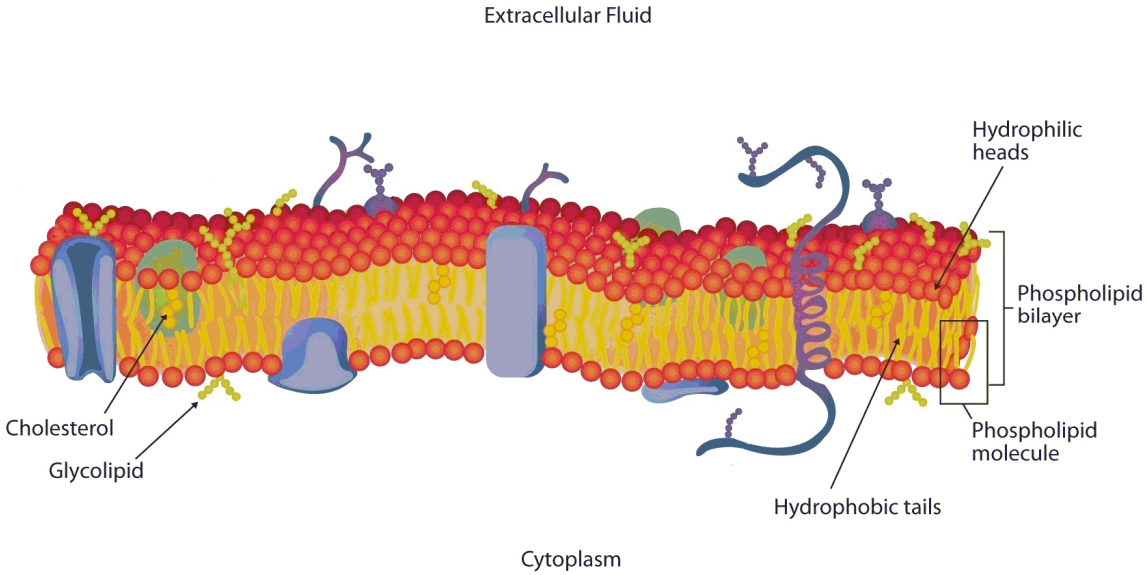

Fig. 2 Cellular membranes: a phospholipid bilayer. Cellular membranes are composed of a phospholipid bilayer, containing cholesterol molecules, glycolipids and membrane proteins. Figure adapted from Ball et al. 2012.

1.1.2 Lipogenesis in cancer

First metabolic investigations of human tumors revealed more than 60 years ago that malignant cells are characterised by an increased rate of *de novo* fatty acid synthesis (Medes et al. 1953), even when a high level of extracellular lipids prevails (Ookhtens et al. 1984, Sabine et al. 1967). In accordance with this discovery it was found that lipogenic enzymes, like FAS and ACC, were overexpressed in various types of cancer (Milgraum & Pasternack 1997, Swinnen et al. 2000). In normal cells, lipogenesis is accurately regulated and an uncontrolled accumulation of palmitate, the first product of the *de novo* fatty acid synthesis is toxic to cells (Hardy et al. 2000). Cancer cells with enhanced lipogenesis found strategies to avert this regulatory mechanism by e.g. the inappropriate activation of growth factors. Indeed, the

overexpression of lipogenic enzymes could be linked to the activation of growth factor signaling (Menendez 2010, Yoon et al. 2007). A bidirectional relationship between *de novo* fatty acid synthesis and HER2 oncogene activity has been found, illustrating the ability of lipogenic cells to induce pro-survival pathways (Menendez et al. 2004).

Furthermore, increased lipogenesis strongly affects membrane characteristics. Newly synthesized fatty acids are in most cases saturated in contrast to the polyunsaturated diet-derived fatty acids, thus spawning cell membranes with altered physical and chemical properties. The shift towards fatty acid saturation protects cancer cells from therapeutic interventions as they are less susceptible to chemotherapeutics and reactive oxygen species (Rysman et al. 2010).

Along with the changed membrane characteristics, the lipid profile determines lipid raft composition in cellular membranes, thereby affecting signal transduction, intracellular trafficking and cell migration. In the migratory process lipid rafts are important for the formation of membrane protrusions like invadopodia (Murai, 2012). These are implicated in the process of cell invasion and consist of a complex conglomeration of proteins including actin-modifying proteins, integrins, proteases, multiple kinases and scaffolding proteins, thus mediating the proteolytic invasion of cells into the extracellular matrix (Scott et al. 2012). Several of those proteins have a lipid binding domain, so it is not surprising that lipid rafts and *de novo* fatty acid synthesis were found to be inevitable for invadopodia formation (Scott et al. 2012, Yamaguchi et al. 2009).

Membrane composition also strongly regulates cell deformability, which was in initial studies found to be correlated with the metastatic potential of cells (Swaminathan et al. 2011, Remmerbach et al. 2009, Plodinec et al. 2012). Another important regulator of cell rigidity that is also influenced by membrane characteristics is the cytoskeleton. Actin polymerization is dependent on membrane curvature (Scott et al. 2012) and furthermore, the membrane serves as an anchor for the cytoskeleton (Lodish et al. 2000).

1.2 Acetyl-CoA carboxylase - a key enzyme of the fatty acid metabolism

1.2.1 The role of ACC in the fatty acid metabolism

The acetyl-CoA carboxylase (ACC) is a key enzyme in the fatty acid metabolism, which catalyses the irreversible rate limiting carboxylation of acetyl-CoA to malonyl-CoA (Kim 1997). ACCs are highly conserved, ubiquitous enzymes found in all branches of life including archaea, bacteria, yeast, fungi, plants, animals and humans. The human and plant ACC is a large multi-domain enzyme, that has a biotin carboxylase (BC) domain, a carboxyltransferase (CT) domain and a biotin carboxyl-carrier protein (BCCP). The ACC can be found in dimers, with the BC domains being capable of dimerization (Tong 2005). In eukaryotic and prokaryotic enzymes BC domains are highly conserved, while the CT domains show a weaker sequence homology between the species (Tong & Harwood 2006). The conversion of acetyl-CoA to malonyl-CoA takes place in two steps. First, an ATP-dependent carboxylation of the biotin group, catalysed by the BC activity of the ACC with bicarbonate acting as a donor takes place. In the second step the activated carboxyl group of biotin is transferred to the methyl group of acetyl-CoA by the CT domain of ACC (Tong 2005). A schematic overview of the reactions catalysed by the ACC is given in **Fig. 3**.

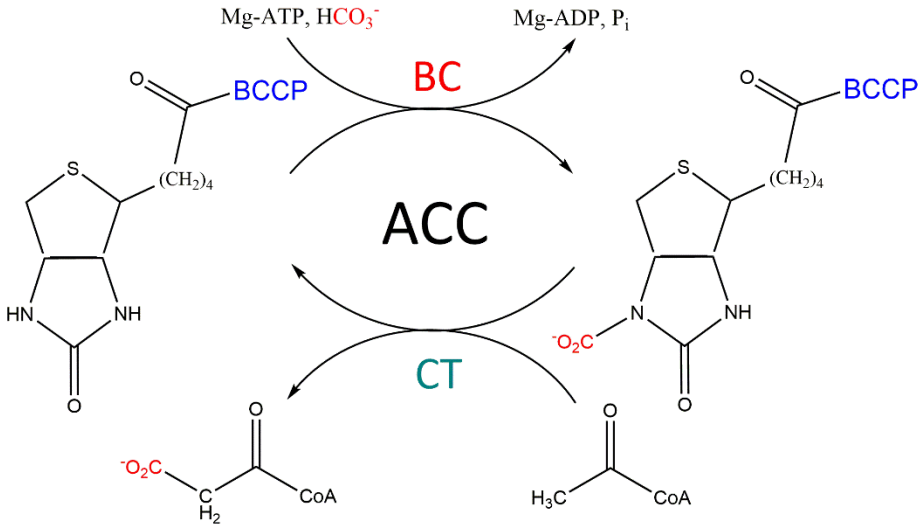

Fig. 3 ACC-catalysed conversion of acetyl-CoA to malonyl-CoA. Biotin carboxylase (BC) domain transfers a carboxyl-group from HCO_3^- to the biotin group of the ACC enzyme in an ATP-dependent reaction. In the next step the carboxyl group is attached to acetyl-CoA by the carboxyltransferase (CT) domain generating malonyl-CoA. BCCP is the biotin carboxyl-carrier protein. Figure adapted from Tong 2005.

There are two isoforms of the mammalian ACC: ACC1 and ACC2 (Tong 2005). ACC1 is largely expressed in lipogenic tissues, like liver and the lactating mammary gland, while ACC2 can mainly be found in the heart and skeletal muscle (Tong 2005). The ATP binding site, the carboxylation site, the acyl-CoA binding site and the phosphorylation sites, which regulate the enzyme activity are nearly identical. An additional sequence of 150 extra amino acids of ACC2 constitutes the main difference between the two isoforms (Kim 1997). This sequence acts to anchor ACC2 to the outer membrane of the mitochondria (Tong 2005).

The generation of malonyl-CoA, which is used for long chain fatty acid synthesis is accomplished by ACC1. Whereas malonyl-CoA, derived from the ACC2-catalysed reaction is responsible for regulation of the mitochondrial ß-oxidation (Kim 1997). To cross the mitochondrial membrane, acyl-CoAs must be converted to acylcarnitines, a reaction that is mediated by carnitine palmitoyltransferase I (CPT-I). CPT-I is inhibited by malonyl-CoA, the product of ACC2 (Abramson 2011). During starvation and exercise, acyl-CoAs are metabolized in the ß-oxidation cycle to acetyl-CoA, which is used for ATP production in the tricarboxylic acid (TCA) cycle and oxidative phosphorylation (OXPHOS) (Rui 2014). A schematic overview of the role of the two ACC isoforms ACC1 and ACC2 in the lipogenesis is given in **Fig. 4**.

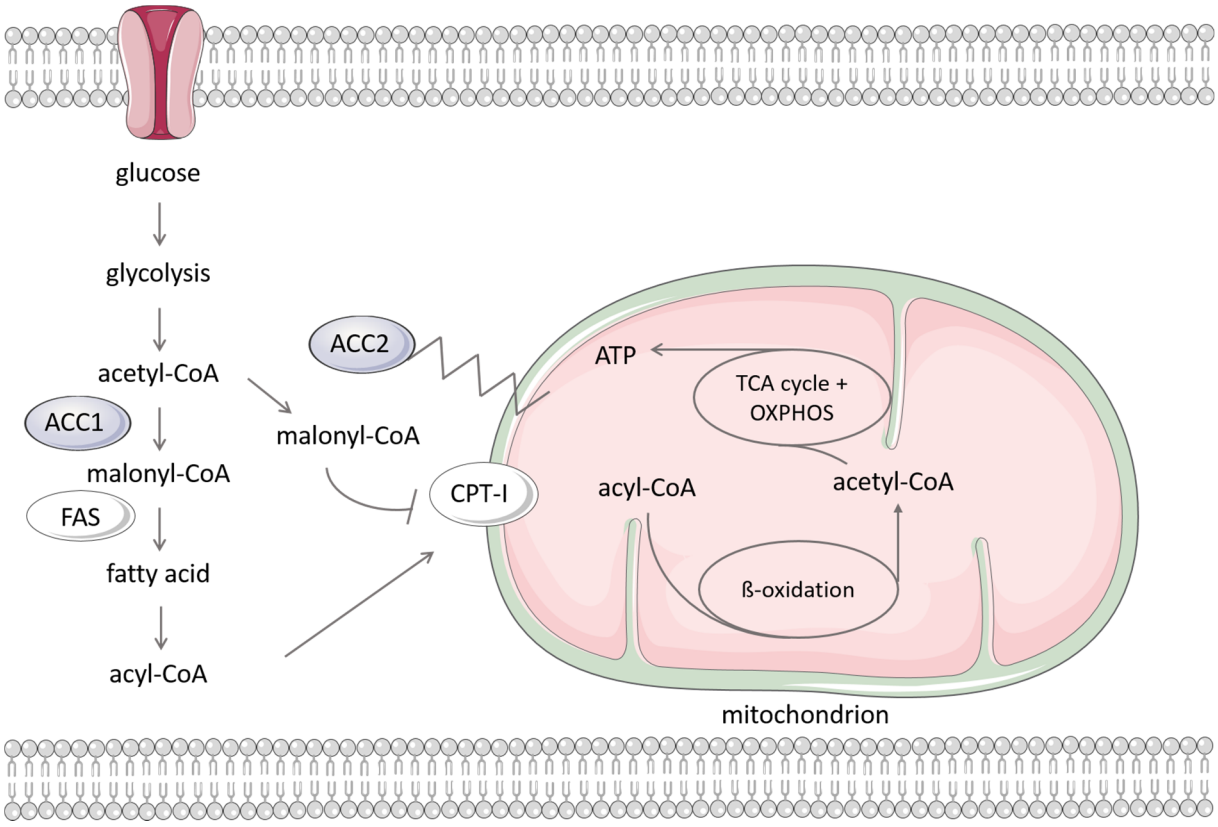

Fig. 4 Role of the ACC in the fatty acid metabolism. Acetyl-CoA, which is derived from glycolysis is converted to malonyl-CoA by ACC1 or ACC2. Malonyl-CoA, the product of ACC1, is used for fatty acid synthesis, which is catalysed by the fatty acid synthase (FAS). Acyl-CoAs can enter the ß-oxidation cycle, where acetyl-CoA is generated. Next, acetyl-CoA is utilized for ATP production through the tricarboxylic acid (TCA) cycle and the oxidative phosphorylation (OXPHOS). Malonyl-CoA, which is derived from the ACC2-catalysed reaction acts as an inhibitor of the carnitine palmitoyltransferase I (CPT-I) and therefore blocks ß-oxidation. Figure adapted from Abramson 2011**.**

1.2.2 ACC as a target in cancer therapy

First, the ACC was discovered as an interesting target for the treatment of the metabolic syndrome, diabetes and obesity as ACC2 deficient mice possessed a reduced body fat mass and body weight (Abu-Elheiga et al. 2003). An inhibition of ACC by the isoform non-selective inhibitor CP-640186 abrogated fatty acid biosynthesis, promoted fatty acid oxidation, led to a lower body fat mass and enhanced insulin sensitivity in test animals (Harwood 2004).

Current focus has centered on the fact, that ACC inhibition could be a promising approach in cancer therapy (Swinnen et al. 2006). It is well established that ACC is overexpressed in several types of cancer like breast, liver, prostate and liposarcoma (Abramson 2011). RNAi-induced inhibition of ACC1 in LNCaP cells was found to decrease proliferation and induce caspase-mediated apoptosis, whereas non-malignant cells with a low

lipogenic activity, were not affected (Brusselmans et al. 2005). Further ACC silencing experiments were conducted in MDA-MB-231 and MCF-7 cells, which resulted in a decreased *de novo* fatty acid synthesis and finally led to apoptosis (Chajès et al. 2006).

Pharmacological inhibition is another approach to target ACC in cancer. Mammalian ACC inhibitors can basically be divided into three classes: The first class are lipophilic fatty acid mimetics, which compete with acetyl-CoA in the CT reaction. Members of the second class are substituted bipiperidylcarboxamides, which reversibly and isoenzyme-nonselectively inhibit the CT reaction. Soraphen A, a polyketide natural product, represents the third group of ACC inhibitors and interferes with the BC activity of ACC (Tong & Harwood 2006).

1.3 Soraphen A - a myxobacterial acetyl-CoA carboxylase inhibitor

1.3.1 Myxobacteria: natural pharmaceutical factories

Myxobacteria are unicellular rod-shaped gram negative bacteria, which have one of the largest bacterial genomes. They can be found in soil, dung of herbivores, bark and rotting wood. Myxobacteria exhibit a unique life cycle and are prominent for their ability to form multicellular fruiting bodies by directed cell movement upon starvation. Vegetative cells within the fruiting bodies convert into myxospores that can endure unfavorable conditions (Shimkets et al. 2006). Of special interest is the fact that myxobacteria are producers of a huge amount of bioactive compounds including polyketides, linear and cyclic peptides and heterocyclic molecules (Shimkets et al. 2006, Wenzel & Müller 2009). A myxobacterial product, the Epothilone B derivative Ixabepilone has been approved in the USA in 2007 for refractory metastatic breast cancer (Puhalla & Brufsky 2008). Epothilone B shows a taxol-like antitumor activity by stabilizing the tubulin skeleton of eukaryotic cells (Gerth et al. 2003). Another potent myxobacterial metabolite, produced by the myxobacterium *Sorangium cellulosum* (**Fig. 5**) is the ACC inhibitor Soraphen A (Gerth et al. 1993).

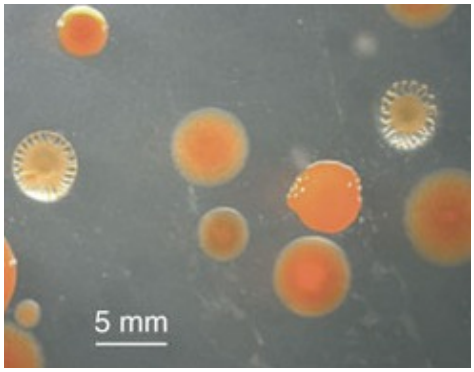

Fig. 5 *Sorangium cellulosum* colonies. Figure from Schneiker et al. 2007.

1.3.2 Structure of Soraphens

Soraphens are a class of at least 40 chemically related secondary metabolites isolated from the myxobacterial strain *Sorangium cellulosum* So ce26 (Gerth et al. 1993). The main compound, Soraphen A contains an unsaturated 18-membered lactone ring, an extracyclic phenyl ring, two hydroxyl groups, three methyl groups and three methoxy groups (Bedorf et al. 1993, Ligon et al. 2002) and is depicted in **Fig. 6 A**. In a genetic approach study using *Saccharomyces cerevisiae,* ACC was identified as the primary target of Soraphen A (Vahlensieck 1994). Soraphen A was found to inhibit the BC domain of the eukaryotic ACC, whereas the bacterial ACC remained unaffected due to large structural differences between the eukaryotic and the bacterial BC domain in the Soraphen A binding site (Shen et al. 2004). As shown in **Fig. 6 B** crystallographic analysis revealed that Soraphen A binds in the allosteric site, 25 Å from the active site of the BC domain (Tong 2005). Furthermore, the crystal structure of the BC domain in complex with Soraphen A suggests that there are extensive interactions between Soraphen A and its binding site, which is in line with the nanomolar binding affinity of Soraphen A (Shen et al. 2004).

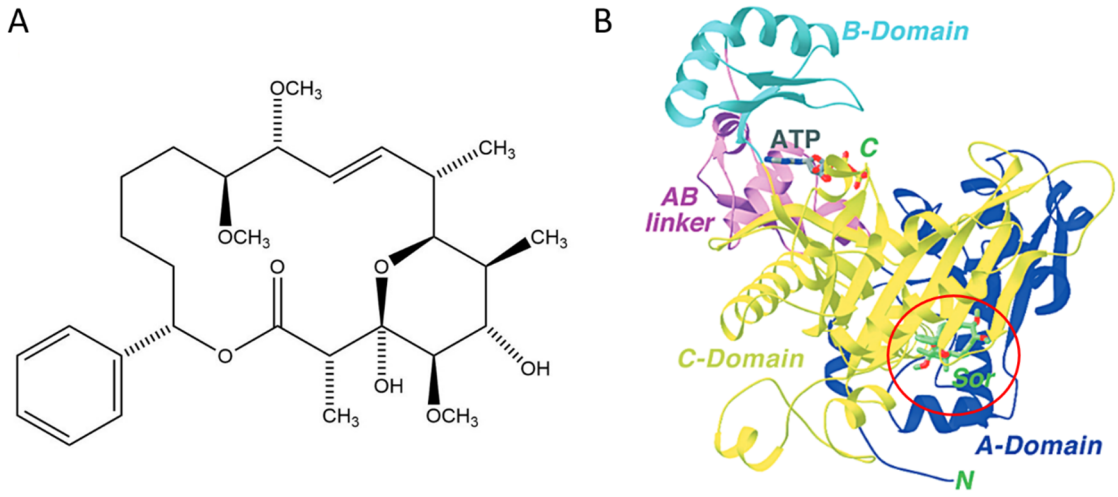

Fig. 6 Soraphen A: chemical structure and binding to the BC domain of the ACC. (A) Chemical structure of Soraphen A. (B) Structure of the yeast BC domain in complex with Soraphen A. The A, B and C sites of the BC domain are shown. Soraphen A (Sor) is marked in green (stick model). Figure adapted from Tong 2005.

Mechanistically, Soraphen A binding in the dimer interface of the ACC leads to a disturbed oligomerization of the BC domain. Thereby, Soraphen A stabilizes the inactive monomer conformation, which is not capable of forming dimers (Shen et al. 2004). A schematic illustration of the mechanism of Soraphen A action is given in **Fig. 7**.

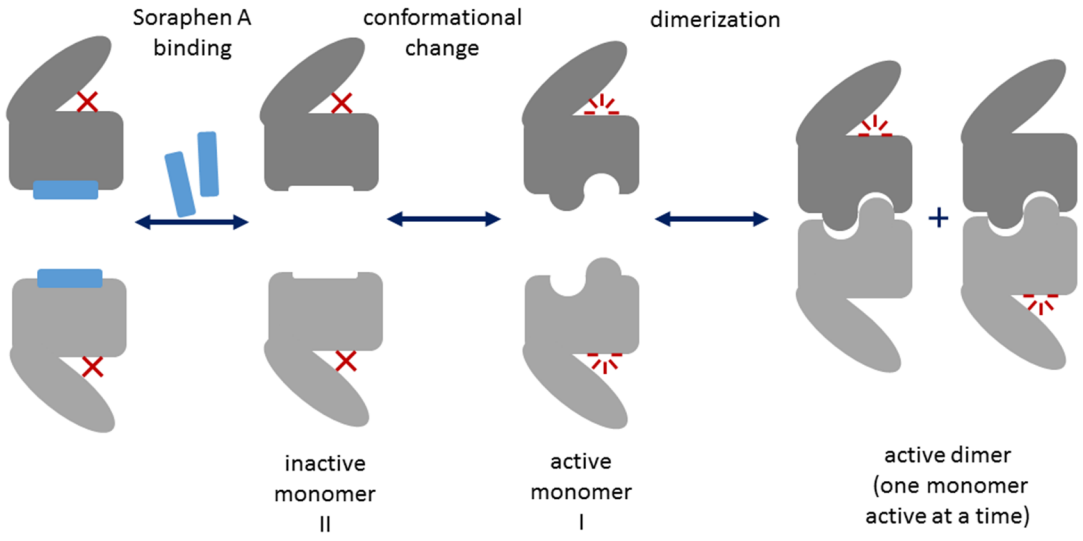

Fig. 7 Mechanism of the inhibition of the BC domain of ACC by Soraphen A. The dimerization domain of BC can switch between the two conformations I and II. Conformation I can be defined as the active state that is able to form dimers, whereas conformation II does not dimerize. Soraphen A stabilizes the inactive conformation and thereby prevents dimerization. Figure adapted from Tong & Harwoord 2006.

1.3.3 First cancer-related studies on Soraphen A

First studies assessed the effect of Soraphen A on cancer cells. *Inter alia* Soraphen A was found to inhibit the fatty acid synthesis and evoke anti-proliferative effects in LNCaP and PC-3M prostate cancer cells (Beckers et al. 2007). Rysman and colleagues extended the investigations on the effects of Soraphen A on LNCaP cells, showing a changed cellular lipid composition and altered membrane dynamics after treatment (Rysman et al. 2010). Going one step further, Jump and colleagues report that Soraphen A inhibits the *de novo* fatty acid synthesis and the elongation of fatty acids in LNCaP and HepG2 cells (Jump et al. 2011). These studies published on Soraphen A in context of cancer are mainly descriptive and limited to a few cell lines. So far, little is known about its mechanism of action.

1.4 Aim of the study

Finding new targets for cancer treatment is of immense clinical importance as therapeutic success is often limited by strong side effects of today's anti-cancer drugs, resistance formation and dissemination. With the discovery that cancer cells are characterised by an enhanced *de novo* fatty acid synthesis 60 years ago (Medes et al. 1953), key enzymes of the fatty acid metabolism like the acetyl-CoA carboxylase have gained attraction as potential targets. Nevertheless, therapeutic exploitation of this knowledge has been poor so far. Recently, first descriptive studies have introduced the acetyl-CoA carboxylase inhibitor Soraphen A as a potential anti-proliferative agent, but little is known about its mode of action.

The aim of the study was to investigate the potential of Soraphen A as an anti-metastatic and anti-proliferative compound and to decipher the mechanism of its action. Thereby, the focus was set on unraveling the underlying signaling mechanisms and implications of a disturbed lipid homeostasis on cell mechanics and thus cancer progression. Modulation of the physical characteristics of cells and membranes was exploited as a novel strategy to fight malignant tumors.

2 Materials and Methods

2.1 Materials

2.1.1 Compounds

The myxobacterial compound Soraphen A was obtained from Prof. Dr. Rolf Müller (Pharmaceutical Biotechnology, University of Saarland, Saarbrücken, Germany). Soraphen A was dissolved in ethanol and stored as 10 mM stocks at -20 °C. Trastuzumab was provided by Roche (Mannheim, Germany).

2.1.2 Inhibitors, reagents, dyes and technical equipment

Tab. 1 Inhibitors

Inhibitor	Distributor/Producer
Complete® mini EDTA free	Sigma Aldrich, Taufkirchen, Germany
Phenylmethylsulfonyl fluoride (PMSF)	Sigma Aldrich, Taufkirchen, Germany
Sodium fluoride (NaF)	Merck, Darmstadt, Germany
Sodium orthovanadate (Na_3VO_4)	ICN Biomedicals, Aurora, OH, USA

Tab. 2 Reagents and dyes

Reagent/Dye	Distributor/Producer
Formaldehyde solution 10 % phosphate buffered	AppliChem, Darmstadt, Germany
BCA Protein Assay Reagent (Kit)	Thermo Fisher Scientific, Waltham, MA, USA
Bovine serum albumin (BSA)	Sigma Aldrich, Taufkirchen, Germany
Cholera Toxin from *Vibrio cholerae*	Sigma Aldrich, Taufkirchen, Germany
Crystal violet	Carl Roth, Karlsruhe, Germany
Dimethyl sulfoxide (DMSO)	AppliChem, Darmstadt, Germany
Epidermal growth factor (EGF)	PeproTech Inc., Rocky Hill, NJ, USA
EGF tetramethylrhodamine conjugate	Life technologies, Carlsbad, CA, USA

FluorSave™ Reagent mounting medium	Merck, Darmstadt, Germany
Formaldehyde, 16 % ultrapure	Polysciences Europe GmbH, Eppelheim, Germany
Glutamine	Sigma Aldrich, Taufkirchen, Germany
Hoechst (bisBenzimide H33342)	Sigma Aldrich, Taufkirchen, Germany
Horse serum	Invitrogen, Karlsruhe, Germany
Hydrocortisone	Sigma Aldrich, Taufkirchen, Germany
Insulin from bovine pancreas	Sigma Aldrich, Taufkirchen, Germany
Matrigel™	BD Biosciences, Heidelberg, Germany
Methylcellulose	Sigma Aldrich, Taufkirchen, Germany
Non-fat dry milk powder (MP)	Carl Roth, Karlsruhe, Germany
Page Ruler™ Prestained Protein Ladder	Fermentas, St.Leon-Rot, Germany
Polyacrylamide (Rotiphorese® Gel A 30 %)	Carl Roth, Karlsruhe, Germany
Poly (2-hydroxyethyl methacrylate) (Poly-HEMA)	Sigma Aldrich, Taufkirchen, Germany
Propidium iodide	Sigma Aldrich, Taufkirchen, Germany
Sodium borohydride ($NaBH_4$)	Sigma Aldrich, Taufkirchen, Germany
Sodium citrate	Carl Roth, Karlsruhe, Germany
Transferrin from human serum tetramethylrhodamine conjugate	Invitrogen, Karlsruhe, Germany
Tris-HCl	Sigma Aldrich, Taufkirchen, Germany
Triton X-100	Merck, Darmstadt, Germany
Tween® 20	BDH/Prolabo®, Ismaning, Germany
XenoLight D-Luciferin Potassium Salt	PerkinElmer, Waltham, MA, USA

All other reagents and biochemicals not listed in **Tab.2** were purchased from Sigma-Aldrich, AppliChem, Carl Roth or Merck.

Tab. 3 Cell culture reagents

Cell culture reagent	Producer/Distributor
Collagen G	Biochrom AG, Berlin, Germany
Dulbecco`s modified Eagle`s medium (DMEM)	PAA Laboratories, Pasching, Austria
DMEM/F12 Mix 1:1	PAN Biotech, Aidenbach, Germany
DMEM-powdered cell culture medium	PAA Laboratories, Pasching, Austria
ethylenediaminetetraacetic acid (EDTA)	Carl Roth, Karlsruhe, Germany
ethylene glycol tetraacetic acid (EGTA)	AppliChem, Darmstadt, Germany
Fetal calf serum (FCS)	PAN Biotech, Aidenbach, Germany
McCoy´s medium	PAA Laboratories, Pasching, Austria
Penicillin/streptomycin 100 x	PAA Laboratories, Pasching, Austria
RMPI 1640	PAA Laboratories, Pasching, Austria
Trypsin	PAN Biotech, Aidenbach, Germany

Tab. 4 Technical equipment

Technical equipment	Producer /Distributor
Axiovert 25	Zeiss, Oberkochen, Germany
BD FACS Canto™ II	BD Biosciences, Heidelberg, Germany
Canon EOS 450C camera	Canon, Tokyo, Japan
ChemiDoc™ Touch Imaging system	Bio-Rad, Hercules, CA, USA
Curix 60	Agfa, Cologne, Germany
FACSCalibur	BD Biosciences, Heidelberg, Germany
IVIS Lumina system	Caliper Life Science, Hopkinton, MA, USA
Leica DM IRB	Leica Microsystems Inc., IL, USA
Leica TCS SP5 X	Leica Microsystems Inc., IL, USA
Mikro 22R centrifuge	Hettich, Tuttlingen, Germany
Nucleofector™II Device	Lonza, Basel, Switzerland
Odyssey 2.1	LI-COR Biosciences, Lincoln, NE, USA
Olympus CK30	Olympus Deutschland GmbH, Hamburg, Germany

Open u-IMIC	Fei, Oregon, USA
Rotational Vacuum Concentrator RVC 2-18	Martin Christ Gefriertrocknungsanlagen GmbH, Osterode am Harz Germany
SpectraFluor Plus™	Tecan, Männedorf, Switzerland
Suprafuge 22	Heraeus Sepatch, Osterode am Harz, Germany
Thermoshake, Laboshake	Gerhard Analytical Systems, Königswinter Germany
Ultrasonic cleaner	VWR International GmbH, West Chester, PA, USA
Vi-Cell™ XR	Beckman Coulter, Brea, CA, USA
xCELLigence System	Omni Life Science GmbH & Co. KG, Bremen, Germany
Zeiss LSM 510 Meta confocal laser scanning microscope	Zeiss, Oberkochen, Germany

2.2 Cell culture

2.2.1 Buffers and solutions

Tab. 5 Cell buffers and solutions

Buffers/solutions	Composition
PBS (pH 7.4)	NaCl (123.3 mM), Na_2HPO_4 (10.4 mM) KH_2PO_4 (3.2 mM) in H_2O
PBS + Ca^{2+}/Mg^{2+} (pH 7.4)	NaCl (123.3 mM), KCl (2.7 mM), Na_2HPO_4 (10.4 mM), KH_2PO_4 (3.2 mM), $MgCl_2$ (0.5 mM), $CaCl_2$ (0.7 mM) in H_2O
Trypsin/EDTA	trypsin (0.05 %), EDTA (0.02 %) in PBS
Collagen G	collagen G (0.001 %) in PBS

2.2.2 Culture and passaging of cancer cells

The invasive mammary carcinoma cell line MDA-MB-231 was obtained from Cell Line Services (CLS, Eppelheim, Germany). T24, a bladder carcinoma cell line was kindly provided by Dr. Barbara Mayer (Department of Surgery, University of Munich, Germany) and authenticated by the German Collection of Microorganisms and Cell Cultures (DSMZ, Braunschweig, Germany). The non-cancerous mammary MCF10A cells were obtained from American Type Culture Collection (ATCC, Wesel, Germany). The mammary carcinoma cell line SKBR3 was purchased from Cell Line Services (CLS, Eppelheim, Germany). The hepatocellular carcinoma cell lines Huh7 and HepG2 cells were derived from the Japanese Collection of Research Bioresources (JCRB, Osaka, Japan) and the DSMZ, respectively. MDA-MB-231, SKBR3, Huh7 and HepG2 cells were cultured in DMEM supplemented with 10 % fetal calf serum (FCS) and 1 % penicillin/streptomycin (1.5 mM). Huh7 and HepG2 were cultured in collagen G coated flasks. T24 cells were maintained in McCoy`s medium with 10 % FCS and 1 % penicillin/streptomycin (1.5 mM). MCF10A cells were cultivated in DMEM/F12 Mix 1:1 supplemented with 5 % horse serum, 20 µg/l EGF, 10 mg/l insulin, 0.5 mg/l hydrocortisone, 0.1 mg/l cholera toxin, and 1 % penicillin/streptomycin (1.5 mM). All cell lines were passaged twice a week: MDA-MB-231, T24 and Huh7 cells in a ratio of 1:10 and the SKBR3, HepG2 and MCF10A cells in a ratio of 1:3. Therefore, the culture medium was removed, cells were washed with PBS, detached by Trypsin/EDTA for 2 min at 37 °C and the trypsinization was stopped by adding 5 ml of culture medium. The cells were pelleted (5 min, 1000 rpm) to completely remove Trypsin/EDTA, resuspended in culture medium and passaged as described.

2.2.3 Thawing and freezing of cells

For storage, cells were detached, counted and resuspended in culture medium supplemented with 20 % FCS and 1 % penicillin/streptomycin (1.5 mM). $2 \cdot 10^6$ cells/900 µl medium were transferred into cryo vials and 100 µl DMSO was added. Cells were immediately frozen at - 20 °C, next day transferred first to - 80 °C and after at least 6 h to liquid nitrogen for storage. For thawing, the frozen cells were warmed up in a water bath at 37 °C and transferred into 7 ml culture medium. The cells were pelleted and the supernatant was discarded to remove DMSO. Subsequently cells were resuspended in culture medium and placed into a culture flask. Next day the culture medium was changed and the cells were passaged when they reached confluence.

2.3 Cell proliferation assays

2.3.1 CellTiter-Blue® cell viability assay

CellTiter-Blue® cell viability assay (Promega, Madison, WI, USA) was used to analyse cell proliferation. 1500 cells per well were seeded into a 96-well plate and stimulated as indicated. According to manufacturer`s instruction CellTiter-Blue®- reagent was added, incubated for 2 h and the absorbance was measured at 550 nm using a microplate reader (Tecan, Männedorf, Switzerland). The initial conversion rate of the living cells was determined on day 0 and subtracted from the measured values to calculate the proliferation rate.

2.3.2 Crystal violet proliferation assay

To determine cell proliferation rate, cells were treated as indicated, washed with PBS, stained with 500 µl crystal violet solution per well (0.5 % crystal violet (w/v), 20 % methanol (v/v) in H_2O) for 15 min under shaking, washed three times with distilled water and dried overnight. Next crystal violet was dissolved in 200 µl ethanol/sodium citrate solution (50 % ethanol (v/v), 0.1 M sodium citrate in H_2O) and the absorbance was measured at 540 nm using a microplate reader (Tecan, Männedorf, Switzerland). At day 0 blank value was determined, which was subtracted from the measured values.

2.4 Cell attachment assay

Cell attachment was assessed by the impedance-based real-time cell analyzer (xCELLigence system, Omni Life Science GmbH & Co. KG, Bremen, Germany). Therefore cells were pretreated with Soraphen A for 4 h, detached and 5000 cells per well were seeded into the E-plates according to manufacturer`s instruction. Before seeding, the plate was equilibrated by adding 100 µl cell culture medium per well and the background was measured. Cell attachment rate was determined for 4 h after seeding, with cell index assessment every 2 min for 140 min and then every 15 min for the remaining time.

2.5 Flow cytometric analysis

2.5.1 Measurement of apoptosis

Cell apoptosis was assessed by measuring the subG1 population, which is characterised by DNA fragmentation and loss of nuclear DNA according to Nicoletti and colleagues (Nicoletti et al. 1991). Therefore cells were detached, washed with PBS and resuspended in 100 µl HFS solution (sodium citrate (0.1 % w/v), Triton X-100 (0.1 % v/v) in PBS) containing 50 µg/ml propidium iodide (PI) and incubated for 30 min at 4 °C. Apoptotic DNA was determined by FACS analysis using FACSCalibur (BD Biosciences, Heidelberg, Germany) or BD FACS Canto™ II (BD Biosciences). Data evaluation was performed with the flow cytometry analysis software FlowJo 7.6.

An alternative method for apoptosis rate determination is the PI exclusion assay, where the enhanced permeabilization rate of apoptotic cells is utilized. Therefore the same protocol as described above was followed, but instead of the permeabilizing HFS solution PBS was used to dilute PI. Furthermore, cells were immediately analysed by flow cytometry.

2.5.2 Cell cycle analysis

Cell cycle analysis was accomplished by determining the cellular chromatin status. Therefore cells were detached, washed with PBS and incubated with 100 µl HFS solution (sodium citrate (0.1 % w/v), Triton X-100 (0.1 % v/v) in PBS) containing 50 µg/ml propidium iodide (PI) for 30 min at 4 °C. Fluorescence intensity was measured by flow cytometry using FACSCalibur (BD Biosciences, Heidelberg, Germany) or BD FACS Canto™ II (BD Biosciences) and data were evaluated by flow cytometry analysis software FlowJo 7.6.

2.6 Cell transfection

2.6.1 Plasmid transfection

Cell transfection was performed by electroporation according to manufacturer`s instruction (Nucleofector™ Kit T, Lonza, Basel, Switzerland). Briefly, cells were detached by trypsinization and counted. $5 \cdot 10^5$ cells were transferred into a tube, centrifuged and the supernatant was discarded. The cell pellet was resuspended in 100 µl Nucleofector™ solution and 2 µg plasmid

DNA was added. The cell suspension was transferred into a cuvette and transfected by applying the E-009 program for SKBR3 cells and the A-023 program for MDA-MB-231 cells. For imaging 40.000 transfected cells per well were plated into ibiTreat 8-well µ-Slides (ibidi GmbH, Munich, Germany).

2.6.2 RNAi transfection

Cell transfection for ACC1 and ACC2 silencing was performed with ON-TARGETPlus SMARTpool siRNA by using Dharmafect® transfection reagent (Thermo Fisher Scientific, Waltham, MA, USA). Therefore cells were seeded in 6-well plates in medium without penicillin/streptomycin the day before transfection. 10 µl of siRNA (5 µM) were diluted with 190 µl medium without supplements. 5 µl of Dharmafect® Transfection reagent were mixed with 195 µl medium without supplements and incubated for 5 min. For complex formation the diluted siRNA was combined with the Dharmafect® transfection reagent solution and incubated for 20 min. 1.6 ml of medium supplemented with 10 % FCS were added to the complex solution and vortexed thoroughly. Next, cell medium was replaced by the siRNA/Dharmafect® transfection reagent complex solution and incubated for 72 h.

2.7 Migration and invasion assays

2.7.1 Transwell migration and invasion assay

Cells were stimulated with Soraphen A for 2 h. For invasion assays matrigel™ was thawed on ice and diluted 1:10 in medium without FCS. 100 µl of the diluted matrigel™ was filled into the upper Boyden chamber compartment (Transwell Permeable Supports 8 µm and 5 µm pore polycarbonate inserts, Corning Incorporated, New York, NY, USA) and allowed to polymerize for 1 h at 37 °C. For both the migration and invasion assay the lower compartment was filled with medium containing 10 % (v/v) FCS and 100 ng/ml EGF. After stimulation $7 \cdot 10^4$ cells in 100 µl medium were seeded into the top of the Boyden chamber filter. For MDA-MB-231 and MCF10A cells Boyden chamber inserts with 8 µm pore size were used and for T24 cells inserts with a pore size of 5 µm were applied. MDA-MB-231 cells were allowed to migrate for 4 h, MCF10A cells for 6 h and T24 cells for 16 h. Invasion of both MDA-MB-231 and T24 cells proceeded for 40 h. After migration or invasion, cells were fixed with crystal violet solution (0.5 % crystal violet (w/v), 20 % methanol (v/v) in H_2O) and cells in the upper compartment

were removed with a q-tip. Cells on the bottom of the insert were imaged using an axiovert 25 microscope (Zeiss, Oberkochen, Germany) and an EOS 450C camera (Canon, Tokyo, Japan).

2.7.2 Chemotaxis migration assay

For chemotaxis migration assay, cells were starved overnight and incubated with Soraphen A for 2 h. Next, cells were detached and $3 \cdot 10^5$ cells were seeded into a chemotaxis µ-Slide (ibidi GmbH, Munich, Germany). 2 h after seeding a gradient between 0 % to 10 % FCS/100 ng/µl EGF was established according to manufacturer`s instructions. Cell migration was observed for 20 h using an open u-iMIC microscope (Fei, Oregon, USA), while taking images every 10 min. Data evaluation was performed with the Image J plugin chemotaxis and the ibidi Software chemotaxis and migration tool.

2.7.3 Spheroid invasion and proliferation assay

For spheroid generation cells were detached and adjusted to a concentration of $5 \cdot 10^4$ cells/ml. 2 ml of the cell suspension were mixed with 500 µl of a methylcellulose solution (20 % (w/v) in medium). A 60 mm cell culture dish was filled with 5 ml PBS and 25 µl drops of the cell suspension were placed in lines with a multi-channel pipette into the lid. Next, the lid was inverted, placed over the PBS filled culture dish and the spheroids were incubated at 37 °C for 72 h. Spheroids were either embedded in collagen for invasion monitoring or applied for a CellTiter-Blue® cell viability assay.

For embedding spheroids in collagen, approximately 50 spheroids were collected in medium and allowed to sediment for 30 min at RT. The supernatant was removed leaving 150 µl of medium. 25 µl 10 x DMEM were mixed with 25 µl bicarbonate, 300 µl of collagen G solution (#7213, Biochrom AG, Berlin, Germany) and Soraphen A or vehicle, respectively, on ice. The mixture was added to the spheroids and 400 µl of the spheroid collagen solution were transferred into the middle of a 6-well plate and allowed to polymerize for 10 min at 37 °C. Next, spheroids were covered with 2 ml of medium supplemented with 20 % FCS. The size of the spheroids was monitored for 72 h by using an Axiovert 25 microscope (Zeiss, Oberkochen, Germany) and a Canon EOS 450C camera (Canon, Tokyo, Japan).

For proliferation assay of spheroids, 96-well plates were coated with poly-HEMA solution. Therefore the poly-HEMA stock solution (120 mg/ml in 99 % EtOH) was diluted 1:10 in 99 % EtOH and incubated at 37 °C for 30 min to prevent precipitation before coating. Coated

plates were allowed to dry overnight. Seven spheroids were transferred to each well and stimulated with the respective Soraphen A concentration. 96 h after stimulation the proliferation rate was determined by the CellTiter-Blue® cell viability assay (Promega, Madison, WI, USA).

2.8 *In vivo* experiments

Mice were housed in individual ventilated cages with a 12 h day- and night cycle and *ad libitum* access to autoclaved water and standard food.

For the 4T1-Luc dissemination experiment 4T1-Luc cells were pretreated with Soraphen A for 6 h and 72 h or the vehicle as indicated, detached, resolved in PBS and $1 \cdot 10^5$ cells were injected into the tail vein of six-week old Balb/c mice (Harlan Laboratories GmbH, Eystrup, Germany). Four days after injection, mice were anesthetized (1.5-2 % isoflurane in oxygen) and the bioluminescence of metastases was measured 10 min after luciferin injection (6 mg in PBS) by the IVIS Lumina system using Living Image software 4.4 (Caliper Life Science, Hopkinton, MA, USA). The total flux/area was determined as photons/second/cm^2.

Tumor growth was assessed *in vivo* by the Huh7 xenograft model. Therefore Huh7 cells were harvested and $3 \cdot 10^6$ cells dissolved in 100 µl PBS were injected into the flank of eight-week old SCID mice (Charles River Laboratories, Sulzfeld, Germany). After tumors have developed, mice were treated daily with 40 mg/kg Soraphen A for nine days. Tumor volume was assessed by using a digital caliper (Emil Lux, Wermelskirchen, Germany), thereby length (l), wide (w) and height (h) of the tumor was measured. The tumor volume was calculated by the formula $V = (\pi/6)\ l \cdot w \cdot h$.

Animal experiments were approved by the government of Bavaria and performed according to the guidelines of the German legislation for the protection of animals. *In vivo* experiments were done by Melanie Ulrich and Kerstin Loske (Group of Prof. Dr. Angelika M. Vollmar, University of Munich, Pharmaceutical Biology).

2.9 Microscopy

2.9.1 Fixation and staining of cells

Cells were seeded on an ibiTreat 8-well µ-slide (ibidi GmbH, Munich, Germany) and stimulated the next day with Soraphen A as indicated. Fixation of cells was performed with 4 % PFA in PBS at RT for 10 min or with ice-chilled methanol for 10 min at -20 °C, respectively. After fixation cells were washed three times with PBS + Ca^{2+}/Mg^{2+} and permeabilized with 0.2 % Triton in PBS. If extracellular receptors were stained the permeabilization step was omitted. Next, unspecific binding sites were blocked with 0.1 % Triton/1 % BSA in PBS for 10 min at RT. Primary antibodies were diluted in 0.1 % Triton/1 % BSA in PBS as indicated and given to the samples for 2 h. After three washing steps the cells were incubated with Alexa Fluor® labeled secondary antibodies and Hoechst for nuclei staining for 1 h. Another three washing steps with PBS + Ca^{2+}/Mg^{2+} and once with distilled water followed before mounting of cells with PermaFlour™ mounting medium (Beckman Coulter, Brea, CA, USA).

Tab. 6 Primary antibodies used for immunohistochemistry

Antigen	Source	Dilution	Producer/Distributor	Product #	Fixation
EEA1	goat	1:50	Santa Cruz	sc-6415	4 % PFA
HER2	rabbit	1:200	Cell Signaling	2156	methanol
LAMP1	mouse	1:50	Developmental Studies Hybridoma Bank	H4A3	4 % PFA
Rac1	mouse	1:100	Upstate	05-389	4 % PFA
Vinculin	mouse	1:100	Santa Cruz	sc-25336	4 % PFA

Tab. 7 Secondary antibodies and dyes used for immunohistochemistry

Antibody/Dye	Dilution	Producer/Distributor	Product #
Alexa Fluor® 488, goat anti-rabbit IgG (H+L)	1:400	Molecular Probes	A - 11008
Alexa Fluor® 546, goat anti-mouse IgG (H+L)	1:400	Molecular Probes	A - 11003

Alexa Fluor® 546, donkey anti-goat IgG (H+L)	1:400	Molecular Probes	A - 11056
Hoechst (bisBenzimide H33342)	1:400	Sigma Aldrich	B-2261
Rhodamine-phalloidin	1:400	Invitrogen	R-415

2.9.2 FRAP analysis

FRAP analysis was performed to assess lateral membrane fluidity. Therefore, cells were transfected with the plasmid pMyrPalm-mEGFP (#21038, Addgene, Cambridge, MA, USA) and engineered to express MyrPalm-mEGFP, in order to visualize cellular membranes. The transfection was accomplished by electroporation as described in 2.6.1. 24 h after transfection cells were stimulated with Soraphen A for 72 h. 48 h after treatment, cells were kept in Soraphen A stimulated starvation medium. Next, the EGFP fluorescence in a defined region of interest (ROI) of randomly chosen cells was bleached and the fluorescence recovery was measured for 10 min. Cells were analysed with the TCS SP5 X microscope (Leica Microsystems Inc., IL, USA) in a humidified climate chamber (5 % CO_2, 37 °C).

2.9.3 Receptor internalization assay

For receptor internalization analysis 10.000 cells per well were seeded into an ibiTreat 8-well µ-Slide (ibidi GmbH, Munich, Germany) and stimulated with Soraphen A as indicated. 24 h before performing the internalization assay the culture medium was replaced by Soraphen A stimulated starvation medium. Rhodamine-conjugated Transferrin or EGF were diluted 1:100 in medium supplemented with 10 % FCS. Hoechst was added for nuclei staining at a dilution of 1:400. The culture medium was removed, 100 µl of the solution were added per well and incubated for 15 min. After the incubation time, cells were washed three times with PBS + Ca^{2+}/Mg^{2+}, fixed with 4 % PFA for 10 min at RT, washed another three times with PBS + Ca^{2+}/Mg^{2+} and once with distilled water and mounted with PermaFlour™ mounting medium.

2.9.4 Microtubules staining

Cells were cultivated in ibiTreat 8-well µ-Slides (ibidi GmbH, Munich, Germany) and treated as indicated. Culture medium was discarded, cells were washed twice with PBS + Ca^{2+}/Mg^{2+} and covered with 270 µl extraction buffer (80 mM PIPES pH 6.8, 1 mM $MgCl_2$, 5 mM EGTA, 0.5 % Triton-X, H_2O) for 30 s to remove monomeric and dimeric tubulin subunits. Next 30 µl 5 % glutaraldehyde were directly added to the extraction buffer and incubated for 10 min. After fixation the extraction buffer was removed and excess glutaraldehyde was quenched with 270 µl freshly made 0.1 % $NaBH_4$ in PBS for 7 min. The cells were washed with PBS + Ca^{2+}/Mg^{2+} three times for 5 min by gentle shaking. Unspecific binding sites were blocked with 0.2 % BSA in PBS for 10 min at RT. The anti-α tubulin antibody (#18251, abcam, Cambridge, UK) was diluted 1:400 in 0.2 % BSA in PBS and incubated for 30 min at RT. After four washing steps the secondary antibody and Hoechst were diluted in 0.2 % BSA in PBS, added and incubated for another 30 min. The secondary antibody was removed and after washing the cells four times with PBS + Ca^{2+}/Mg^{2+} and once with distilled water, the samples were mounted with PermaFlour™ mounting medium.

2.10 Receptor dimerization assays

2.10.1 Proximity ligation assay: Duolink®

Receptor dimerization and receptor dimer localization were assessed by the Duolink® proximity ligation assay (Sigma-Aldrich, St. Louis, MO, USA). Therefore, cells were seeded in 16-well glass slides (Lab-Tek®) and stimulated with Soraphen A for 72 h. 48 h after treatment cells were cultivated in starvation medium. Next, cells were fixed with methanol for 10 min at - 20 °C, washed three times with PBS + Ca^{2+}/Mg^{2+} and the unspecific binding sites were blocked for 10 min at RT with 2 % BSA in PBS. HER2 (#2156, Cell Signaling, Danvers, MA, USA) and EGFR (#2239, Cell Signaling, Danvers, MA, USA) antibodies were diluted 1:100 in blocking solution, added to the cells and incubated for 2 h. After the antibodies were removed and the samples washed thoroughly with PBS + Ca^{2+}/Mg^{2+}, PLA probes were diluted 1:5 in 2 % BSA in PBS and added to the cells for 1 h at 37 °C. For the ligation reaction the ligation stock was diluted 1:5 in high purity water. Next, the PLA probe solution was tapped off and the cells were washed two times for 5 min with washing buffer A. Immediately before usage the ligase

was added to the ligation solution at a 1:40 dilution and mixed. Cells were covered with the solution and incubated for 30 min at 37 °C. After the incubation time was completed, the ligase solution was tapped off and the cells were washed with washing buffer A twice for 2 min. For the amplification reaction the amplification stock was diluted in high purity water 1:5 and the polymerase was added at a 1:80 dilution directly before usage. The amplification reaction proceeded for 100 min at 37 °C. Next the solution was removed and the cells were washed twice for 10 min with washing buffer B. For nuclei staining Hoechst was added at a dilution of 1:400 to the washing buffer B in the first washing step. Before mounting, the slides were incubated with 0.01 % washing buffer B for 1 min. After mounting with FluorSave™ Reagent mounting medium the slides were stored at RT in the dark overnight and analysed by evaluating the fluorescent signal.

Tab. 8 Buffers for Duolink® Proximity Ligation Assay

Buffer	Composition
Washing buffer A	Tris (0.01 M), NaCl (0.15 M), Tween-20 (0.05 %) in H_2O
Washing buffer B	Tris (0.2 M), NaCl (0.1 M) in H_2O

2.10.2 Co-IP assay

Protein interactions were analysed by using the Pierce™ Crosslink Magnetic IP/Co-IP Kit (Thermo Fisher Scientific, Waltham, MA, USA). Cells were seeded in dishes, stimulated with Soraphen A for 2 h and treated with 100 ng/ml EGF 15 min before harvesting. For the Co-IP reaction Src antibody (#2110, Cell Signaling, Danvers, MA, USA) was diluted 1:12.5, coupled to the magnetic beads and crosslinked by DSS according to manufacturer`s instruction. Cells were washed with PBS and lysed by adding 500 µl provided IP lysis/wash buffer on ice for 5 min. The lysed cells were transferred into a tube and centrifuged for 10 min at 13.000 g to remove cell debris. Next, protein concentration was demined by BCA assay (Thermo Fisher Scientific, Waltham, MA, USA). The protein concentration of the control and Soraphen A treated cells was aligned by adding IP lysis/wash buffer. Cell lysate was mixed with the crosslinked magnetic beads and the immunoprecipitation was performed according to manufacturer’s instruction. The interaction partners could be detected by immunoblotting.

2.11 Phospholipid analysis

2.11.1 Lipid extraction

Lipid extraction for LC-MS/MS sample analysis was performed according to Bligh and Dyer (Bligh & Dyer 1959). Therefore cells were stimulated as indicated, harvested and frozen in liquid nitrogen. For lipid extraction the pellet was resuspended in 150 µl PBS then 552.5 µl chloroform were given to the sample and vortexed for 30 s. Another 187.5 µl of chloroform were added and vortexed for 30 s. Next 187.5 µl PBS were given to the sample and vortexed for 30 s. To separate the chloroform phase, which contained the lipid fraction from the aqueous phase the sample was centrifuged at 4000 rpm for 5 min. The lower chloroform phase was transferred to a new tube and the chloroform was evaporated for 30 min at 30 °C by using a rotational vacuum concentrator RVC 2-18. Lipid films were stable and were next used for LC-MS/MS analysis, which was performed by Dr. Andreas Koeberle (Group of Prof. Dr. Oliver Werz, University of Jena, Chair of Pharmaceutical and Medical Chemistry, Institute of Pharmacy).

2.11.2 Phospholipid rescue experiments

For phospholipid rescue experiments cell culture medium was supplemented with 100 µM of the respective phospholipid species listed in **Tab. 9** (purchased from Avanti Polar Lipids Inc., AL, USA). Therefore phospholipids, which were dissolved in chloroform, were transferred into a falcon tube and the chloroform was removed under nitrogen stream. Next, the respective amount of medium was added to obtain a 100 µM solution of the phospholipid. The mixture was vortexed and treated with ultrasound for 30 min at 40 °C. To prevent formation of vesicle agglomerates, the solution was always kept at 37 °C. Cells were treated with medium containing the phospholipid and stimulated with Soraphen A as indicated. 96 h after treatment cell proliferation was determined by crystal violet staining.

Tab. 9 Phospholipids used for rescue experiments

Phospholipid	Abbreviation	Avanti Polar Lipids Product #
1-palmitoyl-2-oleoyl-*sn*-glycero-3-phosphocholine	PC (16:0-18:1)	850457C
1-palmitoyl-2-arachidonoyl-*sn*-glycero-3-phosphocholine	PC (16:0-20:4)	850459C
1,2-dipalmitoleoyl-*sn*-glycero-3-phosphocholine	PC (16:1-16:1)	850358C
1,2-dipalmitoyl-*sn*-glycero-3-phosphocholine	PC (16:0-16:0)	850355C

2.12 Measurement of cell and membrane deformation

2.12.1 RT-DC measurement

The real-time deformability cytometry (RT-DC) measurements were performed according to Otto and colleagues (Otto et al. 2015) by Dr. Maria Winzi (Group of Prof. Dr. Jochen Guck, Biotec, TU Dresden). Therefore cells were stimulated with Soraphen A as indicated, trypsinized, washed with PBS and resuspended in PBS + 0.5 % methylcellulose or PBS + 0.63 % methylcellulose, respectively to a final concentration of $3 \cdot 10^5$ cells/ml. The measurement was performed in a 30 µm x 30 µm channel at flow rates of 0.16 µl/s, 0.24 µl/s and 0.32 µl/s. As a reference, non-deformed cells were measured in the reservoir outside the channel. The relative deformation (RD) was calculated as follows with d (deformation), treat (treatment), co (control), chan (channel) and res (reservoir):

$$RD = \frac{(d_{chan}^{treat} - d_{res}^{treat})}{(d_{chan}^{co} - d_{res}^{co})}$$

Statistical analysis was performed by using the bootstrapping algorithm to test for the significance of control versus Soraphen A treated cells. Therefore data from the channel and the reservoir were resampled for both control and Soraphen A treated cells and the RD values were determined, which follow a Gaussian distribution. P-values were obtained by dividing

the count of resamples that had an RD equal or larger than one by the number of total resamples.

2.12.2 Optical stretcher measurement

Cells were treated with Soraphen A as indicated, trypsinized, resuspended in cell culture medium and applied for the optical stretcher measurement. A dual laser beam fiber optical stretcher setup was used (Lincoln et al. 2007). Image series (30 fps) were recorded for whole deformation measurement at a constant temperature of 23 °C. For each experiment a minimum of 300 cells was assessed. Data are presented as median creep deformation J. For statistical analysis bootstrapping was applied to estimate the 95 % confidence interval. At the end of the stretch phase a two-sample Kolmogorov-test was used to determine if there is a difference between control and Soraphen A treated cells. The experiments were performed by Sebastian Schmidt (Group of Prof. Dr. Josef A. Käs, Leipzig University, Faculty of Physics and Earth Sciences, Institute of Experimental Physics I).

2.12.3 GPMV deformability analysis

To assess the deformability of giant plasma membrane vesicles (GPMV), cells were grown to 90 % confluence and treated as indicated with Soraphen A or the vehicle only. The culture medium was removed and cells were washed with GPMV buffer (150 mM NaCl, 10 mM HEPES and 2 mM $CaCl_2$ in H_2O). To induce vesiculation, 25 mM PFA and 4 mM DTT were freshly added to the GPMV buffer. Next cells were covered with the PFA and DTT containing GMPV buffer and incubated at 37 °C, 5 % CO_2 and 60 cycle/min for 120 min. The upper ¾ of the solution was pipetted on an object plate and the vesicles were imaged with an optical phase contrast microscope (DM IRB, Leica Microsystems Inc., IL, USA). Membrane fluctuations were analysed by Fourier analysis, which is described in detail in Braig et al. 2015. The experiments were performed by Chris Händel (Group of Prof. Dr. Josef A. Käs, Leipzig University, Faculty of Physics and Earth Sciences, Institute of Experimental Physics I).

2.13 Western blot analysis

Cells were trypsinized, washed with PBS and lysed in RIPA buffer supplemented with the protease inhibitor cocktail complete® (Sigma-Aldrich, St. Louis, MO, USA), 1 mM PMSF and 2 mM Na_3VO_4. Protein concentration was determined by BCA assay according to manufacturer´s instructions (Thermo Fisher Scientific, Waltham, MA, USA). Equal amounts of proteins were separated by SDS-electrophoresis (100 V, 500 mA, 150 W, 21 min/ 200 V, 500 mA, 150 W, 40 min) and proteins were transferred onto nitrocellulose membranes for 90 min and 100 V at 4 °C. Next, unspecific binding sites were blocked for 2 h with 5 % milk powder (MP) solution in PBS. Membranes were incubated with the primary antibody overnight, washed three times with TBS-T and incubated with secondary antibodies for 2 h. Protein detection was performed by the chemiluminescence-based ECL detection system (Amersham Pharmacia Biotech, Amersham, UK), the ChemiDoc™ Touch Imaging system (Bio-Rad, Hercules, CA, USA) or the fluorescence-based Odyssey Infrared Imaging System 2.1 (LI-COR Biosciences, Lincoln, NE, USA). Western blots were quantified with Image J or the Image Lab Software (Bio-Rad).

Tab. 10 Solutions and buffers for Western blot analysis

Solution	Composition
Electrophoresis buffer	Tris (4.9 mM), glycine (38 mM), SDS (0.1 %), in H_2O
RIPA lysis buffer	Tris-HCl (pH 7.4, 50 mM), NaCl (150 mM), nonidet NP 40 (1 %), deoxycholic acid (0.25 %), SDS (0.1 %) Na_3VO_4 (2 mM)*, complete® mini EDTA free (4 mM)*, PMSF (1 mM)*, in H_2O
5x SDS sample buffer	Tris-HCl (pH 6.8, 3.125 mM), glycerol (10 ml), SDS (5 %), DTT (2 %), pyronin Y (0.025 %), in H_2O
Stacking gel	Rotiphorese™ Gel 30 17 %, Tris (125 mM, pH 6.8), SDS (0.1 %), TEMED (0.2 %), APS (0.1 %) in H_2O

Separation gel 10 %	Rotiphorese™ Gel 30 (33 %), Tris (375 mM, pH 8.8), SDS (0.1 %), TEMED (0.1 %), APS (0.05 %) in H_2O
Tank buffer 5x	Tris-Base (240 mM), Glycine (195 mM), in H_2O
Tank buffer 1x	Tank buffer 5x (20 %), Methanol (20 %), in H_2O
TBS-T (pH = 8)	Tris-Base (24.76 mM), NaCl (189.9 mM), Tween 20 (0.1 %) in H_2O

* added directly before usage

Tab. 11 Primary antibodies used for Western blot analysis

Antigen	Source	Dilution	Solvent	Producer/Distributor	Product #
actin	mouse	1:1000	BSA 1 %	Merck Millipore	MAB 1501
EEA1	goat	1:1000	BSA 1 %	Santa Cruz	sc-6415
EGFR	mouse	1:1000	MP 5 %	Cell Signaling	2239
EGFR pTyr1068	rabbit	1:1000	BSA 5 %	Cell Signaling	2234
FAK	mouse	1:1000	BSA 5 %	Santa Cruz	sc-1688
FAK pTyr397	rabbit	1:1000	BSA 5 %	Santa Cruz	Sc-11765
HER2	rabbit	1:1000	MP 5 %	Cell Signaling	2156
HER2 pTyr1221/1222	rabbit	1:1000	BSA 5 %	Cell Signaling	2243
LAMP1	mouse	1:1000	BSA 5 %	Developmental Studies Hybridoma Bank	H4A3
Src	mouse	1:1000	MP 5 %	Cell Signaling	2110
Src pTyr416	rabbit	1:1000	BSA 5 %	Cell Signaling	6943
Tubulin beta	rabbit	1:1000	BSA 5 %	Cell Signaling	2146

Tab. 12 Secondary antibodies used for Western blot analysis

Antibody	Dilution	Solvent	Producer/Distributor	Product #
Goat-anti-mouse IgG1 HRP	1:1000	MP 1 %	Biozol	BZL07046
Goat-anti-rabbit IgG HRP	1:1000	MP 1 %	Bio-Rad	172-1019
Donkey-anti-goat IgG HRP	1:1000	MP 1 %	Santa Cruz	Sc- 2020
IRDye 800CW Goat-anti-rabbit	1:20 000	MP 1 %	LI-COR GmbH	926-32211D
IRDye 800 Goat-anti-rabbit IgG (H+L)	1:20 000	MP 1 %	Rockland	611-132-122
Alexa Fluor 680, Goat-anti-mouse IgG (H+L)	1:20 000	MP 1 %	Molecular Probes	A – 21057

2.14 Statistical analysis

Three independent experiments were performed and statistically analysed by the GraphPad PRISM Software 5.04 unless noted otherwise. Data are expressed as means + SEM or ± S.E.M and analysed using Student`s t test. P-values of * $p < 0.05$, ** $p < 0.01$, *** $p < 0.001$ were considered as significant. Synergism was calculated using the Bliss formula (Bliss 1956).

3 Results

3.1 Soraphen A – an anti-migratory compound

3.1.1 Inhibition of cell migration and invasion by Soraphen A *in vitro*

Lipogenesis and lipid homeostasis are known to be linked with cancer risk and progression (Azrad et al. 2013), therefore, a disruption of the fatty acid metabolism could be a therapeutic approach in cancer treatment. To characterise the cellular effects of the acetyl-CoA carboxylase (ACC) inhibitor Soraphen A, we initially examined cell migration and invasion of the carcinoma cell lines MDA-MB-231 and T24. Therefore, cells were stimulated for 2 h with Soraphen A and analysed in a Boyden chamber migration and invasion assay. Boyden chamber invasion experiments were performed by using matrigel™ coated inserts. As shown in **Fig. 8**, Soraphen A significantly reduced migration and invasion in both MDA-MB-231 and T24 cells.

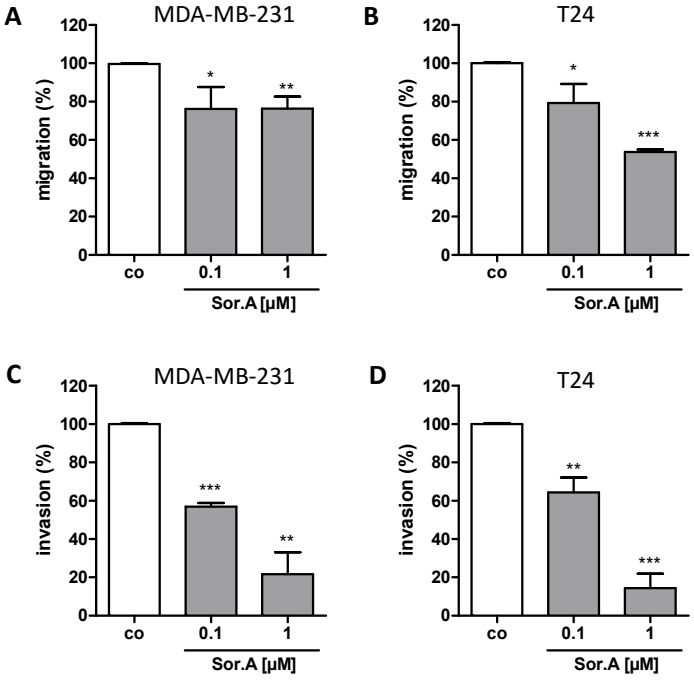

Fig. 8 Soraphen A inhibits migration and invasion of MDA-MB-231 and T24 cells. Cells were treated with increasing Soraphen A (Sor.A) concentrations for 2 h and (A, B) migration and (C, D) invasion of MDA-MB-231 and T24 were analysed by a Boyden chamber migration and invasion assay. For invasion assays, the upper Boyden chamber insert was filled with matrigel™. Error bars are given as the SEM of three independent experiments. * $p < 0.05$, ** $p < 0.01$, *** $p < 0.001$ (Student`s t-test).

Of note, migration of the non-invasive MCF10A cells was not inhibited by Soraphen A, which is depicted in **Fig. 9**.

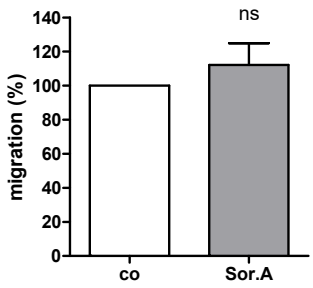

Fig. 9 Migration of the non-invasive MCF10A cells after Soraphen A treatment. MCF10A cells were treated with 1 µM Soraphen A (Sor.A) for 2 h, plated into Boyden chamber inserts and allowed to migrate 6 h. Error bars are presented as the SEM of three independent experiments. Statistical analysis was accomplished by Student`s t-test (ns = non-significant). Performed by Eva-Maria Baur.

Silencing of the Soraphen A target ACC1 by siRNA also diminished the migratory and invasive potential of cells in comparison to the control (**Fig. 10**), suggesting that ACC1 inhibition is responsible for the reduction of the migratory capacity.

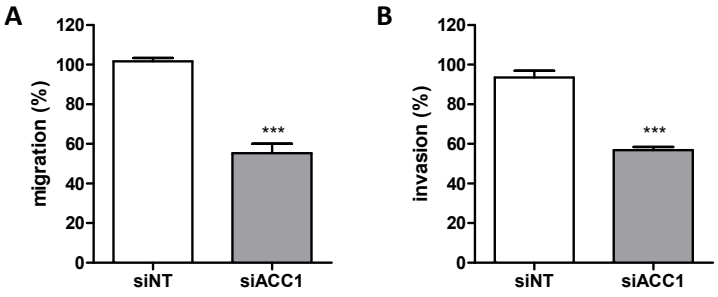

Fig. 10 Influence of ACC1 silencing on migration of MDA-MB-231 cells. ACC1 was silenced by siRNA in MDA-MB-231 cells and the (A) migration and (B) invasion were assessed in a Boyden chamber setup. For invasion assays, the upper Boyden chamber insert was filled with matrigel^{TM}. Error bars represent the SEM of three independent experiments. *** $p < 0.001$ (Student`s t-test).

The results observed in the Boyden chamber assay could be confirmed in a 3D spheroid invasion assay with T24 cells. Therefore, spheroids were embedded in collagen to mimic the *in vivo* tumor and the surrounding matrix interface, treated with Soraphen A and allowed to invade for 72 h. As demonstrated in **Fig. 11**, Soraphen A significantly abrogated cell invasion of spheroids.

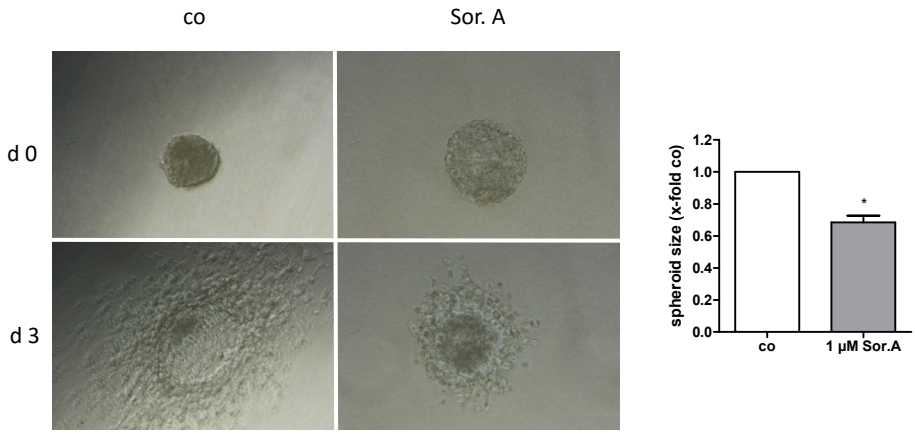

Fig. 11 3D spheroid invasion after Soraphen A treatment. T24 spheroids were stimulated with 1 µM Soraphen A (Sor.A) and imbedded in collagen. Pictures were taken on day 0 (d 0) and day 3 (d 3). The diameter of spheroids was measured and the quantification (day 3) depicted in the right panel. Left panel shows one representative spheroid. Error bars represent the SEM of three independent experiments. In one experiment at least 10 spheroids per condition were measured. * $p < 0.05$ (Student`s t-test).

Beyond the classical Boyden chamber assay for analysis of cell migration, we also performed a chemotaxis migration experiment in 2D and 3D. To quantify the chemotactic movement of cells, the forward migration indices $FMI_{\parallel}$ and $FMI_{\perp}$ were calculated, with $FMI_{\parallel}$ defining the migration parallel to the gradient and $FMI_{\perp}$ perpendicular to the gradient. The larger the FMI values are, the stronger is the chemotactic migration in the respective direction. To evaluate the overall travel trend of cells, the center of mass (M_{end}) was used, which represents the average point of all endpoints of the travelled cells. Furthermore, velocity of cells was determined. In the 3D setting, migration of cells was monitored in matrigel^{TM}. For both the MDA-MB-231 and T24 cells we found a reduced $FMI_{\parallel}$ index in the 2D and 3D setting after Soraphen A treatment, which is depicted in **Fig. 12** and **Fig. 13**, implicating a diminished chemotactic migration towards a gradient of growth factors. Interestingly, in the 3D setting Soraphen A treated MDA-MB-231 cells showed an enhanced velocity in comparison to non-treated cells. However, this effect was not significant and could neither be found in the 3D setup for T24 nor in the 2D setting for MDA-MB-231 or T24 cells. The 3D chemotaxis experiments were performed by Kerstin Kick (Group of Prof. Dr. Angelika M. Vollmar, University of Munich, Pharmaceutical Biology).

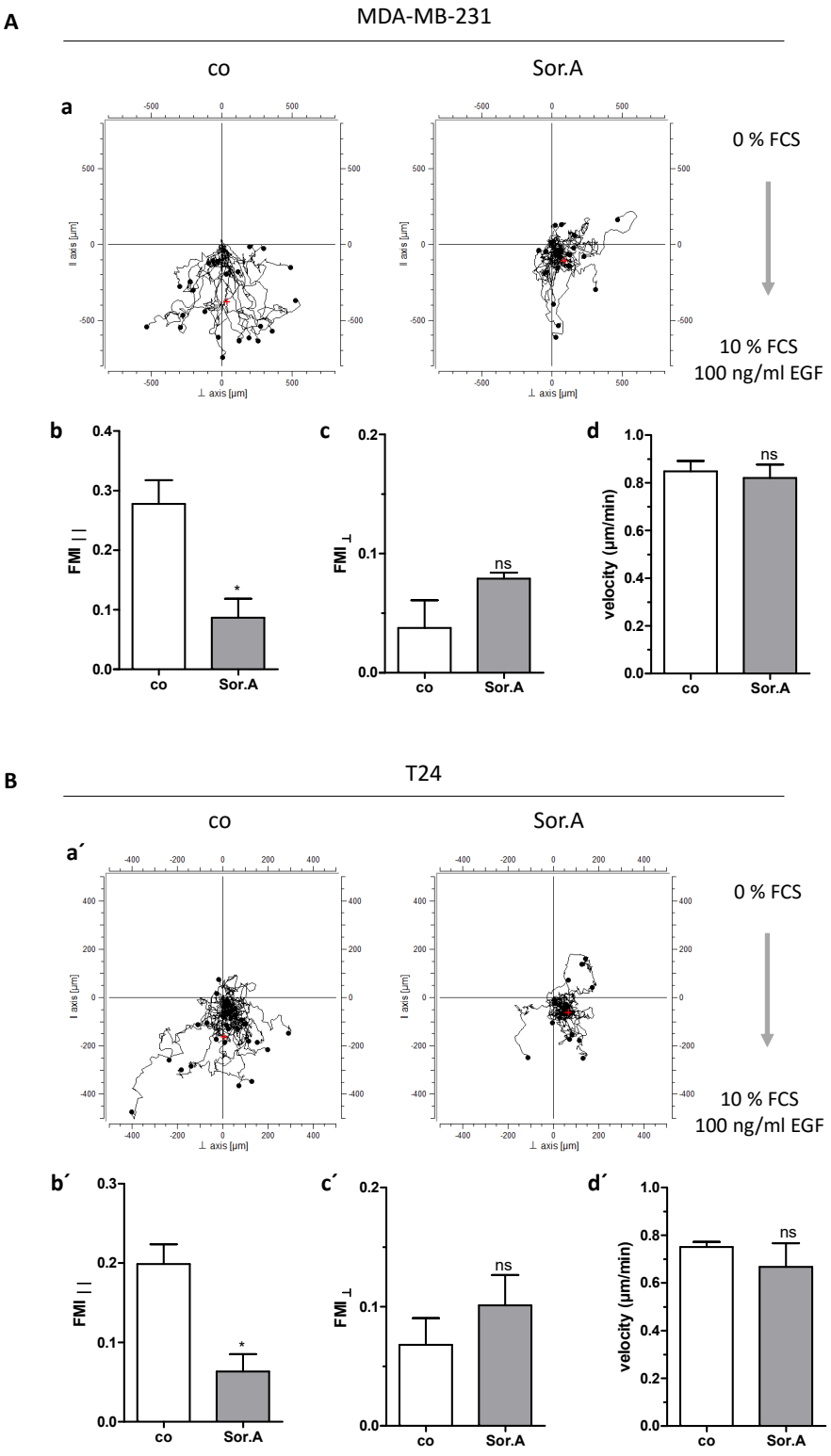

Fig. 12 2D chemotaxis after Soraphen A treatment. (A) MDA-MB-231 and (B) T24 cells were pretreated for 2 h with 1 µM Soraphen A (Sor.A) and (a, a´) the migration towards a 10 % FCS/100 ng/ml EGF gradient was monitored for 16 h. The center of mass (M_{end}) is marked in red. The quantitative parameters (b, b´) $FMI_{\parallel}$, (c, c´) $FMI_{\perp}$ and (d, d´) the velocity of cells were determined. Error bars are given as the SEM of three independent experiments. * $p < 0.05$, ns = non-significant (Student`s t-test).

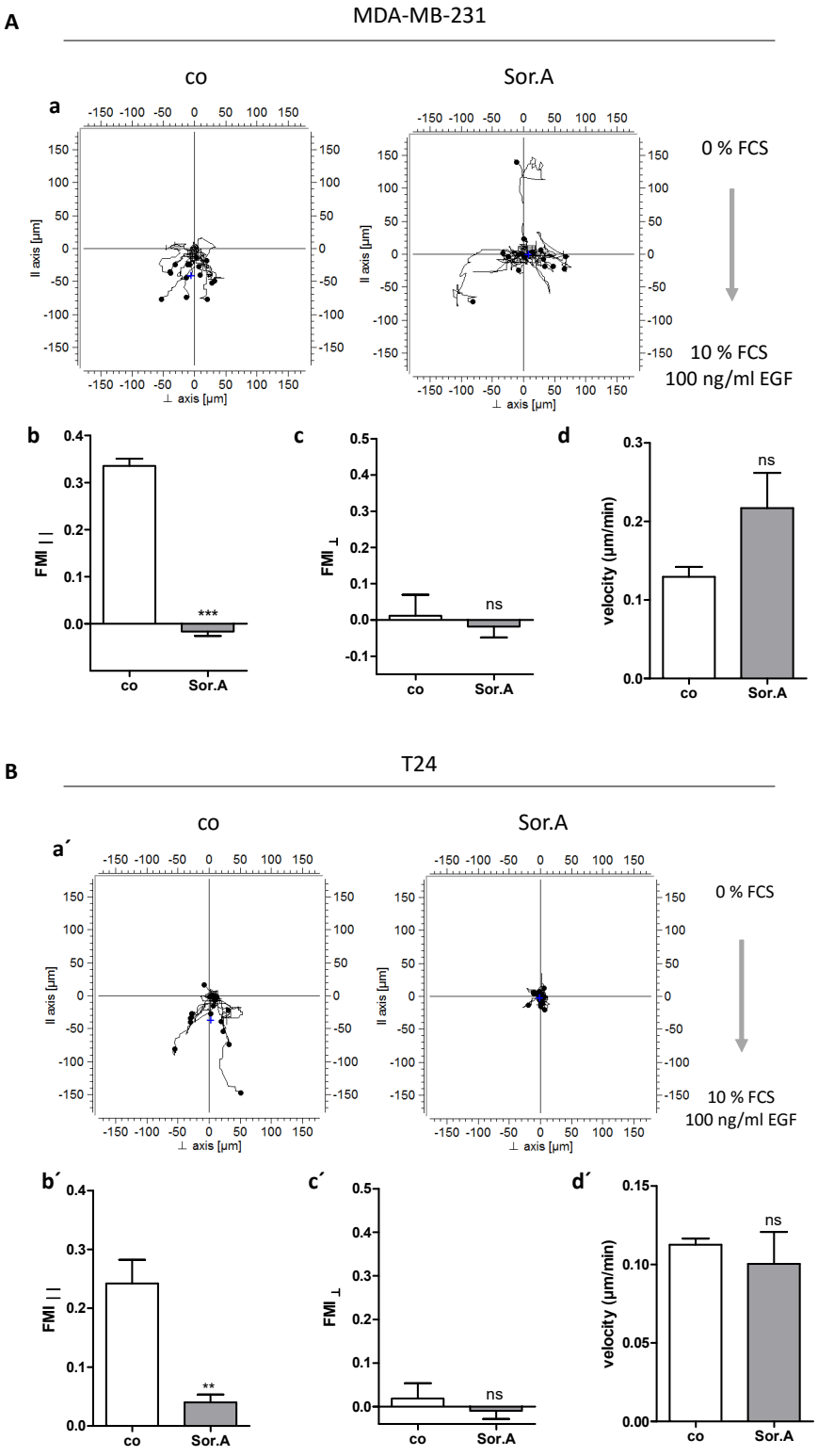

Fig. 13 3D chemotaxis after Soraphen A treatment. (A) MDA-MB-231 and (B) T24 cells were pretreated for 2 h with 1 µM Soraphen A (Sor.A) and (a, a´) the migration towards a 10 % FCS/100 ng/ml EGF gradient was monitored for 16 h. The center of mass (M_{end}) is marked in blue. The quantitative parameters (b, b´) $FMI_{\parallel}$, (c, c´) $FMI_{\perp}$ and (d, d´) the velocity of cells were determined. Error bars are given as the SEM of three independent experiments. ** $p < 0.01$, *** $p < 0.001$, ns = non-significant (Student`s t-test). Performed by Kerstin Kick (Group of Prof. Dr. Angelika M. Vollmar, Pharmaceutical Biology, University of Munich).

To exclude that the reduced migratory capacity of cells after Soraphen A treatment results from other Soraphen A-induced cellular processes, we analysed whether cell attachment, proliferation and apoptosis rate were changed in treated cells. Therefore, cell attachment was measured 4 h after seeding by an impedance-based real-time cell analyzer setup, showing no effect of Soraphen A (**Fig. 14 A, B**). Furthermore, cell death was determined by PI exclusion assay in Soraphen A and vehicle treated cells (**Fig. 14 C, D**) and the influence of Soraphen A on the proliferation rate was assessed by CellTiter-Blue® cell viability assay (**Fig. 14 E, F**). Neither cell death was induced nor was the proliferation rate affected after Soraphen A treatment.

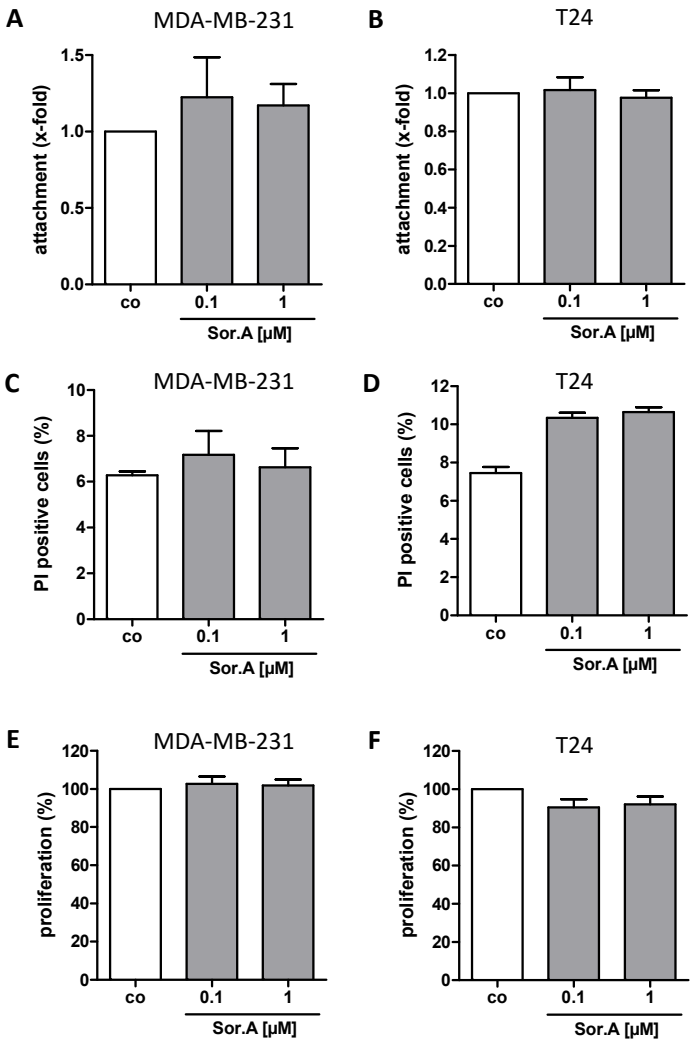

Fig. 14 Analysis of cell attachment, cell death induction and proliferation after Soraphen A treatment. Attachment of (A) MDA-MB-231 and (B) T24 cells was determined via real-time cell analyzer impedance measurement 4 h after cell seeding. Therefore, cells were pretreated with Soraphen A (Sor.A) for 4 h before seeding. Cell death rate was measured 24 h after Sor.A treatment in (C) MDA-MB-231 and (D) T24 cells by PI exclusion assay. The proliferation rate was assessed 72 h after Sor.A treatment in (E) MDA-MB-231 and (F) T24 cells by CellTiter-Blue® cell viability assay. Error bars are given as the SEM of three independent experiments performed in duplicate or triplicate, respectively.

3.1.2 Soraphen A as a potent inhibitor of migration *in vivo*

Since *in vitro* experiments showed a strong anti-migratory potential of Soraphen A, we next analysed the *in vivo* effects of Soraphen A on tumor cell dissemination, using the 4T1-Luc murine breast cancer cell model. The 4T1-Luc cells metastasize to the lungs and recombinantly express luciferase, which allows real-time imaging of tumors by using the IVIS Lumina system. Therefore Soraphen A or vehicle pretreated cells were injected intravenously in Balb/c mice. Mice challenged with Soraphen A stimulated cells showed a strongly reduced formation of lung metastases in comparison to the control group both 6 h and 72 h after Soraphen A treatment (**Fig. 15**). The inhibitory effect on metastasis formation was significant 72 h after stimulation. *In vivo* experiments were performed by Melanie Ulrich and Kerstin Loske (Group of Prof. Dr. Angelika M. Vollmar, University of Munich, Pharmaceutical Biology).

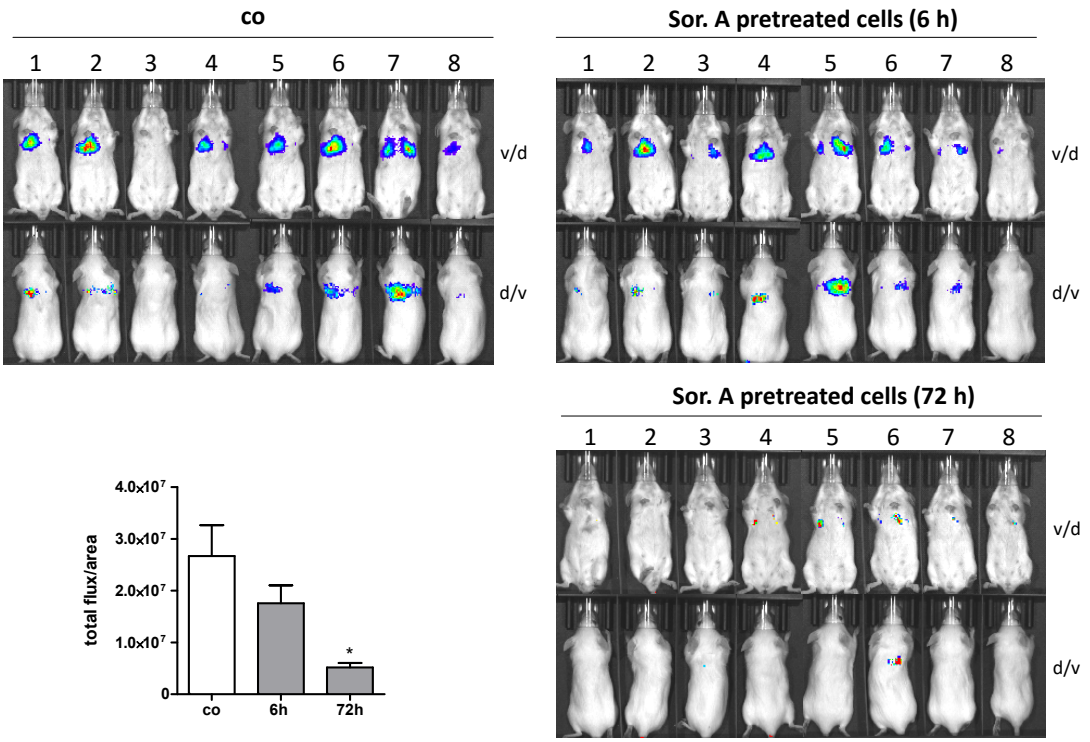

Fig. 15 Soraphen A inhibits metastasis *in vivo*. 4T1-Luc cells were pretreated with 1 µM Soraphen A (Sor.A) for 6 h or with 25 nM Sor.A for 72 h, respectively. $1 \cdot 10^5$ cells were injected intravenously in Balb/c mice, with eight mice per group. Lung dissemination was analysed four days post injection (v/d = ventrodorsal, d/v = dorsoventral). The quantitative bioluminescence signal evaluation is depicted in the left lower panel. Data analysis was accomplished by one-way ANOVA + Dunnett`s multiple comparison test with * $p < 0.05$. *In vivo* experiments were performed by Melanie Ulrich and Kerstin Loske (Group of Prof. Dr. Angelika M. Vollmar, University of Munich, Pharmaceutical Biology).

To exclude cytotoxic effects being responsible for the reduced dissemination in the *in vivo* experiment, apoptosis rate of 4T1-Luc cells was assessed after Soraphen A treatment. As demonstrated in **Fig. 16**, we could show that Soraphen A does not induce apoptosis.

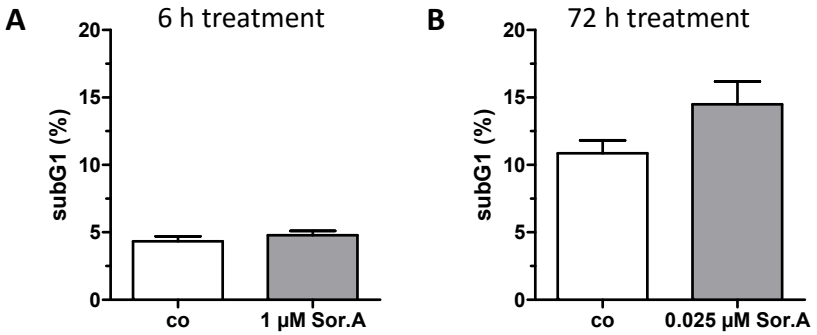

Fig. 16 Evaluation of apoptosis induction in 4T1-Luc cells after Soraphen A treatment. 4T1-Luc cells were treated with 25 nM Soraphen A (Sor.A) for 72 h or 1 µM Sor.A for 6 h. Apoptosis rate was assessed by PI staining. Error bars are presented as the SEM of three independent experiments performed in triplicate. Conducted by Eva-Maria Baur.

3.1.3 Alteration of phospholipid composition by Soraphen A

To understand the underlying mechanism behind the arresting effects of Soraphen A on cell migration and metastasis formation, we examined the phospholipid composition of the invasive breast cancer cell line MDA-MB-231 after acetyl-CoA carboxylase inhibition. Therefore, cells were treated for 6 h with Soraphen A or vehicle only, lipids were extracted, separated by reverse phase liquid chromatography and analysed by ESI tandem mass spectrometry by Dr. Andreas Koeberle (Group of Prof. Dr. Oliver Werz, University of Jena, Chair of Pharmaceutical and Medical Chemistry, Institute of Pharmacy). After the stimulation no significant changes were recorded in the total amount of phosphatidylcholine (PC), phosphatidylethanolamine (PE), phosphatidylserine (PS) and phosphatidylinositol (PI) species (**Fig. 17 A**). However, the phospholipid composition of all species was profoundly changed after treatment, with the amount of some species being enhanced (e.g. PC (16:0/16:0), PC (16:0/18:2), PC (18:0/18:2)), others decreased (e.g. PC (16:0/16:1)) and a few not significantly regulated (e.g. PC (16:0/18:1)) by Soraphen A (**Fig. 17 B**).

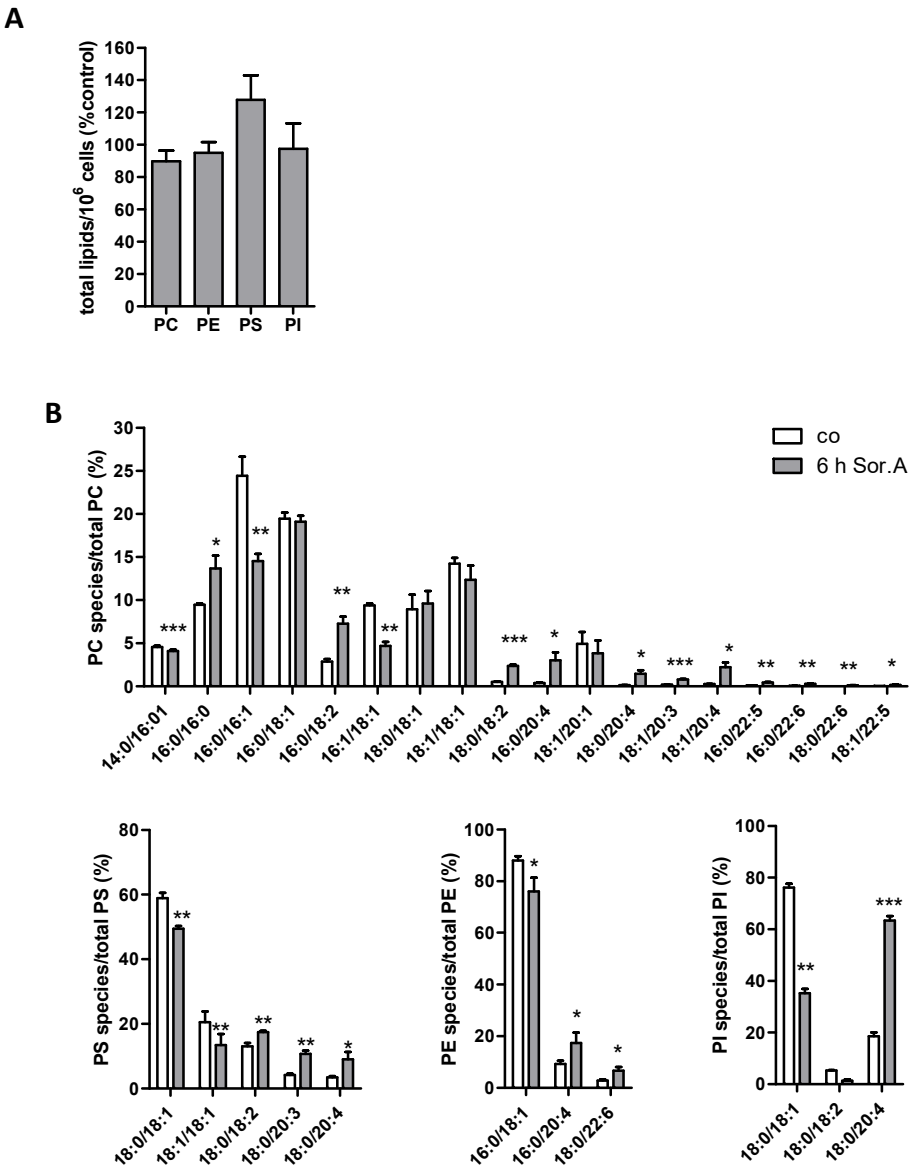

Fig. 17 Soraphen A changes the phospholipid composition of MDA-MB-231 cells. Cells were treated with Soraphen A (Sor.A) or vehicle for 6 h, lipids were extracted and analysed by liquid chromatography ESI tandem mass spectrometry. (A) Total signal intensities of phospholipid species in Sor.A treated cells normalized to control. A value of 100 % was assigned for the signal intensities of control cells. (B) Distribution of phospholipid species in control (co) and in Sor.A treated cells, given as the percentage of the sum of all species in the respective subclass. Data analysis was performed by repeated measures ANOVA + Turkey's post-hoc test (* $p < 0.05$, ** $p < 0.01$, *** $p < 0.001$). Experiments were conducted by Dr. Andreas Koeberle (Group of Prof. Dr. Oliver Werz, University of Jena, Chair of Pharmaceutical and Medical Chemistry, Institute of Pharmacy).

The phospholipidome data presented in **Fig. 17** were also analysed according to fatty acid desaturation index and fatty acid chain length, as shown in **Fig. 18**. The number of double bonds and the fatty acid chain length were significantly increased after Soraphen A treatment in PC, PS and PI species. PE species also exhibited a clearly higher desaturation level and longer fatty acid chain lengths, though these effects were not significant.

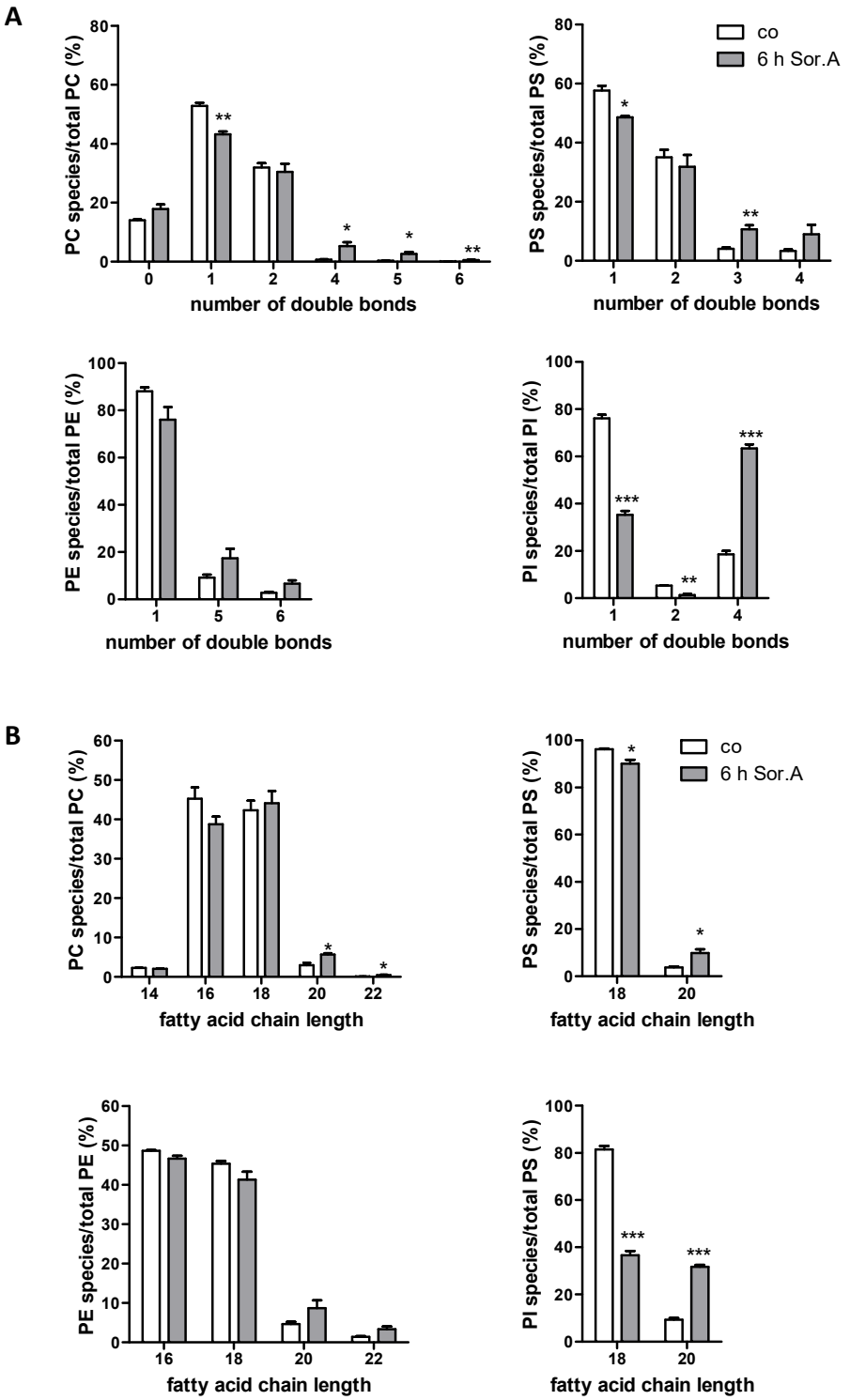

Fig. 18 Soraphen A enhances fatty acid desaturation and fatty acid chain length in MDA-MB-231 cells. Cells were treated with Soraphen A (Sor.A) or vehicle for 6 h, lipids were extracted and analysed by liquid chromatography ESI tandem mass spectrometry. (A) Distribution of the phospholipid species depending on their desaturation. The signal intensities are depicted relative to the summarized signal intensities of all subclass intensities. (B) Distribution of the phospholipid species depending on their fatty acid chain length given as the percentage of the sum of all species in the respective subclass. Data analysis was accomplished by repeated measures ANOVA + Turkey's post-hoc test (* $p < 0.05$, ** $p < 0.01$, *** $p < 0.001$). Experiments were performed by Dr. Andreas Koeberle (Group of Prof. Dr. Oliver Werz, University of Jena, Chair of Pharmaceutical and Medical Chemistry, Institute of Pharmacy).

3.1.4 Influence of Soraphen A on filopodia formation and the cytoskeleton

Another important regulator of migration is the cytoskeleton, with the reorganization and turnover of the actin cytoskeleton being the driving force for cellular movement. Actin filaments *inter alia* regulate the formation of cellular protrusions (Yamaguchi & Condeelis 2007). Based on the data published by Swaminathan and colleagues, proposing that invasive cells express a higher amount of cortical actin in comparison to their non-invasive counterparts (Swaminathan et al. 2011), we first analysed whether the actin localization was changed after Soraphen A treatment. Cortical actin could be found in control cells as well as in Soraphen A treated cells (**Fig. 19**), demonstrating that the cellular organization of actin was not affected by Soraphen A.

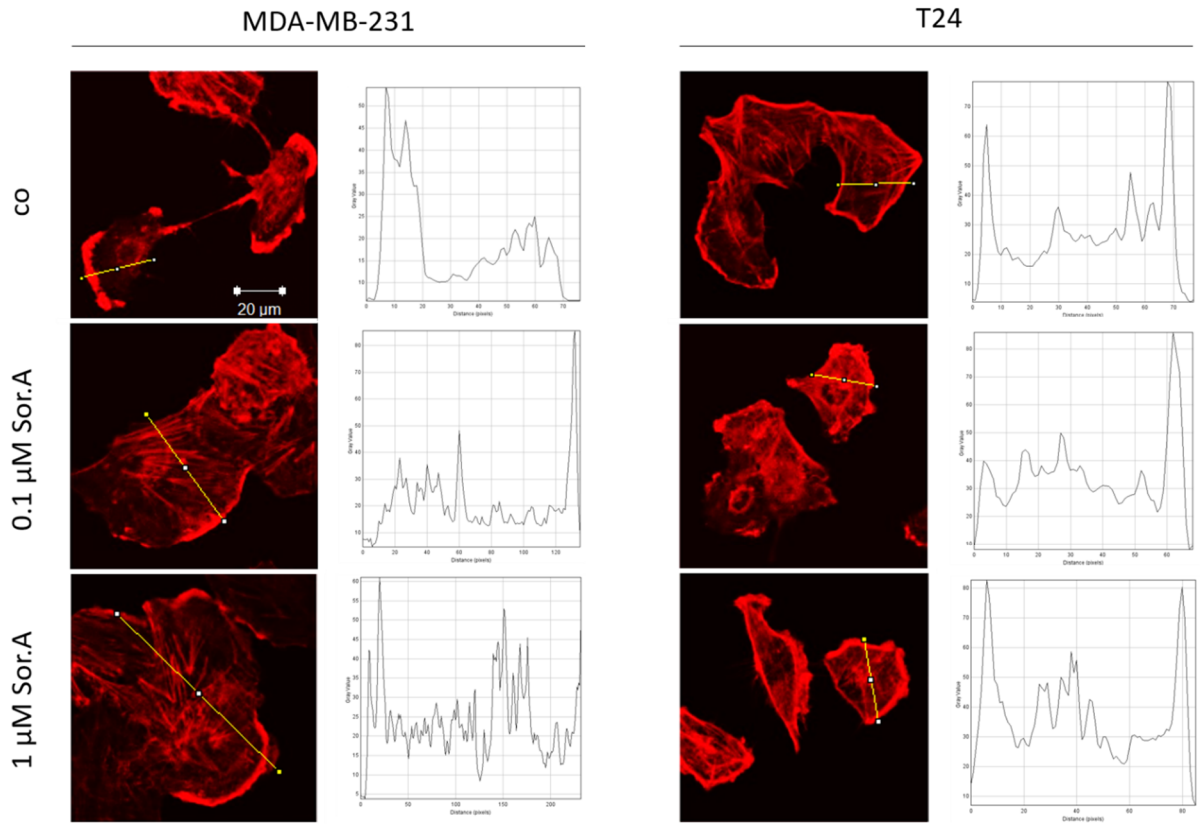

Fig. 19 Actin profile after Soraphen A treatment. MDA-MB-231 and T24 cells were treated with increasing concentrations of Soraphen A (Sor.A) or vehicle for 4 h, fixed and actin was stained. Actin profiles across the lines depicted in yellow were analysed using ImageJ and are shown in the right panels. One representative experiment out of three is shown.

Microtubules are a major constituent of the cytoskeleton, thus we also tested whether their structure is influenced by Soraphen A. Microtubules seem, as actin, not to be regulated by

Soraphen A as shown in **Fig. 20**, implicating that Soraphen A has no direct effects on the cytoskeleton of cells.

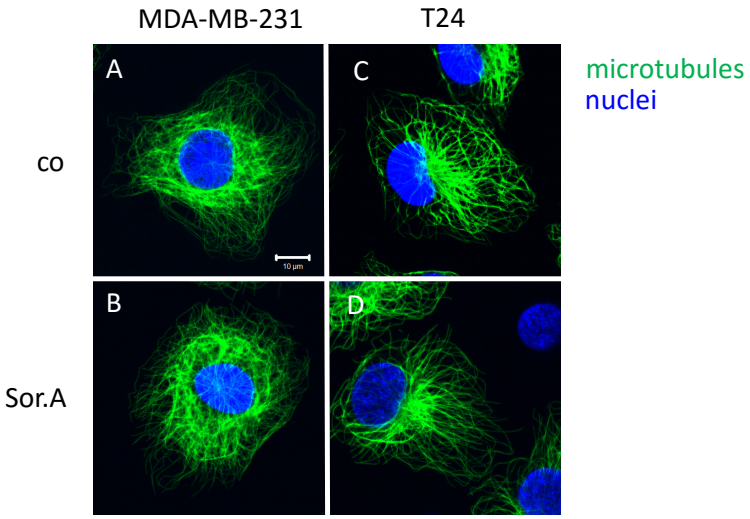

Fig. 20 Effect of Soraphen A on microtubules. MDA-MB-231 and T24 cells were treated with Soraphen A (Sor.A) for 2 h or vehicle, respectively and microtubules were visualized by α-tubulin staining.

Next, we assessed whether Soraphen A influences filopodia formation and interestingly found cell line-dependent effects. In MDA-MB-231 cells the number of filopodia per cell was significantly reduced, whereas in T24 cells no effect of Soraphen A could be determined. Filopodia were analysed in spreading MDA-MB-231 cells. In T24 cells the experiment was conducted in adherent cells, as T24 did not form filopodia in the spreading state (**Fig. 21**).

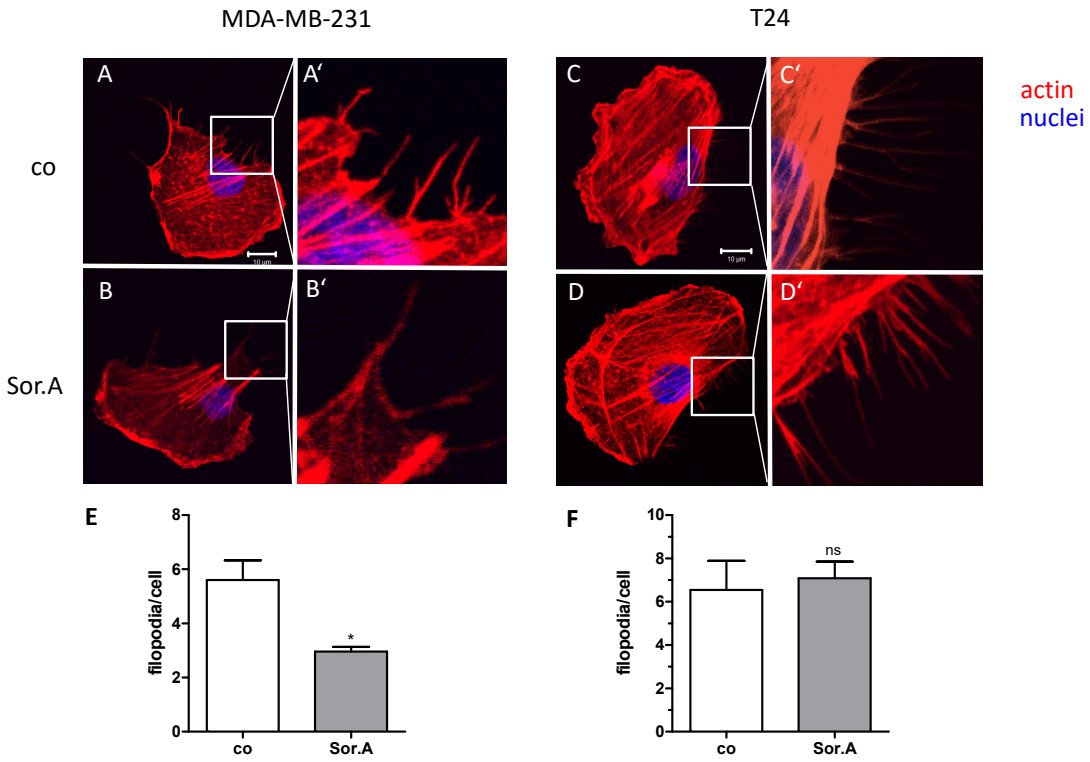

Fig. 21 Effect of Soraphen A on filopodia formation. MDA-MB-231 cells were seeded, stimulated with (A) vehicle or (B) Soraphen A (Sor.A) for 2 h, detached, seeded in 8-well µ-Slides, allowed to adhere for 2 h, fixed and stained for actin. T24 cells were seeded in 8-well µ-Slides, stimulated with (C) vehicle or (D) Sor.A for 2 h, fixed and actin was stained. Quantification of filopodia is depicted in (E) for MDA-MB-231 cells and (F) for T24 cells. Error bars show the SEM of three independent experiments. * $p < 0.05$, ns = non-significant (Student`s t-test).

To understand the underlying mechanism that evokes the reduced number of filopodia after Soraphen A treatment, we analysed two proteins that influence the formation of membrane protrusions, namely Rac and Vinculin. Rac is a GTPase that influences cell motility and controls filopodia and membrane ruffles formation (Ridley et al. 1999), whereas Vinculin effects mechanotransduction of cells at adhesion sites by regulating cell adhesion, cell spreading and the generation of traction forces (Jannie et al. 2015). **Fig. 22** shows the Rac and Vinculin staining in spreading MDA-MB-231 cells 2 h after Soraphen A treatment, revealing no differences between treated and untreated cells. Thus we supposed that the altered membrane characteristics are responsible for the diminished filopodia formation and in the next step analysed the biophysical membrane and cell properties.

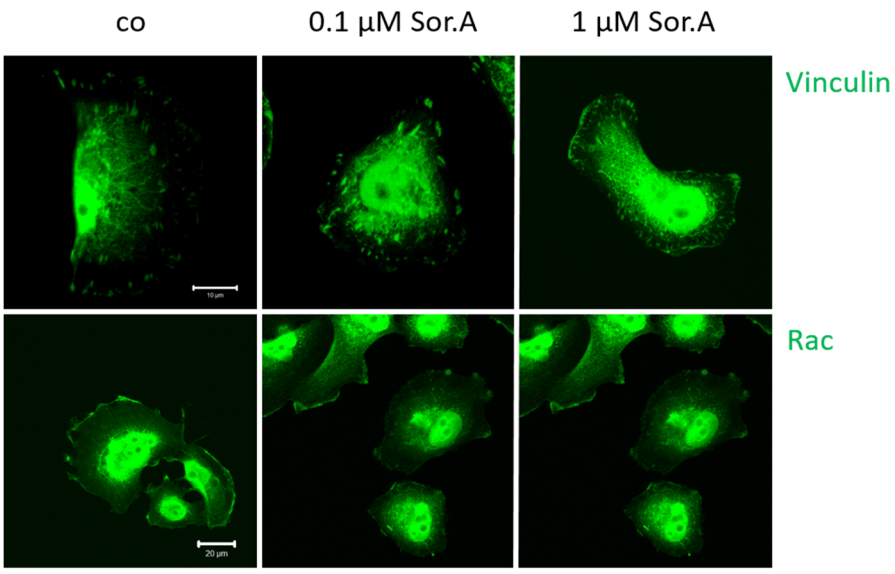

Fig. 22 Effect of Soraphen A on Vinculin and Rac localization. MDA-MB-231 cells were treated with increasing concentrations Soraphen A (Sor.A) for 2 h, fixed and stained for Vinculin or Rac, respectively, before mounting. One representative experiment out of three is shown.

3.1.5 Biomechanical analysis of cells after Soraphen A treatment

As phospholipids are the most abundant building blocks of cellular membranes, we hypothesized that a changed phospholipid profile could affect biomechanical properties of cells. First membrane rigidity, which excludes factors like cytoskeletal restraints, was determined by preparing giant plasma membrane vesicles (GPMVs). Therefore, MDA-MB-231 and T24 cells were treated for 2 h with 1 µM Soraphen A, before GPMVs were generated and analysed. GPMVs gained from both Soraphen A treated MDA-MB-231 and T24 cells had an increased median bending rigidity compared to the vehicle treated GMPVs, indicating that Soraphen A enhances membrane rigidity (**Fig. 23 A, B**).

Second, cell stiffness of whole cells was analysed by optical stretcher setup. Therefore, cells were trapped between two laser beams and stretched for 2 s by enhancing the laser power. MDA-MB-231 cells were found to be stiffer after Soraphen A treatment, whereas no changes in the whole cell stiffness could be measured in T24 cells (**Fig. 23 C, D**). The endpoint of the stretcher phase measurement was plotted in **Fig. 23 E** and **F**. The experiments were performed by Chris Händel and Sebastian Schmidt (Group of Prof. Dr. Josef A. Käs, Leipzig University, Faculty of Physics and Earth Sciences, Institute of Experimental Physics I).

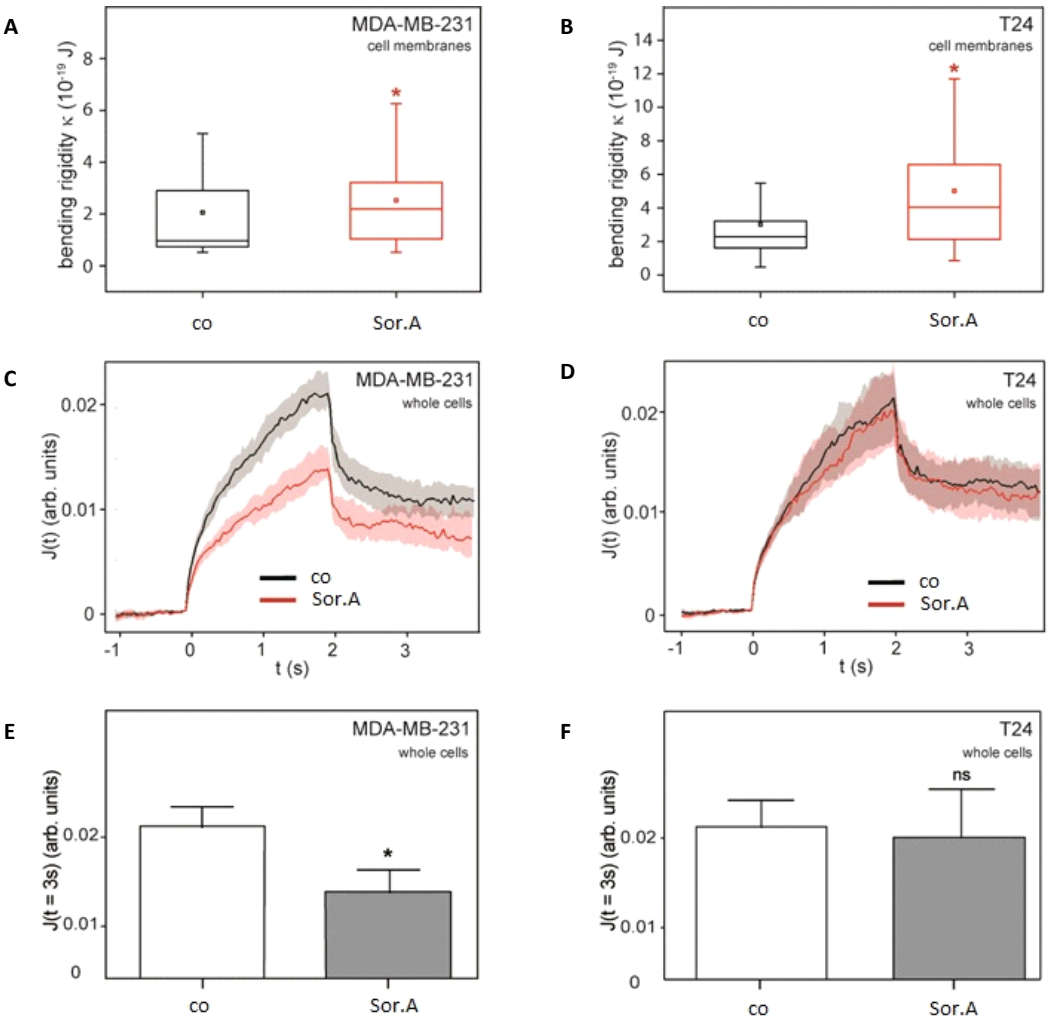

Fig. 23 Biochemical characterisation of MDA-MB-231 and T24 cells after Soraphen A treatment. Boxplots of bending elastic moduli κ of GPMVs obtained from Soraphen A (Sor.A) or vehicle treated (A) MDA-MB-231 and (B) T24 cells. Statistical analysis was done with the Kolmogorov-Smirnov test (* $p < 0.05$, ns = non-significant). Median relative deformation of whole (C) MDA-MB-231 and (D) T24 cells in optical stretcher measurements was plotted over time. The stretch phase ranged from 0 s to 2 s with 800 mW. Evaluation of the optical stretcher measurement at the end of the stretch phase for (E) MDA-MB-231 and (F) T24 cells. Performed by Chris Händel and Sebastian Schmidt (Group of Prof. Dr. Josef A. Käs, Leipzig University, Faculty of Physics and Earth Sciences, Institute of Experimental Physics I).

3.1.6 Effect of Soraphen A on membrane-dependent cellular processes

Cell migration is a complex process that involves many molecular components. As we found that membrane characteristics and not the classical key players of migration are affected by Soraphen A, we concentrated on membrane-dependent cellular processes which are associated with cell migration. First we focused on membrane recycling and assessed the effect of Soraphen A on the endosomal and lysosomal marker proteins EEA1 and LAMP1, as lysosomes and endosomes are inevitable for recycling processes. In MDA-MB-231 cells a

reduced level of the EEA1 protein 6 h after Soraphen A treatment could be detected, whereas in T24 cells no effect was visible (**Fig. 24 A, B**). In contrast to that, LAMP1 expression was reduced in T24 cells but not in MDA-MB-231 cells, as depicted in **Fig. 24 C** and **D**.

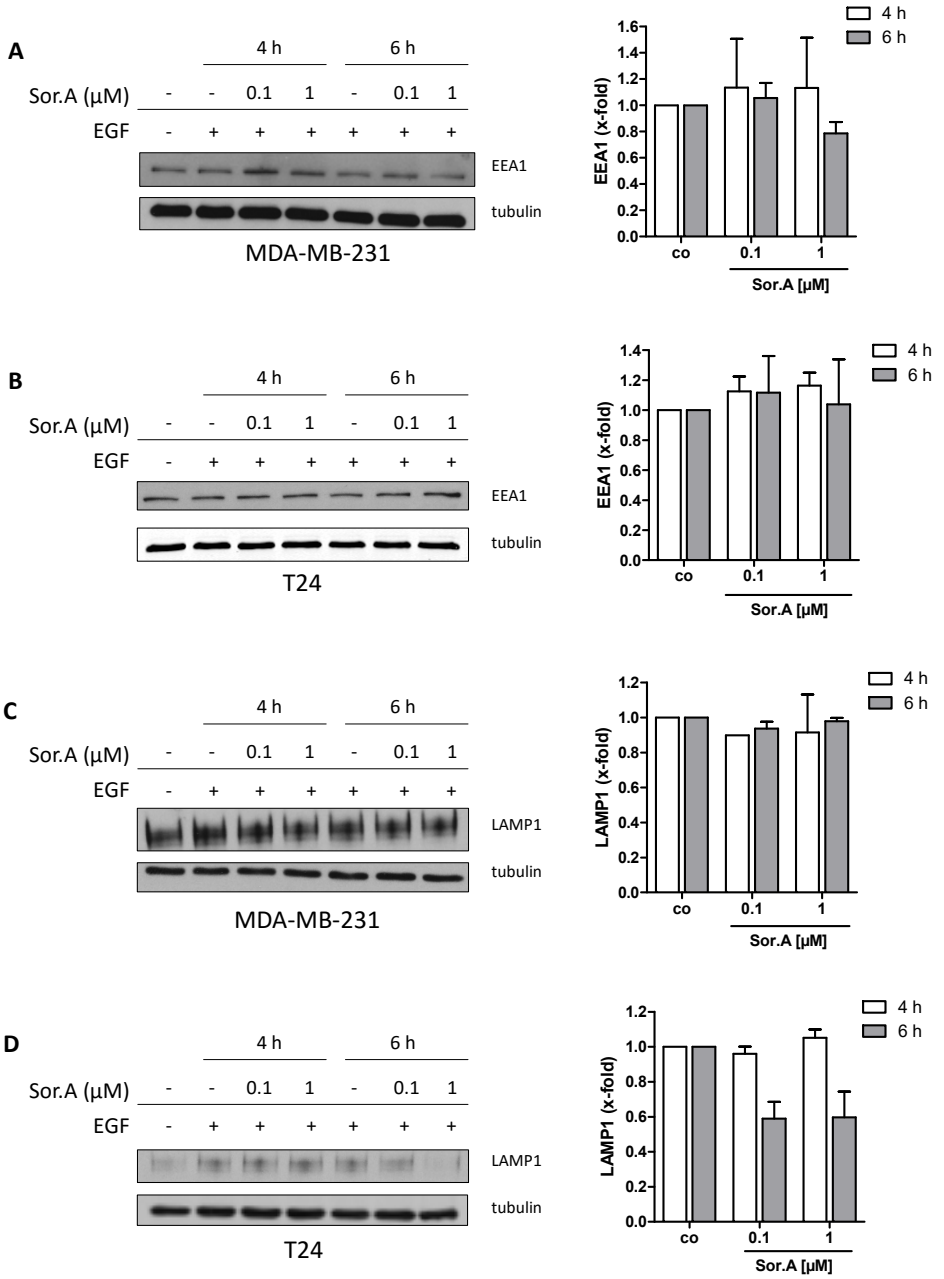

Fig. 24 EEA1 and LAMP1 protein expression after Soraphen A treatment. MDA-MB-231 and T24 cells were stimulated with increasing concentrations of Soraphen A (Sor.A) for 4 h and 6 h, respectively. To induce the recycling machinery cells were additionally treated with 100 ng/ml EGF for 15 min. EEA1 expression in (A) MDA-MB-231 and (B) T24 cells. LAMP1 expression in (C) MDA-MB-231 and (D) T24 cells. Quantification was conducted by ImageJ. Error bars represent the SEM of two (LAMP1) or three (EEA1) independent experiments.

We next assessed whether the signaling of the membrane-associated receptor EGFR, which is also known to be involved in cell migration, is regulated by Soraphen A treatment. In MDA-MB-231 cells we found a slightly reduced phosphorylation of the EGFR. In T24 cells the

phosphorylation of EGFR was strongly diminished 4 h after stimulation, whereas the effect was alleviated again after 6 h of Soraphen A treatment (**Fig. 25**).

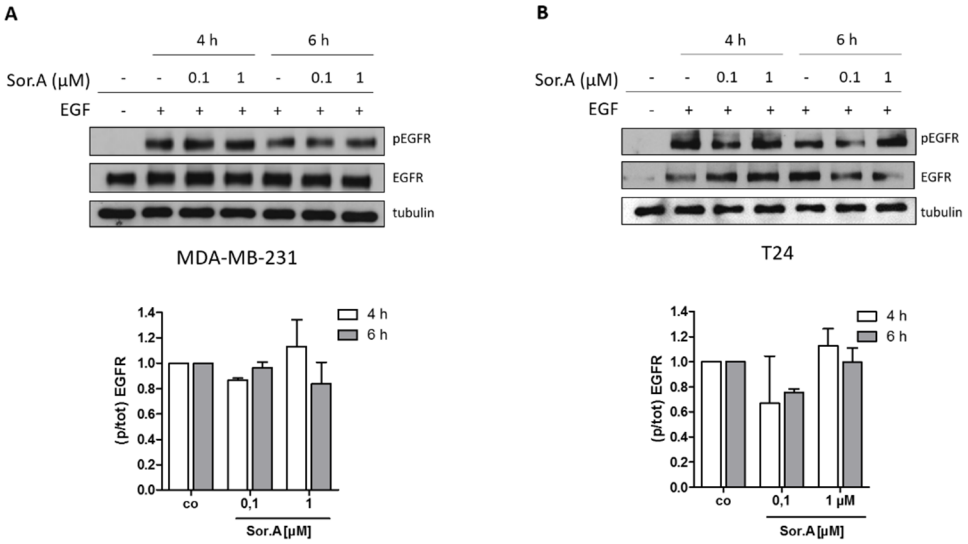

Fig. 25 pEGFR/EGFR expression after Soraphen A treatment. (A) MDA-MB-231 and (B) T24 cells were treated with increasing concentrations of Soraphen A (Sor.A) for 4 h or 6 h, respectively. EGFR phosphorylation was induced with the EGFR ligand EGF (100 ng/ml). Western blot quantification, performed by Image J can be found in the lower panel. Error bars represent the SEM of three independent experiments.

Another mediator of migration, which binds to transmembrane integrins is the focal adhesion kinase FAK (Sieg et al. 1999). FAK is not directly anchored, but can be recruited to the membrane to activate downstream signaling pathways. We were interested whether Soraphen A influences FAK and found that FAK phosphorylation was not changed after treatment (**Fig. 26**).

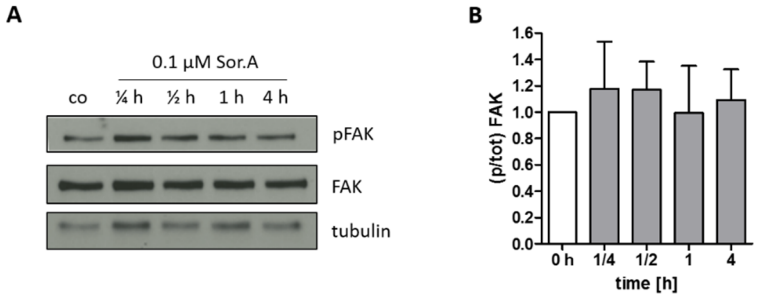

Fig. 26 Effect of Soraphen A on phosphorylation of FAK. (A) MDA-MB-231 cells were stimulated with Soraphen A (Sor.A) for 15 min, 30 min, 1 h and 4 h and the phosphorylation of FAK was assessed by Western blot analysis. (B) Quantification of the Western blots was performed by Image J. Error bars represent the SEM of two independent experiments.

3.2 Soraphen A – an anti-proliferative compound

3.2.1 Anti-proliferative effects of Soraphen A on cancer cells *in vitro*

Beyond the anti-metastatic potential of Soraphen A we analysed its effects on cell proliferation of the breast cancer cell lines SKBR3 and MDA-MB-231 and the hepatocellular carcinoma cells Huh7 and HepG2. While anti-migratory effects occurred after short stimulation times of 2 h, longer stimulation times of 96 h resulted in a dose-dependent inhibition of proliferation in all cell lines. Of note, SKBR3 cells were particularly sensitive to Soraphen A treatment (**Fig. 27**).

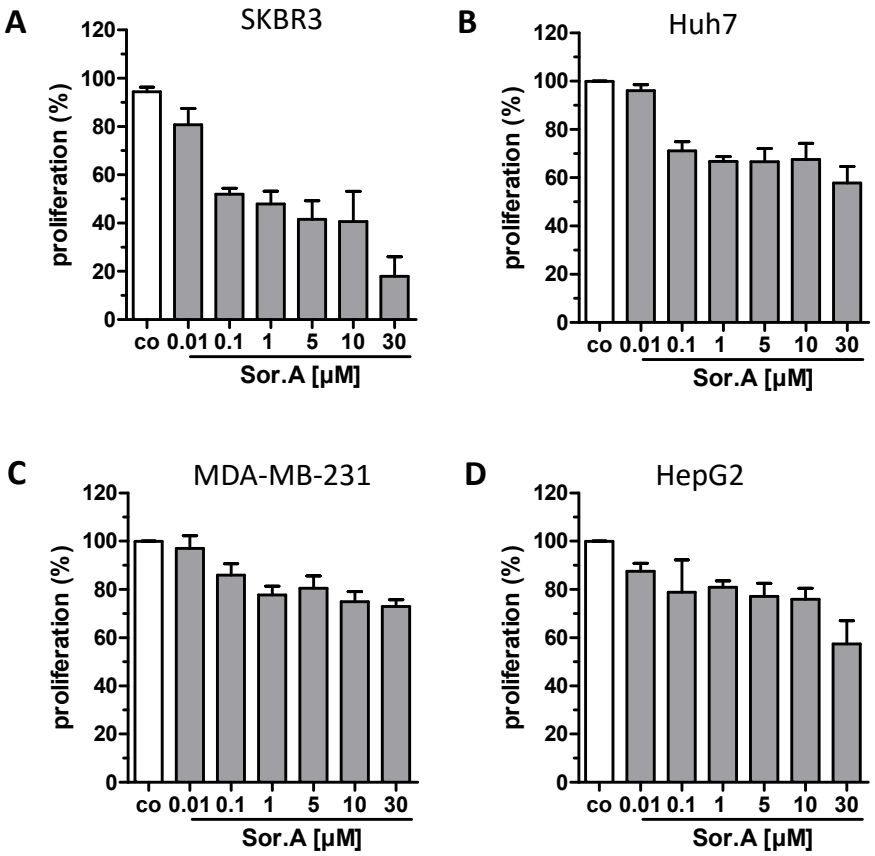

Fig. 27 Soraphen A inhibits proliferation of SKBR3, Huh7, MDA-MB-231 and HepG2 cells. (A) SKBR3, (B) Huh7, (C) MDA-MB-231, (D) HepG2 cells were treated with increasing concentrations of Soraphen A (Sor.A) for 96 h and the proliferation was assessed by CellTiter-Blue® cell viability assay. Error bars represent the SEM of three independent experiments performed in triplicate.

The anti-proliferative effects of SKBR3 cells were not due to apoptosis induction (**Fig. 28**), but rather to a G1-arrest of cells which could be revealed by cell cycle analysis (**Fig. 29**).

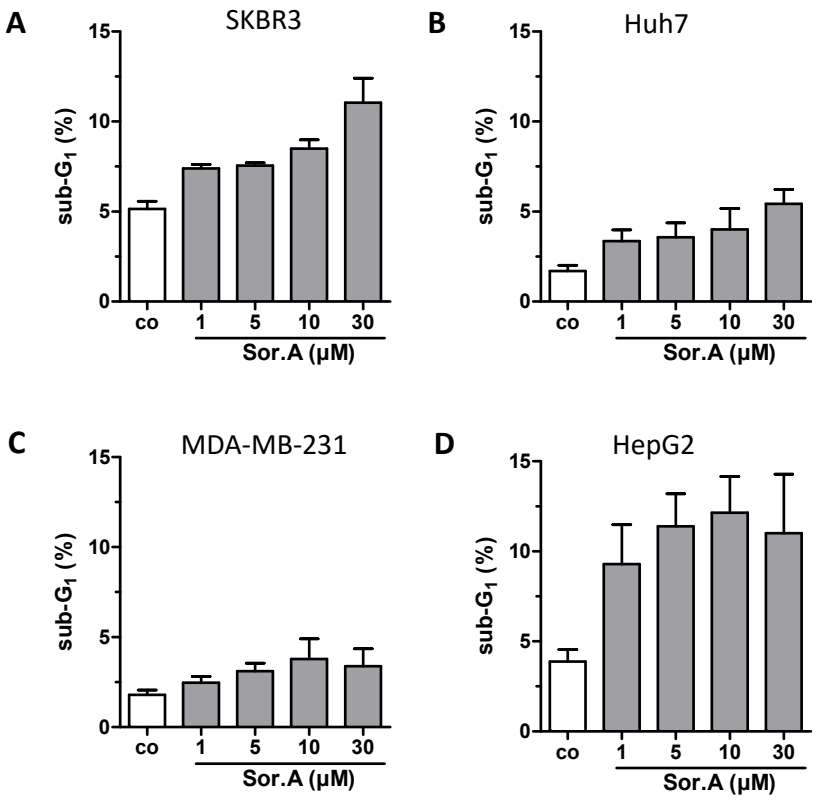

Fig. 28 Effect of Soraphen A on apoptosis. (A) SKBR3, (B) Huh7, (C) MDA-MB-231 and (D) HepG2 cells were treated with increasing concentrations of Soraphen A (Sor.A) for 96 h. Apoptosis rate was assessed by PI staining and flow cytometry. Error bars represent the SEM of three independent experiments performed in triplicate. Conducted by Eva-Maria Baur.

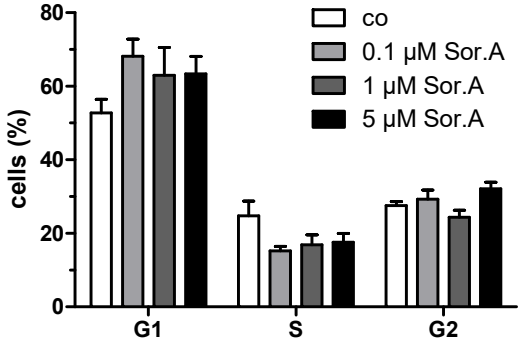

Fig. 29 Soraphen A induces a G1-arrest in SKBR3 cells. SKBR3 cells were treated with increasing concentrations of Soraphen A (Sor.A) for 72 h. Cell cycle was assessed by PI staining and flow cytometry. Error bars represent the SEM of three independent experiments performed in triplicate. Conducted by Eva-Maria Baur.

Proliferation of spheroids, which are utilized to mimic the three dimensionality of tumors cultured on poly-HEMA coated plates, was also reduced after Soraphen A treatment (**Fig. 30**).

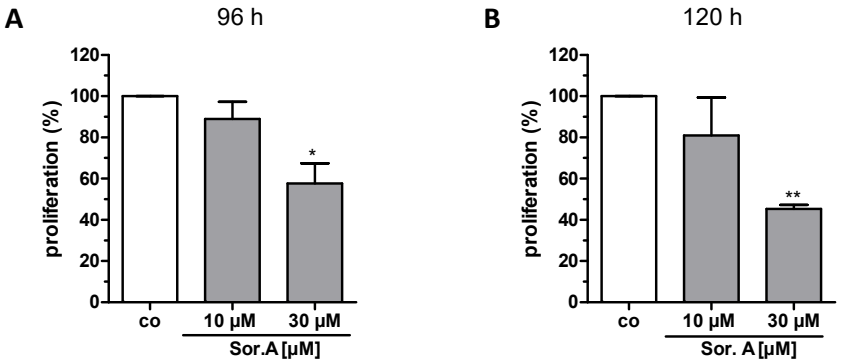

Fig. 30 Inhibition of spheroid proliferation after Soraphen A treatment. Huh7 spheroids were seeded onto poly-HEMA coated plates and treated with Soraphen A (Sor.A) for (A) 96 h or (B) 120 h, respectively. Proliferation rate was determined by CellTiter-Blue® cell viability assay. Error bars represent the SEM of two independent experiments performed in triplicate. * $p < 0.05$, ** $p < 0.01$ (Student`s t-test).

Next we addressed, whether a deprivation of exogenous nutrients is able to potentiate Soraphen A action as cells could obtain lipids from exogenous sources upon ACC inhibition to maintain their lipid homeostasis. Furthermore, we analysed the effects of growth medium supplementation with the phospholipids PC (16:0/16:0), PC (16:1/16:1), PC (16:0/20:4) and PC (16:0/18:1) in combination with Soraphen A. As expected, we first could see that FCS deprivation enhances Soraphen A-mediated inhibition of proliferation. Secondly, in the combination treatment of cells, all phospholipid species could slightly rescue the inhibitory effect of Soraphen A on proliferation, but the rescue effects were only significant for PC (16:1/16:1) in both cultivation settings (10 % FCS and 1 % FCS) and for PC (16:0/20:4) in the 1 % FCS experimental setup (**Fig. 31**).

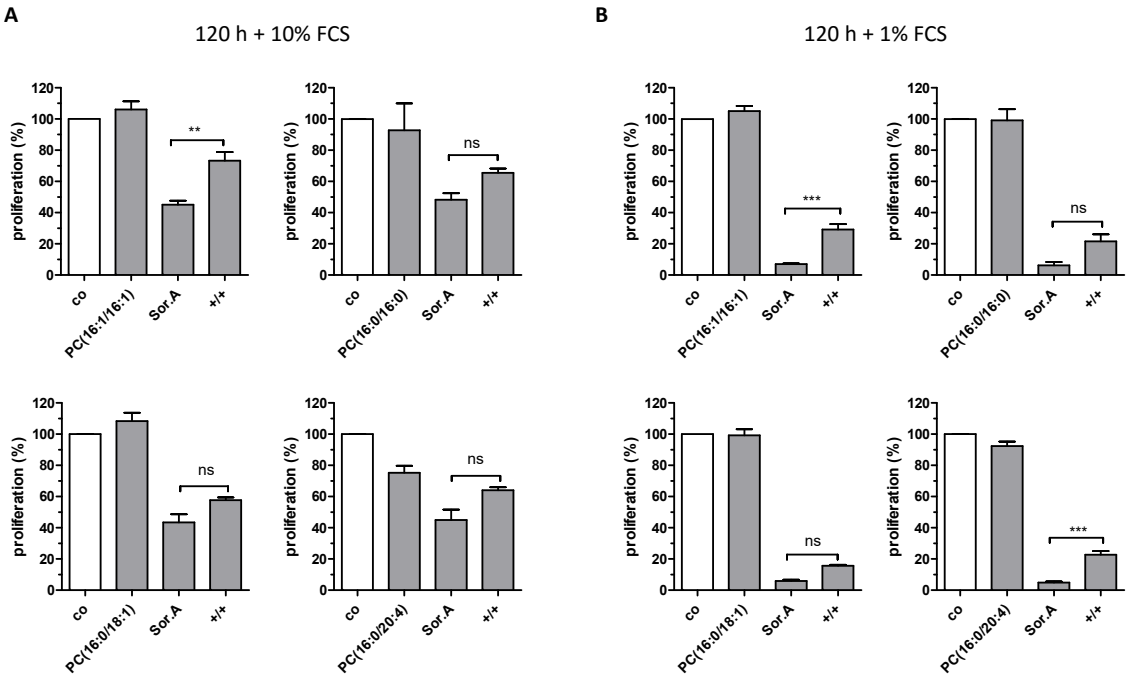

Fig. 31 Rescue of Soraphen A effect by phospholipid supplementation in MDA-MB-231 cells under normal and starvation cultivation conditions. MDA-MD-231 cells were cultivated in (A) medium containing 10 % FCS or (B) starvation medium with 1 % FCS. Cells were treated with 0.1 µM Soraphen A (Sor.A), 100 µM of the respective phospholipid or the combination (+/+), respectively for 120 h. Cell proliferation was determined by crystal violet proliferation assay. Error bars represent the SEM of three independent experiments performed in triplicate. ** $p < 0.01$, *** $p < 0.001$, ns = non-significant (Student`s t-test).

3.2.2 Soraphen A-mediated inhibition of tumor growth *in vivo*

The effect of Soraphen A *in vivo* was analysed in a Huh7 xenograft tumor model. Thereby mice were treated with 40 mg/kg Soraphen A daily. Tumor growth was significantly inhibited by Soraphen A over time as demonstrated in **Fig. 32 A** and **B**. Moreover, mice showed a good tolerability of Soraphen A as assessed by weight measurements **Fig. 32 C**.

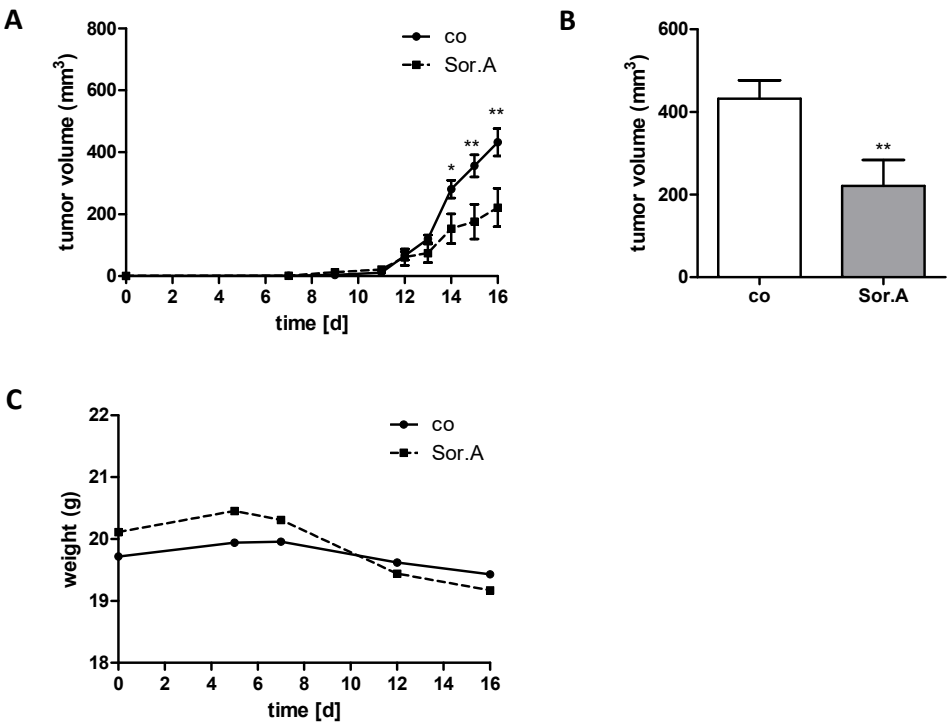

Fig. 32 Inhibitory effect of Soraphen A in a Huh7 xenograft model *in vivo*. SCID mice were treated daily with 40 mg/kg Soraphen A (Sor.A). (A) Tumor growth was measured by assessing tumor volume over time. (B) Endpoint measurement of the tumor volume at day 16. (C) Mouse weight was depicted over time. Error bars are presented as the SEM. * $p < 0.05$, ** $p < 0.01$ (Student`s t-test). *In vivo* experiments were performed by Melanie Ulrich and Kerstin Loske (Group of Prof. Dr. Angelika M. Vollmar, University of Munich, Pharmaceutical Biology).

3.2.3 Regulation of phospholipid composition by Soraphen A

To unravel the underlying mechanism behind the Soraphen A-induced inhibition of cell proliferation, the following experiments addressed whether the lipid homeostasis is affected after Soraphen A treatment. We focused on phospholipids, which are major components of cell membranes and performed an ESI tandem mass spectrometry analysis of various phospholipid species. The measurements were conducted by Dr. Andreas Koeberle (Group of Prof. Dr. Oliver Werz, University of Jena, Chair of Pharmaceutical and Medical Chemistry, Institute of Pharmacy). Soraphen A reduced the amount of phosphatidylcholines (PC), phosphatidylinositols (PI) and phosphatidylethanolamines (PE), whereas the phosphatidylserines (PS) remained nearly unaffected (**Fig. 33 A**). **Fig. 33 B** illustrates the profound change of the lipid composition after Soraphen A treatment, suggesting a disturbed phospholipid equilibrium. To further understand how the lipid homeostasis was changed, data shown in **Fig. 33** were plotted in regard to the fatty acid desaturation index and the fatty acid

chain length, revealing that the number of double bonds in all phospholipid species was significantly enhanced in treated cells, simultaneously the fatty acid chain length increased in PC, PE and PI species (**Fig. 34**).

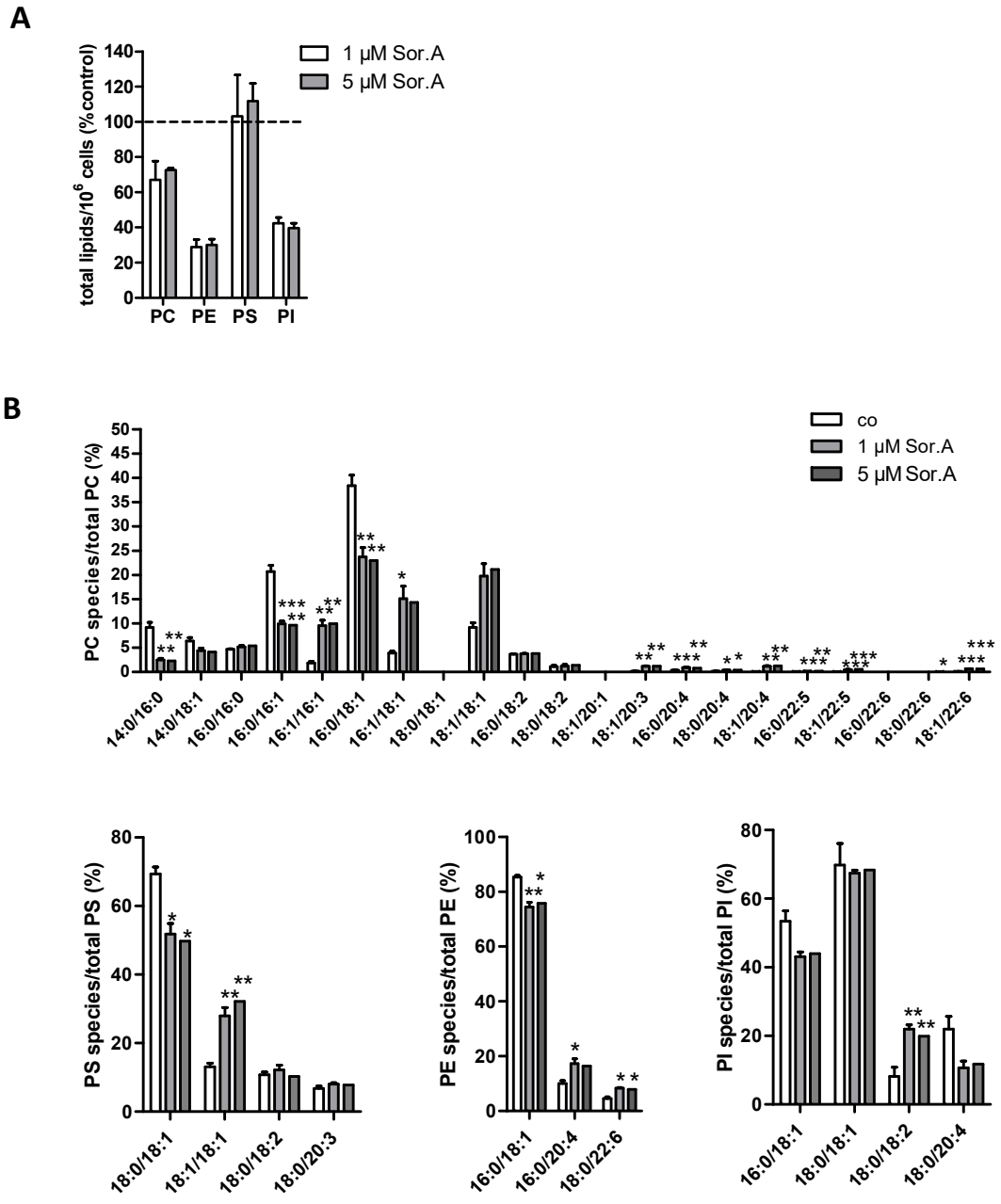

Fig. 33 Soraphen A changes the phospholipid composition of SKBR3 cells. Cells were treated with Soraphen A (Sor.A) or vehicle for 72 h, lipids were extracted and analysed by liquid chromatography ESI tandem mass spectrometry. (A) Total signal intensities of phospholipid species in Sor.A treated cells normalized to control. A value of 100 % was assigned to the signal intensities of control cells. (B) Distribution of phospholipid species in control and in Sor.A treated cells, given as the percentage of the sum of all species in the respective subclass. Data analysis was performed by repeated measures ANOVA + Turkey's post-hoc test (* $p < 0.05$, ** $p < 0.01$, *** $p < 0.001$). Experiments were performed by Dr. Andreas Koeberle (Group of Prof. Dr. Oliver Werz, University of Jena, Chair of Pharmaceutical and Medical Chemistry, Institute of Pharmacy).

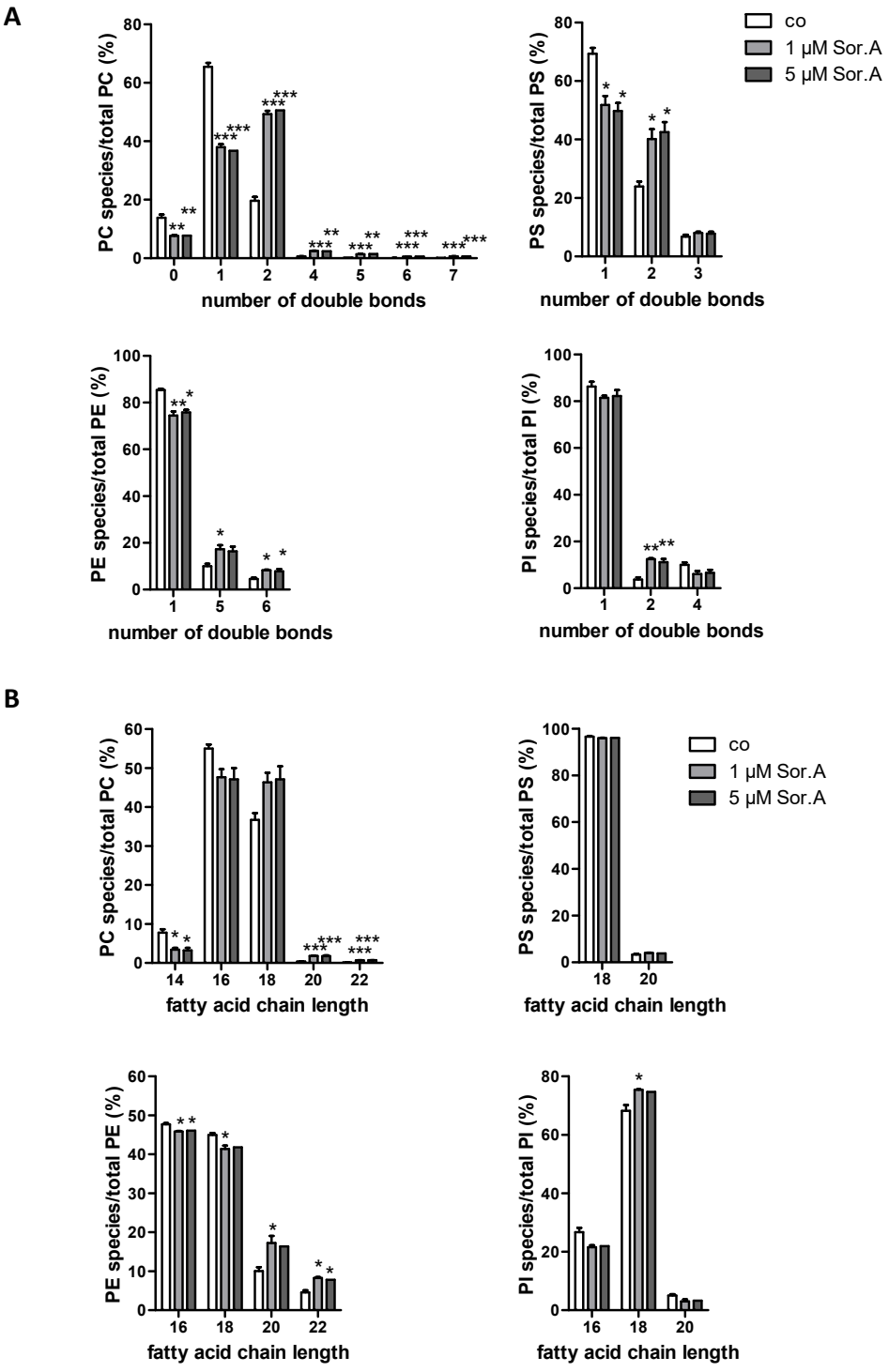

Fig. 34 Soraphen A enhances fatty acid desaturation index and fatty acid chain length in SKBR3 cells. Cells were treated with Soraphen A (Sor.A) or vehicle for 72 h, lipids were extracted and analysed by liquid chromatography ESI tandem mass spectrometry. (A) Distribution of the phospholipid species depending on their desaturation. The signal intensities are depicted relative to the summarized signal intensities of all subclass intensities. (B) Distribution of the phospholipid species depending on their fatty acid chain length given as the percentage of the sum of all species in the respective subclass. Data analysis was performed by repeated measures ANOVA + Turkey's post-hoc test (* $p < 0.05$, ** $p < 0.01$, *** $p < 0.001$). Experiments were performed by Dr. Andreas Koeberle (Group of Prof. Dr. Oliver Werz, University of Jena, Chair of Pharmaceutical and Medical Chemistry, Institute of Pharmacy).

3.2.4 Soraphen A-induced changes in cell and membrane stiffness

So far our data revealed a strong interference of Soraphen A with the phospholipid homeostasis and membrane composition. To evaluate the functional consequences of Soraphen A treatment on membrane characteristics, we next assessed cell deformability by real-time deformability cytometry (RT-DC) in collaboration with Dr. Maria Winzi (Group of Prof. Dr. Jochen Guck, Biotec, TU Dresden), as cell deformability is known to be defined to a high extend by membrane characteristics. In the experimental setup three different flow rates (0.16 µl/s, 0.24 µl/s and 0.32 µl/s) were applied. To exclude that cellular shape is altered by stimulation *per se*, cells were imaged in the reservoir before entering the channel, where stretching was accomplished. 48 h after Soraphen A treatment a clear stiffening of cells in comparison to control could be determined. This effect was significant for the flow rate of 0.24 µl/s (**Fig. 35 A**). Interestingly, 72 h after Soraphen A stimulation cell reversed their deformability state and were found to be softer in comparison to the untreated cells. For the flow rates of 0.16 µl/s and 0.24 µl/s these alterations were significant (**Fig. 35 B**).

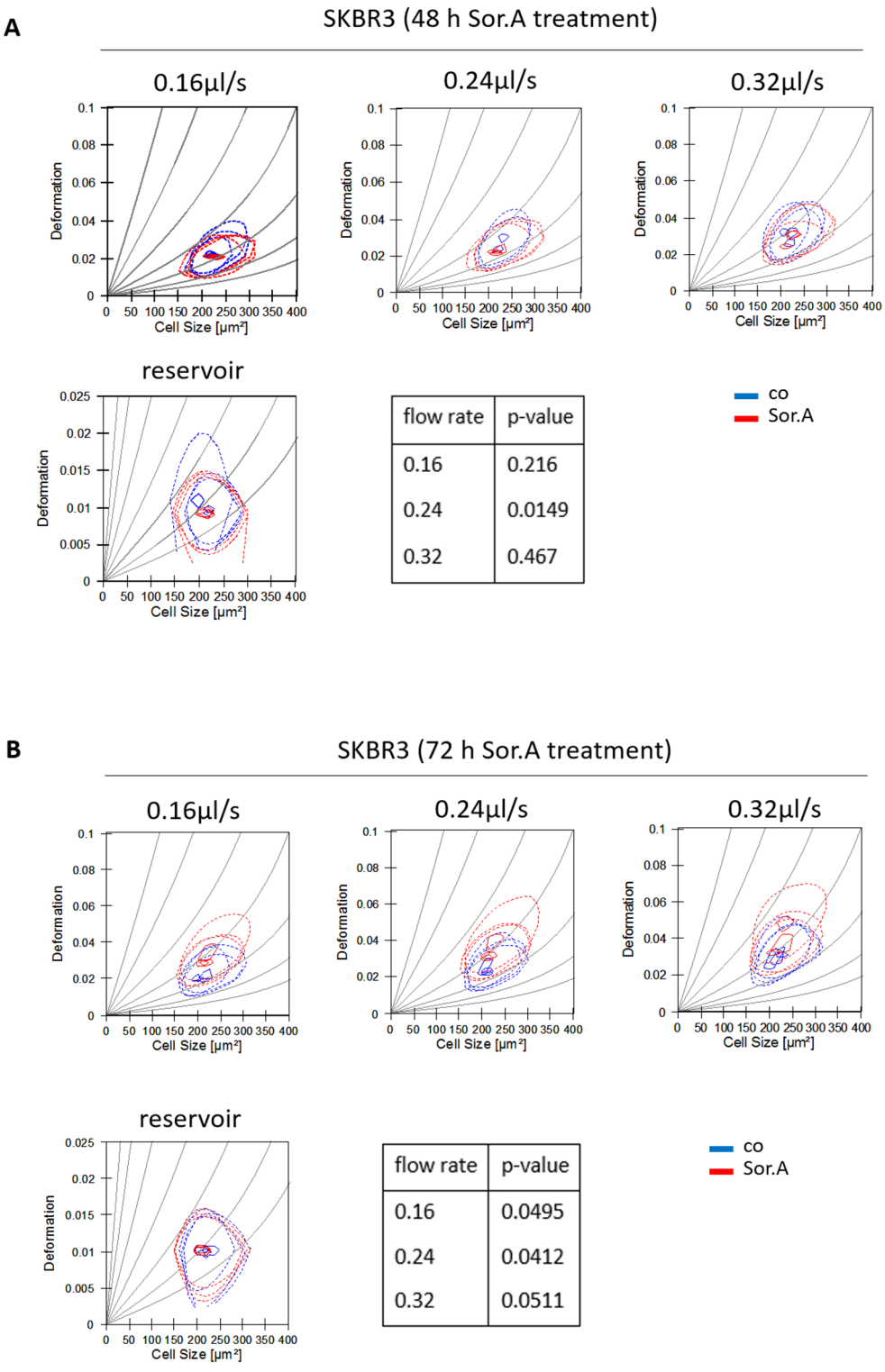

Fig. 35 Effects of Soraphen A on cell deformability. SKBR3 cells were stimulated with Soraphen A (Sor.A) for (A) 48 h and (B) 72 h. 24 h before harvesting, cells were starved. Next, cells were trypsinized, dissolved in PBS containing methylcellulose and assessed in the RT-DC setup at three different flow rates (0.16 µl/s, 0.24 µl/s and 0.32 µl/s). Before entering the channel, cell deformation was measured in the reservoir. Cell size was plotted against the deformation rate. Data show the results of three independent experiments. Data analysis was performed using the bootstrapping algorithm. Experiments were conducted by Dr. Maria Winzi (Group of Prof. Dr. Jochen Guck, Biotec, TU Dresden).

To further study the effects of Soraphen A on membrane characteristics, lateral membrane fluidity, which plays an important role for lipid raft formation, receptor movement and membrane-associated signaling processes was assessed. Therefore, SKBR3 cells were transfected with the vector pMyrPalm-mEGFP and thereby engineered to express an EGFP labeled membrane marker. The EGFP fluorescence was bleached and the fluorescence recovery time was measured. Soraphen A treated cells were characterised by a decreased fluorescence recovery rate, demonstrating that membrane fluidity was disturbed (**Fig. 36 A-C**). ACC1 silencing by siRNA also resulted in a reduced membrane fluidity, which is depicted in **Fig. 36 D** and **E**.

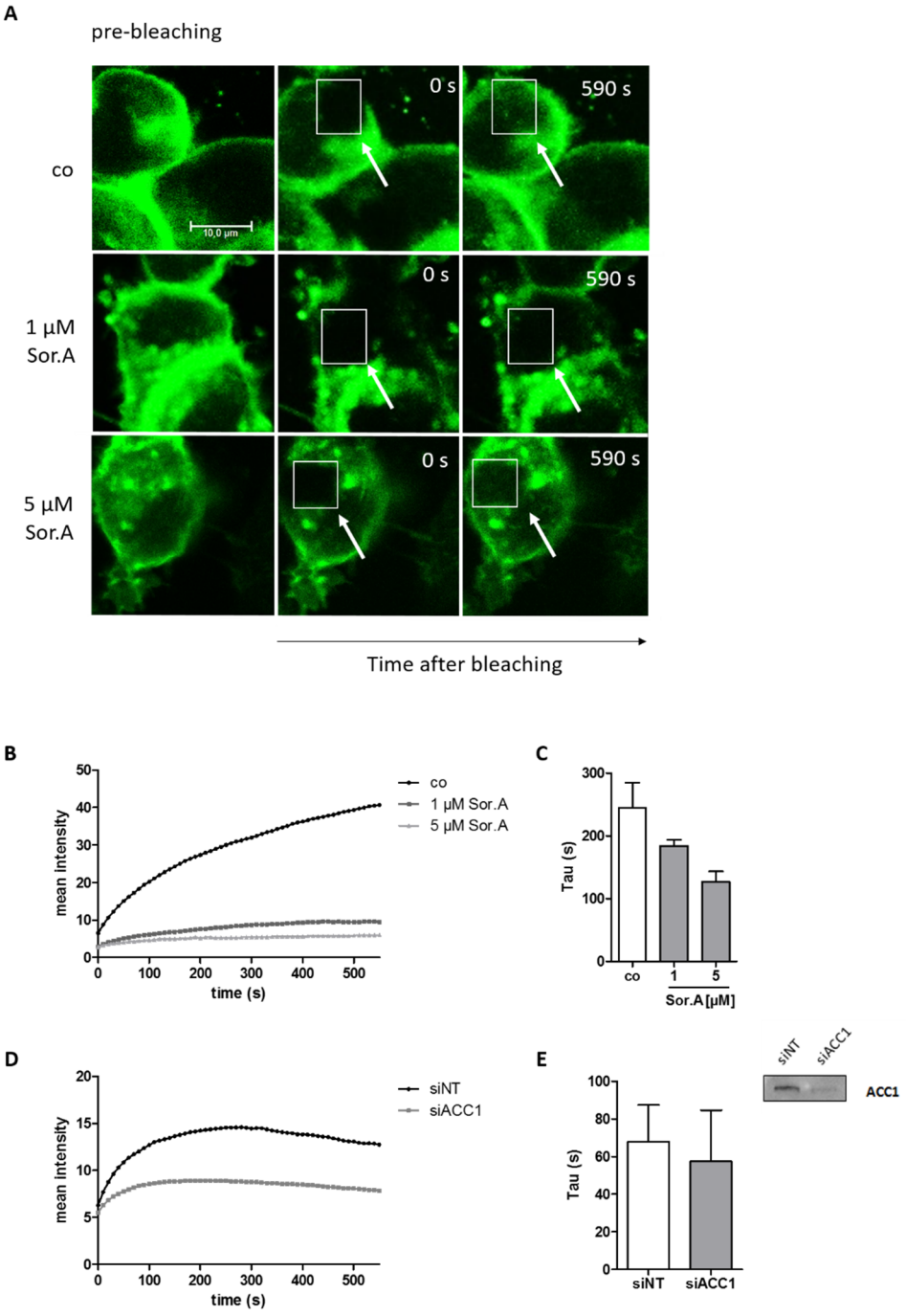

Fig. 36 Lateral membrane fluidity is reduced after Soraphen A treatment. SKBR3 cells were transfected with the plasmid pMyrPalm-mEGFP encoding the EGFP labeled membrane marker and stimulated with Soraphen A (Sor.A) for 72 h. 48 h post stimulation cell were maintained in starvation medium containing the respective concentration of Sor.A or vehicle. For ACC1 silencing experiments, cells were transfected with pMyr-Palm-EGFP and siACC1 or siNT, respectively, and analysed 96 h post transfection. (A) Lateral membrane fluidity was assessed by FRAP assay. White arrows indicate the photobleached area. (B, D) Mean fluorescence recoveries after photobleaching were plotted over time. (C, E) The time constant Tau was calculated by the non-linear equation "one-phase association" in GraphPad PRISM. ACC1 silencing by siRNA was proven by Western blot analysis. (A), (B), (D) show one representative experiment out of three. Error bars represent the SEM of three independent experiments.

3.2.5 Effects of Soraphen A on receptor dimerization

As membrane fluidity and membrane characteristics are strongly interweaved with membrane receptor signaling, we analysed the activation and dimerization of the transmembrane proteins HER2 and EGFR and the membrane-associated protein Src. Receptor dimerization, which is required for receptor activation was stimulated by the ligand EGF. As demonstrated in **Fig. 37 A**, Soraphen A inhibited the phosphorylation of HER2, EGFR and Src receptors. In accordance with that, we could show, that Soraphen A interferes with receptor dimerization. Duolink® Proximity Ligation Assay, which enables HER2-EGFR dimer visualization *in situ*, revealed that HER2-EGFR receptor dimerization could be successfully induced by EGF treatment and was significantly inhibited in Soraphen A stimulated cells (**Fig. 37 B**). Quantification of the data showed a reduced number of HER2-EGFR clusters, whereas the cluster size did not differ in treated and untreated cells. Next, Src-HER2 dimerization was analysed by Co-IP and interestingly showed an enhanced dimer formation after Soraphen A treatment (**Fig. 37 C**), revealing that Soraphen A differently regulates the dimerization capability of receptors.

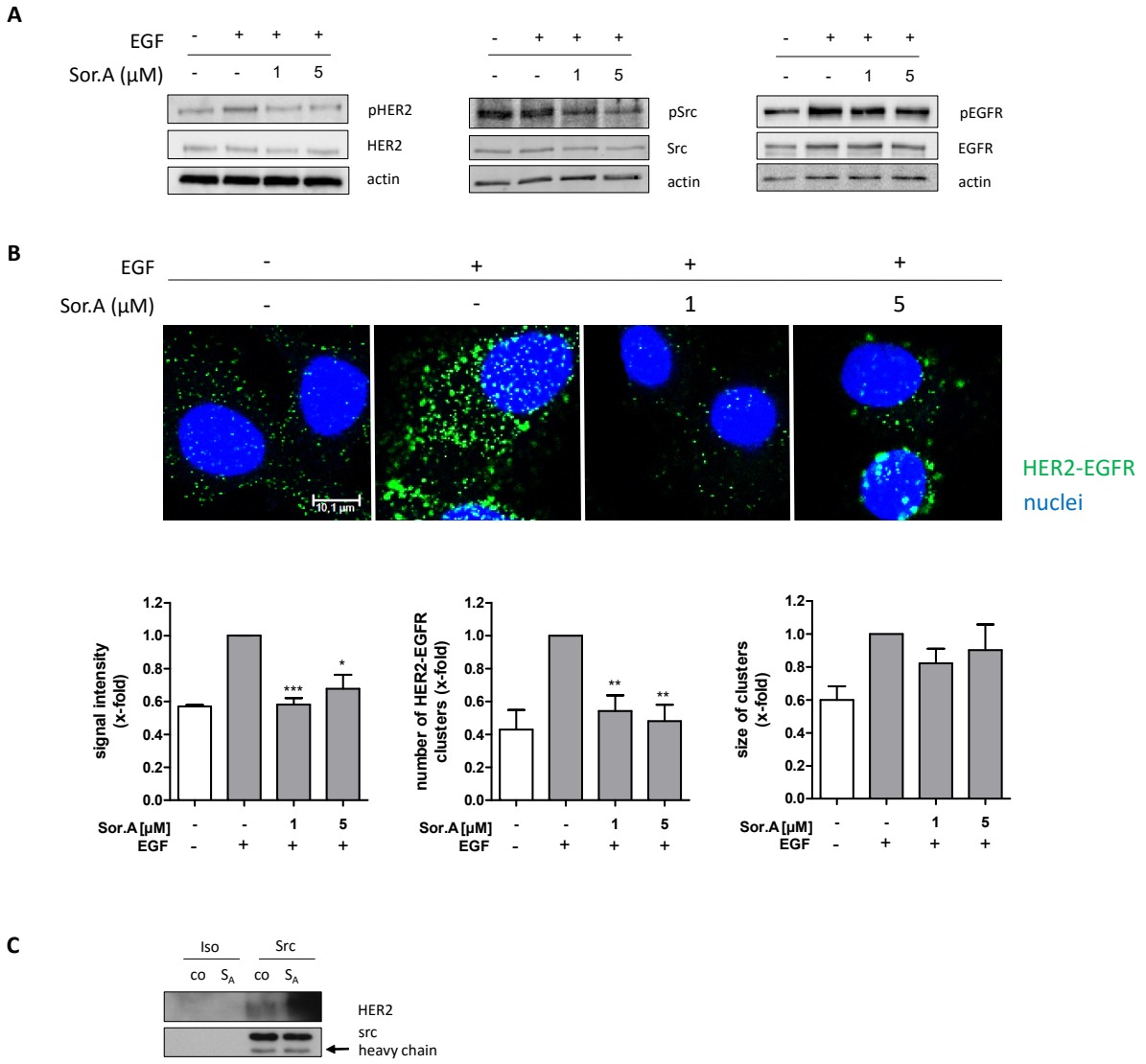

Fig. 37 Effect of Soraphen A on the activation and dimerization of membrane receptors. SKBR3 cells were treated for 72 h with Soraphen A (Sor.A) and cultured in starvation medium 24 h prior to harvesting or fixation. (A) Western blot analysis of the phosphorylation status of HER2, Src and EGFR. 15 min before harvesting cells were treated with 100 ng/ml EGF. (B) HER2-EGF dimerization rate was determined by Duolink® Proximity Ligation Assay. Signal intensities, the number of EGFR-HER2 clusters and cluster size were analysed by Image J. (C) Co-IP analysis of HER2-Src dimerization after Soraphen A (S_A) treatment was performed using Pierce™ Crosslink Magnetic IP/Co-PI Kit. (A) and (C) show one representative experiment. Error bars are presented as the SEM of three independent experiments. * $p < 0.05$, ** $p < 0.01$, *** $p < 0.001$ (Student`s t-test).

3.2.6 Deregulation of receptor recycling after Soraphen A treatment

Beyond receptor signaling, receptor recycling is another cellular process that is strongly regulated by membrane characteristics. Two well characterised receptors, which are commonly used for receptor recycling studies, are the Transferrin receptor and the EGFR. Here, the effect of Soraphen A on receptor recycling was assessed by using a Transferrin-rhodamine or an EGF-rhodamine conjugate, respectively. The labeled ligands were added to the culture medium 20 min before cell fixation and allowed to internalize. Soraphen A treatment induced a crowding of the ligands near the perinuclear compartment (**Fig. 38 A**). This accumulative effect was visible 48 h after Soraphen A treatment, whereas shorter stimulation times did not induce a changed ligand localization (**Fig. 38 B**). Receptor recycling is regulated by endosome and lysosome formation, thus confocal imaging of the endosomal marker EEA1 and the lysosomal marker LAMP1 was performed. Soraphen A treated cells again exhibited an accumulation of both the endosomal and lysosomal marker proteins in the perinuclear compartment, as is demonstrated in **Fig. 38 C** (left panel). Interestingly, apart from the changed localization of the EEA1 and LAMP1 proteins, a reduced protein expression could be revealed by Western blot analysis (**Fig. 38 C**, right panel).

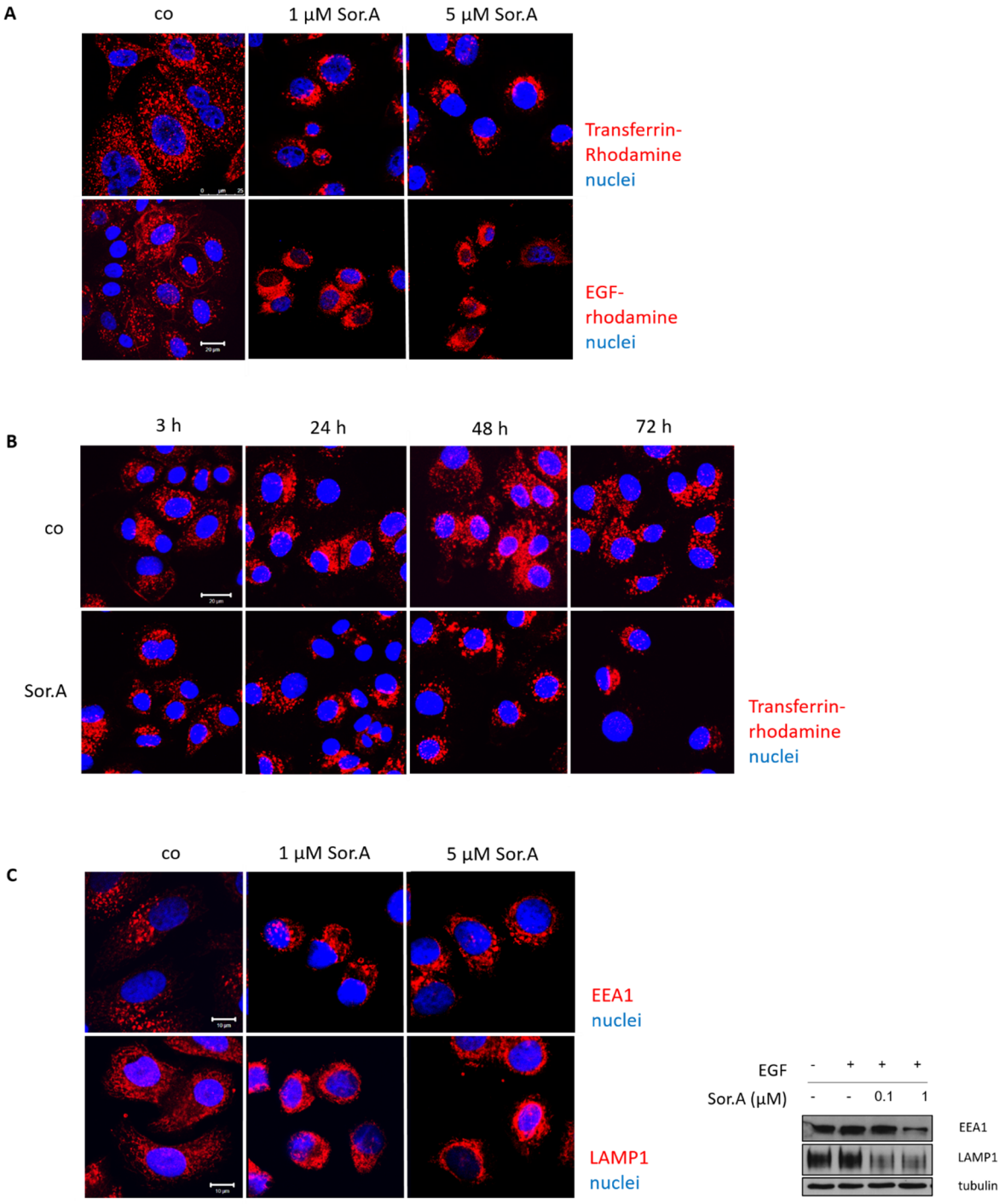

Fig. 38 Soraphen A inhibits receptor recycling. SKBR3 cells were treated with increasing Soraphen A (Sor.A) concentrations as indicated for 72 h. 24 h before imaging or lysate preparation cells were cultured in Sor.A stimulated starvation medium. (A) Transferrin receptor recycling and EGFR recycling in SKBR3 cells. The receptor ligands, Transferrin-rhodamine or EGF-rhodamine were added to cells 20 min prior to cell fixation. (B) Time course experiments of Transferrin recycling 3 h, 24 h, 48 h or 72 h after treatment with 5 µM Sor.A. Transferrin-rhodamine was added to cells 20 min prior to cell fixation. (C) EEA1 and LAMP1 confocal staining (left panel). Western blot analysis of EEA1 and LAMP1 protein expression (right panel). One of three independently performed experiments is shown.

3.2.7 Soraphen A treatment in combination with Trastuzumab

SKBR3 cells, which in this study were used as a model system for the anti-proliferative effects of Soraphen A and showed to be highly sensitive towards treatment are characterised by HER2 overexpression. A common therapy for HER2-overexpressing tumors is Trastuzumab, so we aimed at testing a combination therapy with Trastuzumab. As demonstrated in **Fig. 39 A**, a combination treatment of SKBR3 cells resulted in a synergistic inhibition of proliferation. For the combination therapy 0.1 µM Soraphen A and 10 µg/ml Trastuzumab were applied, a concentration at which no apoptosis was induced (**Fig. 39 B**). A synergistic inhibition of proliferation could also be achieved in ACC1 silenced cells, whereas no synergy was observed in ACC2 silenced cells, demonstrating an ACC1-mediated effect (**Fig. 39 C, D**). To understand the mechanism behind the synergistic effects of the combination treatment, we focused on the HER2 receptor and performed a HER2 staining. **Fig. 39 E** demonstrates that Trastuzumab induced the well described internalization of HER2, whereas Soraphen A treatment led to a slightly enhanced exposure of HER2 on the cell surface. Confocal images of the HER2 receptor were evaluated by categorizing cells according to their HER2 localization: in cells that expressed HER2 on the surface and in cells with internalized HER2.

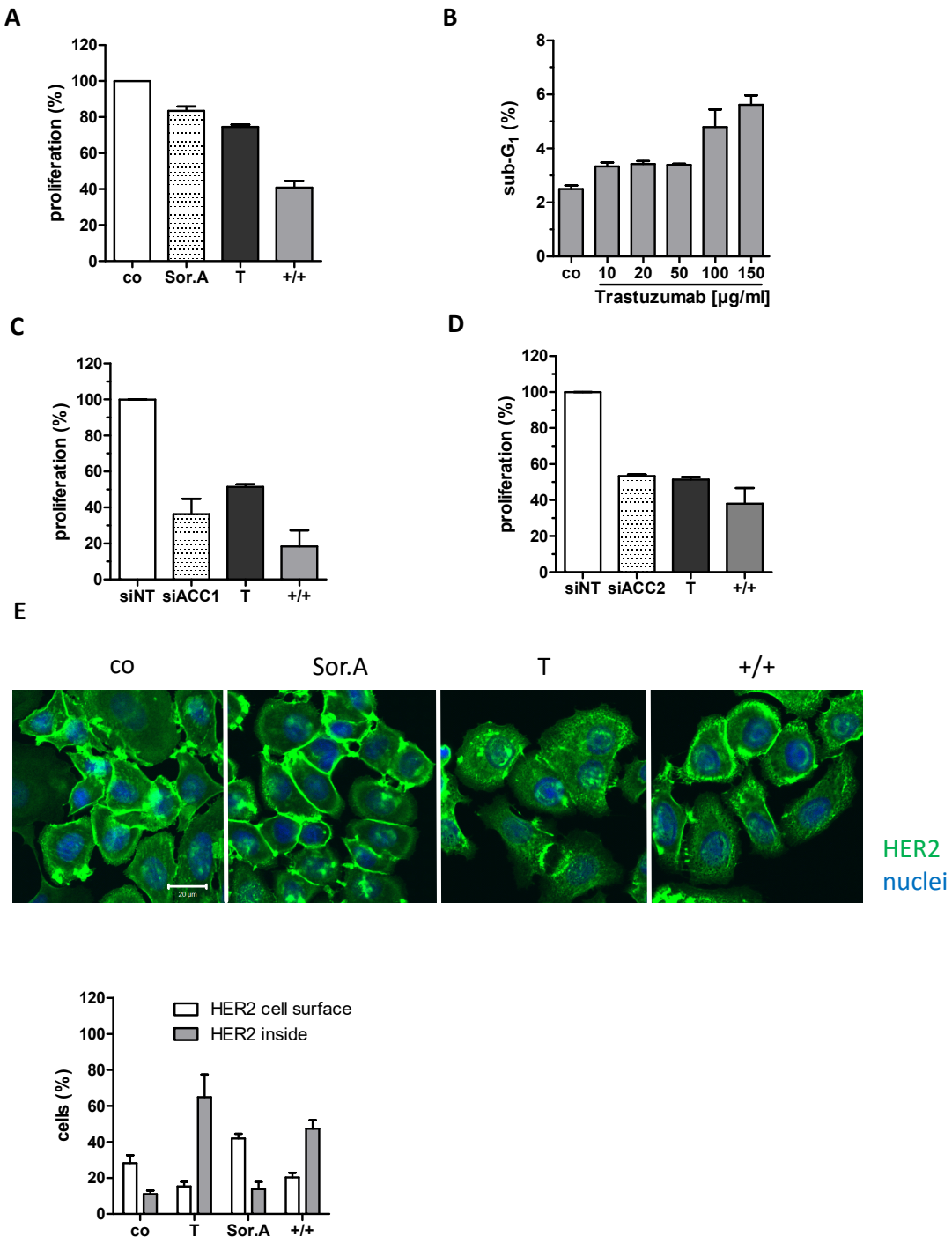

Fig. 39 Soraphen A inhibits cell proliferation synergistically with Trastuzumab. (A) SKBR3 cells were treated with 0.1 µM Soraphen A (Sor.A), 10 µg/ml Trastuzumab (T) or the combination (+/+), respectively. Proliferation rate was determined by CellTiter-Blue® cell viability assay. Synergism was calculated with the Bliss formula (v = 2.28) (B) SKBR3 cells were treated with increasing Trastuzumab concentrations for 72 h and apoptosis rate was measured. Proliferation rate of (C) ACC1 or (D) ACC2 silenced cells in combination with Trastuzumab was assessed by CellTiter-Blue® cell viability assay. (E) HER2 confocal imaging of Sor.A (0.1 µM), Trastuzumab (10 µg/ml) or the combination (+/+) treated cells, respectively. Quantification of confocal HER2 images is shown in the lower panel. Cells were classified in cells exhibiting HER2 on the cell surface or in cells with internalized HER2. Error bars represent the SEM of three independent experiments.

4 Discussion

Since the finding that tumors overexpress lipogenic enzymes, the acetyl-CoA carboxylase (ACC) is in the focus of extensive cancer research (Milgraum & Pasternack 1997). Here we introduced the myxobacterial ACC inhibitor Soraphen A, which is a valuable tool to analyse the role of lipogenesis in cancer progression as a potent anti-migratory and anti-proliferative compound and aimed at unraveling the underlying mechanism behind its action.

4.1 Soraphen A – an anti-migratory and anti-proliferative compound

This study revealed growth inhibitory effects of Soraphen A in SKBR3, MDA-MB-231, Huh7 and HepG2 cells. The anti-proliferative potential of Soraphen A was described before in several other cell lines, among them were LNCaP, PC-3M, HepG2 and LiSa-2 cells (Beckers et al. 2007, Jump et al. 2011, Rysman et al. 2010, Olsen et al. 2010). Concomitantly, RNAi-based studies on ACC inhibition also revealed a reduced proliferation rate and apoptosis induction in LNCaP cells (Brusselmans et al. 2005). Chajès and collegues could confirm the cytotoxic effects of ACC silencing in MDA-MB-231 cells (Chajès et al. 2006). In our study we could not verify apoptosis induction, suggesting that cells exhibit different metabolic requirements and thereby Soraphen A has cell specific effects. Interestingly, we found that cells displayed divergent response rates to Soraphen A treatment with SKBR3 cells being the most sensitive ones. Again, this could be explained by various metabolic states of cells and a different dependence on lipogenic pathways. This notion is supported by data presented by Daniëls and colleagues, who analysed the effects of cell cultivation in a low lipogenic environment on the proliferation rate of the lipogenic cell lines PC3M, HOP62, HepG2 and the non-lipogenic cell line T24 and found differing response rates towards FCS deprivation. In all tested cell lines an enhanced *de novo* lipid synthesis could be induced under starvation conditions (Daniëls et al. 2014). However, the categorization in lipogenic and non-lipogenic cells which is performed under standard culture condition does not always allow to predict the effects of lipid deprivation, proposing a differing capability of cells to outbalance the reduced supply with fatty acids. We could also demonstrate that MDA-MB-231 cells were more responsive to Soraphen A under

starvation conditions, in comparison to the cultivation with excess FCS, implicating that cells are more dependent on extracellular nutrition sources after Soraphen A treatment. This could be exploited in cancer therapy as cells in tumors have often to face reduced supply with nutrients and evade this unfavorable conditions by angiogenesis and extravasation (Hanahan & Weinberg 2000, Daniëls et al. 2014). Even though the anti-proliferative effects of Soraphen A are described in some model systems in literature, little is known about the cellular implications of the underlying mechanism, which awaited further investigations and was the aim of this study.

In contrast to anti-proliferative effects of Soraphen A, to our knowledge we were the first ones to describe Soraphen A as an anti-migratory compound. So far only TOFA, another inhibitor of the ACC was found to inhibit invasion *in vitro* (Scott et al. 2012). Beyond the ACC, the fatty acid synthase (FAS), which is also an important enzyme in the fatty acid metabolism was found to be correlated with the migratory potential of cells, demonstrating the eminent role of *de novo* lipogenesis in migration (Selvendiran et al. 2010, Liu et al. 2013).

Interestingly, in our study inhibition of migration occurred at early time points after stimulation and could be verified in a spheroid invasion assay and *in vivo* by the 4T1-Luc dissemination experiment. The inhibition of proliferation required longer stimulation times of 96 h in comparison to the early effects on migration in our experimental setup. Suppressive effects of Soraphen A on cell proliferation could also be verified *in vivo* by a Huh7 xenograft model. Obviously the early changes in the lipid composition and membrane stiffness after Soraphen A treatment are sufficient to inhibit cell migration as these processes are highly dependent on membrane characteristics. To achieve a suppression of proliferation longer stimulation times are necessary as cell are presumably able to compensate the inhibition of fatty acid synthesis by e.g. the uptake of exogenous fatty acids at the beginning. This notion is supported by our data, demonstrating that cultivation of cells in starvation medium renders them more susceptible to Soraphen A treatment.

4.2 Lipid homeostasis as a target of Soraphen A

As Soraphen A interferes with fatty acid synthesis we focused on the phospholipid composition of cells, which we studied after short and long stimulation times with respect to the anti-migratory and the anti-proliferative effects of Soraphen A. After long stimulation times with Soraphen A, we could demonstrate that the amount of phosphatidylcholines (PC), phosphatidylinositols (PI) and phosphatidylethanolamines (PE) is reduced, whereas phosphatidylserines (PS) were not affected. Short stimulation times did not alter the total amount of phospholipids. Interestingly, the phospholipid composition was profoundly changed both after 6 h and after 72 h of Soraphen A treatment. We could find a shift towards longer fatty acids and reveal a higher degree of desaturation in both setups. This is in concordance with the study presented by Rysman and colleagues, who demonstrated an enhanced desaturation index 72 h after Soraphen A treatment in LNCaP cells (Rysman et al. 2010). The increased desaturation could be beneficial in clinical context, as Rysman proposed that an elevated level of saturated lipids, which can be found in malignant cells protects cancer cells from chemotherapeutics and free radicals (Rysman et al. 2010). Reversing that phenotype by Soraphen A could thereby be a valuable tool to sensitize cells for chemotherapeutics in combination therapies. In contrast to our data Jump and colleagues claim a reduced elongation of fatty acids after Soraphen A treatment in LNCaP and HepG2 cells (Jump et al. 2011). We hypothesize, that Soraphen A disturbs the lipid homeostasis and cells find various ways to compensate for this interference.

4.3 Modulating cell mechanics – a novel anti-neoplastic strategy

Cell mechanics are strongly dependent on the lipid composition and regulate malignancy and metastatic competence of tumor cells (Guck et al. 2005, Simons & Vaz 2004). Therefore we addressed, whether Soraphen A modulates stiffness of cells and membranes. In MDA-MB-231 and T24 cells, which were the model systems for migration and invasion experiments, we found a stiffening of giant plasma membrane vesicles (GPMVs), prepared from cellular membranes after Soraphen A treatment. It is well described that an enhanced rate of longer

fatty acid chains is accompanied by membrane stiffening (Rawicz et al. 2000). On the other hand the observed increased desaturation index would implicate a higher deformability, but in this case the elongated fatty acid chains seem to dominate and evoke the stiffening effect. Apart from GPMV measurements, whole cell stiffness was assessed by optical stretcher setup. Interestingly, Soraphen A was found to enhance cell rigidity in MDA-MB-231 cells, whereas in T24 cells no effect could be measured. Whole cell stiffness is to a high extend determined by cytoskeletal restraints (Yamaguchi & Condeelis 2007) and we found that Soraphen A does not influence actin or microtubules architecture. Most likely, in T24 cells the contribution of the cytoskeleton outrivaled the measurement, whereas we propose that in MDA-MB-231 cells the influence of the membrane stiffness on whole cell rigidity was higher than that of the cytoskeleton and therefore verifiable. So far we are only beginning to understand the implications of cell mechanics on cancer progression and development and there are still many questions to address before this knowledge can be translated into clinical practice and exploited as a therapeutic target. But an ever growing body of experimental evidence illustrates the outstanding role of cancer mechanics in tumor progression. Initial studies introduce, that deformability of cancer cells can be used as a marker to grade metastatic potential of cells (Guck et al. 2005, Remmerbach et al. 2009, Swaminathan et al. 2011). The tested cancer cells in these studies were found to be more deformable than their non-malignant counterparts. Our data for MDA-MB-231 and T24 cells reveal that Soraphen A is able to reverse the mechanical phenotype of malignant cells and thereby could function as a valuable therapeutic tool.

SKBR3 cells, which were used for studies on the anti-proliferative effects of Soraphen A were also applied for measurements of cell stiffness. Therefore, real-time deformability cytometry (RT-DC) was performed, a new method which guarantees a high throughput (Otto et al. 2015). Cell deformation was assessed 48 h and 72 h after Soraphen A treatment and interestingly showed differing results. 48 h post stimulation cell stiffening could be determined, whereas 72 h after treatment cells were found to be more deformable. Our data suggest that inhibition of ACC by Soraphen A induces dynamic remodeling of membrane composition to meet the nutritional needs and therefore gives rise to differing membrane characteristics over time. Interestingly, FRAP analysis, which was performed 72 h after Soraphen A treatment, showed that the lateral membrane fluidity was reduced, implicating that the cells lose their intact membrane homeostasis. Considering this apparently highly

dynamic processes, it is not astonishing that Rysman and colleagues measured – in contrast to our results – an enhanced lateral fluidity rate in Soraphen A treated LNCaP cells (Rysman et al. 2010), as LNCaP cells could have other compensatory effects upon ACC inhibition than SKBR3 cells. Moreover, in the study performed by Rysman and colleagues only one time point was assessed in LNCaP cells, so we cannot exclude a change in the lateral membrane fluidity rate over time.

4.4 Deregulation of membrane-associated processes by Soraphen A

Modulation of membrane composition can have severe effects on membrane organization and membrane-associated signaling and recycling processes. It is well described, that lipids are inhomogeneously distributed within membranes and exhibit a complex phase behavior, forming lipid-ordered and disordered domains. The ordered domains also termed lipid rafts are important signaling platforms for migration and proliferation (Meer et al. 2008, Hryniewicz-Jankowska et al. 2014). The organization of lipid domains and phases depends on lipid composition and even small changes can induce profound alterations in the phase behavior, resulting for example in the disruption of lipid rafts (Hryniewicz-Jankowska et al. 2014). The eminent role of lipid homeostasis was also shown in experiments in which cells were cultured in medium containing polyunsaturated fatty acids, resulting in a dissociation of acetylated proteins from lipid rafts (Webb et al. 2000). This led us to evaluate membrane-dependent processes like signaling or recycling in the context of migration and proliferation after Soraphen A treatment.

4.4.1 Membrane properties and their role for migration

To understand the anti-migratory effects of Soraphen A we analysed Rac and Vinculin, finding that this typical mediators of migration were not affected by Soraphen A. Our data rather support the theory that changed membrane characteristics, triggered by the altered lipid composition could be responsible for the observed effects. In MDA-MB-231 cells we found a reduced formation of filopodia after Soraphen A treatment. Cell protrusions like filopodia or invadopodia are important mediators of migration and their formation is related to the metastatic potential of cells (Yamaguchi & Oikawa 2010). Membrane properties and

membrane curvature are described to regulate the formation of invadopodia (Albiges-Rizo et al. 2009). Furthermore, Yamaguchi and colleagues described that lipids rafts, and therefore membrane organization is inevitable for invadopodia formation and that PI species, which are regulated by Soraphen A, are important for their functionality (Yamaguchi et al. 2009, Yamaguchi & Oikawa 2010). Another study outlining the prominent role of fatty acid homeostasis for the regulation of invadopodia was conducted by Scott and colleagues, that demonstrated a reduction of invadopodia occurrence upon ACC1 inhibition (Scott et al. 2012). In our work, Soraphen A did not affect filopodia formation in T24 cells, whereas membrane stiffness was significantly enhanced. For T24 cells the changed membrane rigidity was obviously sufficient to evoke anti-migratory effects. Of note, migration and invasion of MDA-MB-231 and T24 cells were inhibited to a similar extend by Soraphen A in both cell lines, emphasizing the outstanding role of membrane properties for the migratory process.

4.4.2 Role of membrane characteristics for proliferation

Addressing the underlying mechanism behind the anti-proliferative effects of Soraphen A, we used SKBR3 cells, which were found to be especially sensitive towards Soraphen A treatment. Thereby, we focused on membrane-related signaling and recycling processes. Indeed, an inhibition of the phosphorylation of the prominent oncogenic growth factor receptors HER2, EGFR and Src could be demonstrated. Moreover, we could show that receptor dimerization was strongly affected by Soraphen A. HER2-EGFR receptor dimerization was diminished after treatment, and interestingly the formation of HER2-Src dimers was enhanced, even though the phosphorylation of both HER2 and Src was reduced. We hypothesize that dysfunctional Src-HER2 clusters are formed due to the changed lipid composition.

Considering the inhibitory effects of Soraphen A on the signaling of membrane bound receptors, this could explain the enhanced sensitivity of the HER2-overexpressing SKBR3 cells towards Soraphen A in comparison to other tested cell lines. First mechanistic studies revealed a connection between enhanced lipogenesis and the HER2 signaling pathway, demonstrating that the SKBR3 cells exhibit higher levels of FAS and ACC in comparison to MDA-MB-231 cells which are characterised by a low HER2 level. Moreover, engineered overexpression of HER2 in MDA-MB-231 cells induced elevated levels of ACC1 and FAS (Yoon et al. 2007, Menendez 2010). Another study, supporting the prominent role of HER2 was performed by Corominas-faja and colleagues, showing that MCF7 cells that were engineered

to overexpress HER2 are significantly more sensitive towards Soraphen A than the parental MCF-7 cells (Corominas-faja et al. 2014). Another possible explanation for the different sensitivity of cells towards Soraphen A could be traced back to differing metabolic requirements of cells.

Receptor recycling is a further membrane-dependent cellular process, which is important for cell proliferation. In our study, Soraphen A treated cells exhibited a strongly impaired recycling of the Transferrin receptor and EGFR, which were used as model systems. Transferrin receptor and EGFR were found to be trapped in the perinuclear compartment after Soraphen A treatment. We hypothesize, that receptor internalization from the plasma membrane can proceed after treatment, however the backward recycling of the receptors, after entering the endocytic recycling compartment is disturbed by Soraphen A and leads to an accumulation of the receptors in the perinuclear compartment. It is well described that the organization of lipids is finely tuned during the endocytic pathway (Maxfield & Mondal 2006). Thereby the composition of early endosomes is similar to that of the plasma membrane, whereas late endosomes exhibit a decrease in sterols and PS species. Furthermore, PI species play a prominent role during maturation (Meer et al. 2008), so it is not surprising that Soraphen A-induced perturbations of the lipid homeostasis lead to deregulated recycling. Interestingly, after analyzing HER2 receptor recycling, we could find an enhanced localization of HER2 on the cell surface after Soraphen A treatment, disclosing that HER2 endocytic internalization and recycling is also disturbed.

4.5 Synergism of Soraphen A and Trastuzumab – possible mechanisms

Combination therapy turned out to be an effective strategy in oncology as the response rate can be improved, the huge problem of resistance development can often be averted and side effects can be minimized (Menghua et al. 2015). Therefore, we were interested in studying the potential of Soraphen A in combination treatment. As the HER2-overexpressing SKBR3 cells served as a model system for our study, we decided to analyse the combination treatment of Soraphen A with Trastuzumab, which is a common therapy for HER2-positive tumors. Trastuzumab is an antibody that binds to the extracellular domain of HER2 and thereby inhibits signaling by several mechanisms, among them the antibody-dependent

cellular cytotoxicity and inhibition of intracellular signal transduction (Burstein 2005). We could show that Soraphen A and Trastuzumab synergistically reduce cell proliferation.

It is very challenging to explain the synergistic effect of Soraphen A and Trastuzumab treatment, as proposedly the congregation of several effects is implicated. Most obviously the changed membrane composition and the resulting inhibition of membrane-associated receptor signaling after Soraphen A treatment is involved. In addition, the impaired cellular recycling machinery could also contribute to the synergistic effect of the combination therapy. Some studies describe that HER2 undergoes a very rapid and efficient internalization and the recycling cycle is important for its function. However, results on the internalization mechanism, whether a Clathrin-dependent or independent pathway is utilized are contradictorily (Bertelsen & Stang 2014). Possibly both ways are exploited, depending on the cell line. We could see a slight increase of HER2 on the cell surface after Soraphen A treatment, which would support the theory that Soraphen A interferes with the recycling of HER2 and shifts the equilibrium between internalized and recycled HER2. The enhanced exposure of HER2 on the cell surface offers more extracellular targets for Trastuzumab and could thereby potentiate its action. But this hypothesis needs to be further investigated as so far it is not clear if HER2 is dependent on recycling. Other studies propagate the notion that HER2 does not undergo endocytosis due to lack of internalization signals or active retention. The effect of Trastuzumab on HER2 trafficking is also controversially discussed. Some studies show a Trastuzumab-mediated internalization of HER2 and others claim that Trastuzumab does not induce internalization of HER2 receptors (Bertelsen & Stang 2014). In our experimental setting we could reveal an internalization of HER2 upon Trastuzumab treatment, which was reduced by Soraphen A stimulation, supporting our theory that Soraphen A interferes with recycling processes. Interestingly, we could see that EGFR and Transferrin receptor recycling – but not the internalization – was disturbed. In contrast to that HER2 exhibited an enhanced retention on the cell surface after Soraphen A treatment, suggesting that in SKBR3 cells Transferrin, EGFR and HER2 receptors undergo different internalization pathways. Another interesting aspect which should not be left unmentioned and could be useful to understand the synergistic effects of Soraphen A and Trastuzumab is the finding that Soraphen A treatment improves the cellular uptake of chemotherapeutics like doxorubicin due to the enhanced flip-flop rate of cellular membranes (Rysman et al. 2010). Increased Trastuzumab internalization,

could lead to intracellular HER2 binding and its deactivation, thereby contributing to the synergistic effect of Soraphen A and Trastuzumab treatment.

In conclusion we could show that Soraphen A is able to potentiate the effects of Trastuzumab in the HER2-overexpressing SKBR3 cells. HER2-positive tumors are especially aggressive with an increased risk of recurrence and a poor prognosis (Press et al. 1993). The response rate to Trastuzumab, when administered as monotherapy is limited due to resistance formation (Higgins & Baselga 2011), whereas combination therapies proved to have much higher success rates (Nahta et al. 2006). Therefore, we suggest Soraphen A to be a novel and promising therapeutic option for patients with HER2-positive tumors.

5 Summary

In the last decades *de novo* fatty acid synthesis was found to be of outstanding importance for cancer cell progression. Therefore, key enzymes of the lipid synthesis like the acetyl-CoA carboxylase gained increasing attention as therapeutic targets. This work presents Soraphen A, a myxobacterial acetyl-CoA carboxylase inhibitor, as a potent anti-metastatic and anti-proliferative compound. Most noted, these effects could be demonstrated in a Huh7 xenograft tumor growth model and a 4T1-Luc dissemination experiment *in vivo*. We focused on unraveling the underlying mechanism of Soraphen A action and found that Soraphen A profoundly changes lipid composition, alters biophysical cell properties and thereby deregulates cellular signaling and recycling processes.

In MDA-MB-231 and T24 cells, which were used to study cell migration, an enhanced cell and membrane stiffness could be measured after Soraphen A treatment, resulting in an abrogation of the migratory and invasive capacity of cells. In SKBR3 cells, which were the model system for proliferation studies a dynamic change in cell deformability was observed after Soraphen A treatment. Furthermore, processes which are dependent on membrane characteristics like receptor recycling, receptor signaling and receptor dimerization, were affected by Soraphen A, leading to an inhibition of cell proliferation (**Fig. 40**).

In summary, we could introduce Soraphen A as a potent inhibitor of migration and proliferation and unravel its mechanism of action. We found that Soraphen A evokes modifying effects on cell biomechanics and diminishes cancer progression by inhibiting the acetyl-CoA carboxylase. An ever growing body of experimental evidence suggests that cancer cells exhibit a changed deformability, therefore reversing the biomechanical phenotype of malignant cells by Soraphen A is a novel and promising therapeutic approach in the fight against cancer.

This work was supported by the Nanosystems Initiative Munich (NIM).

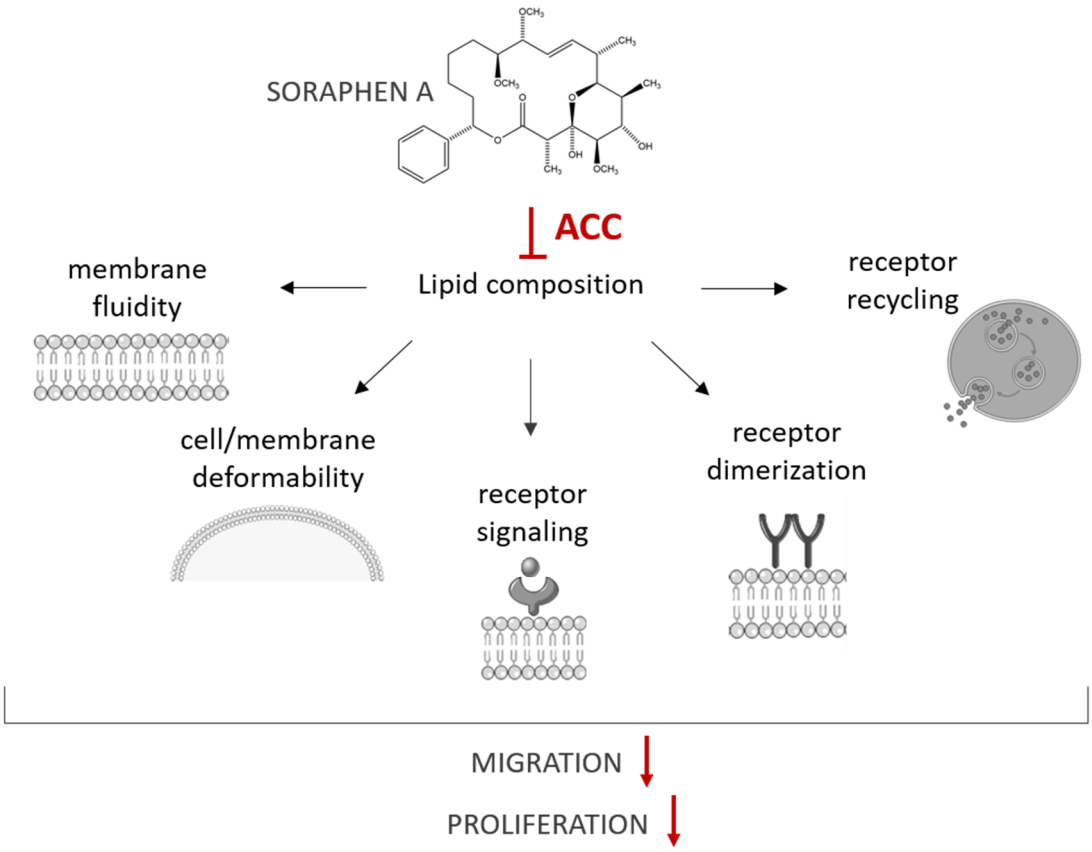

Fig. 40 Mechanism of Soraphen A action as an anti-migratory and anti-proliferative compound. Soraphen A interferes with fatty acid synthesis by acetyl-CoA carboxylase (ACC) inhibition. Fatty acid homeostasis influences membrane fluidity, membrane deformability and thereby membrane-dependent processes like receptor recycling, receptor dimerization and receptor signaling. Deregulation of membrane characteristics leads to an inhibited cell migration and proliferation.

6 References

Abramson, H.N., 2011. The lipogenesis pathway as a cancer target. *Journal of medicinal chemistry*, 54(16), pp.5615–38.

Abu-Elheiga, L. et al., 2003. Acetyl-CoA carboxylase 2 mutant mice are protected against obesity and diabetes induced by high-fat/high-carbohydrate diets. *PNAS*, 100(18), pp.10207–10212.

Albiges-Rizo, C. et al., 2009. Actin machinery and mechanosensitivity in invadopodia, podosomes and focal adhesions. *Journal of Cell Science*, 122(17), pp.3037–3049.

Azrad, M., Turgeon, C. & Demark-Wahnefried, W., 2013. Current evidence linking polyunsaturated fatty acids with cancer risk and progression. *Frontiers in oncology*, 4(3), p.224.

Ball, D.W., Hill, J.W. & Scott, R.J., 2012. Introduction to Chemistry: General, Organic and Biological., pp.957-100.

Beckers, A. et al., 2007. Chemical inhibition of acetyl-CoA carboxylase induces growth arrest and cytotoxicity selectively in cancer cells. *Cancer research*, 67(17), pp.8180–7.

Bedorf, N. et al., 1993. Antibiotics from Gliding Bacteria, LIV. Isolation and Structure Elucidation of Soraphen A1α, a Novel Antifungal Macrolide from Sorangium cellulosum. *Liebigs Annalen der Chemie*, 1993(9), pp.1017–1021.

Berg, J.M., Tymoczko, J.L. & Stryer, L., 2007. Stryer Biochemie., pp.366 - 3.

Bertelsen, V. & Stang, E., 2014. The Mysterious Ways of ErbB2/HER2 Trafficking. *Membranes*, 4(3), pp.424–46.

Bligh, E.G. & Dyer, W.J., 1959. A rapid method for total lipid extraction and purification. *Canadian Journal of Biochemistry and Physiology*, 37(8).

Bliss, C.I., 1956. The calculation of microbial assays. *Bacteriological reviews*, 20(4), pp.243–258.

Braig, S. et al., 2015. Modulation of membrane rigidity in conjunction with cell migration and invasion. *New Journal of Physics*, 17(083007).

Brusselmans, K. et al., 2005. RNA interference-mediated silencing of the acetyl-CoA-carboxylase-alpha gene induces growth inhibition and apoptosis of prostate cancer cells. *Cancer research*, 65(15), pp.6719–25.

Burstein, H.J., 2005. The distinctive nature of HER2-positive breast cancers. *The New England journal of medicine*, 353(16), pp.1652–1654.

Chajès, V. et al., 2006. Acetyl-CoA carboxylase alpha is essential to breast cancer cell survival. *Cancer research*, 66(10), pp.5287–94.

Corominas-faja, B. et al., 2014. Chemical inhibition of acetyl-CoA carboxylase suppresses self-renewal growth of cancer stem cells. *Oncotarget*, 5(18), pp.8306–16.

Daniëls, V.W. et al., 2014. Cancer Cells Differentially Activate and Thrive on De Novo Lipid Synthesis Pathways in a Low-Lipid Environment. *PloS One*, 9(9), p.e106913.

Gerth, K. et al., 2003. Myxobacteria: proficient producers of novel natural products with various biological activities—past and future biotechnological aspects with the focus on the genus Sorangium. *Journal of Biotechnology*, 106(2-3), pp.233–253.

Gerth, K. et al., 1993. The Soraphens: A Family of novel antifungal compounds from Sorangium cellulosum (Myxobacteria). *J Antibiot (Tokyo)*, 47(1), pp.23–31.

Guck, J. et al., 2005. Optical deformability as an inherent cell marker for testing malignant transformation and metastatic competence. *Biophysical journal*, 88(5), pp.3689–3698.

Hanahan, D. & Weinberg, R.A., 2000. The Hallmarks of Cancer. *Cell*, 100, pp.57–70.

Hardy, S., Langelier, Y. & Prentki, M., 2000. Oleate Activates Phosphatidylinositol 3-Kinase and Promotes Proliferation and Reduces Apoptosis of MDA-MB-231 Breast Cancer Cells, Whereas Palmitate Has Opposite Effects. *Cancer Res.*, 15(60(22)), pp.6353–8.

Harwood, H.J., 2004. Acetyl-CoA carboxylase inhibition for the treatment of metabolic syndrome. *Curr Opin Investig Drugs*, 5(3), pp.283–9.

Higgins, M.J. & Baselga, J., 2011. Targeted therapies for breast cancer. *The Journal of Clinical Investigation*, 121(10).

Hryniewicz-Jankowska, A. et al., 2014. Membrane rafts as a novel target in cancer therapy. *Biochimica et biophysica acta*, 1845(2), pp.155–65.

Jannie, K.M. et al., 2015. Vinculin-dependent actin bundling regulates cell migration and traction forces. *Biochem J.*, 465(3), pp.383–393.

Jump, D.B., Torres-Gonzalez, M. & Olson, L.K., 2011. Soraphen A, an inhibitor of acetyl CoA carboxylase activity, interferes with fatty acid elongation. *Biochemical pharmacology*, 81(5), pp.649–60.

Kim, K., 1997. Regulation of Mammalian Acetyl-Coenzyme A Carboxylase. *Annu. Rev. Nutr.*, 17, pp.77–99.

Ligon, J. et al., 2002. Characterization of the biosynthetic gene cluster for the antifungal polyketide Soraphen A from Sorangium cellulosum So ce26. *Gene*, 285(1-2), pp.257–67.

Lincoln, B. et al., 2007. Reconfigurable microfluidic integration of a dual-beam laser trap with biomedical applications. *Biomedical Microdevices*, 9(5), pp.703–710.

Liu, Z.L. et al., 2013. Inhibition of fatty acid synthase suppresses osteosarcoma cell invasion and migration via downregulation of the PI3K/Akt signaling pathway in vitro. *Molecular medicine reports*, 7(2), pp.608–12.

Lodish, H. et al., 2000. Molecular Cell Biology. 4th edition., Section 3.

Maxfield, F.R. & Tabas, I., 2005. Role of cholesterol and lipid organization in disease. *Nature*, 438(7068), pp.612–621.

Maxfield, R. & Mondal, M., 2006. Non-Vesicular Intracellular Traffic. *Biochemical Society Transactions*, 34(3), pp.335–339.

Medes, G., Thomas, A. & Weinhouse, S., 1953. Metabolism of Neoplastic Tissue . IV . A Study of Lipid Synthesis in Neoplastic Tissue Slices in Vitro. *Cancer Res*, (13), pp.27–29.

Meer, G. Van, Voelker, D. & Feigenson, G., 2008. Membrane lipids - where they are and how they behave. *Nat Rev Mol Cell Biol.*, 9(2), pp.112–124.

Menendez, A.J., 2010. Fine-tuning the lipogenic/lipolytic balance to optimize the metabolic requirements of cancer cell growth: Molecular mechanisms and therapeutic perspectives. *Biochimica et biophysica acta*, pp.381–391.

Menendez, J.A. et al., 2004. Inhibition of fatty acid synthase (FAS) suppresses HER2/neu (erbB-2) oncogene overexpression in cancer cells. *PNAS*, 101(29), pp.10715–20.

Menghua, W. et al., 2015. Characteristics of drug combination therapy in oncology by analyzing clinical trial data on ClinicalTrials.gov. *Pac Symp Biocomput. 2015 ;*, pp.68–79.

Milgraum, Z. & Pasternack, R., 1997. Enzymes of the fatty acid synthesis pathway are highly expressed in in situ breast carcinoma. *Clinical Cancer Research*, 3, pp.2115–2120.

Nahta, R. et al., 2006. Mechanisms of disease: understanding resistance to HER2-targeted therapy in human breast cancer. *Nature clinical practice. Oncology*, 3(5), pp.269–80.

Nicoletti, I. et al., 1991. A rapid and simple method for measuring thymocyte apoptosis by propidium iodide staining and flow cytometry. *Journal of immunological methods*, 139(2), pp.271–279.

Olsen, A.M. et al., 2010. Fatty acid synthesis is a therapeutic target in human liposarcoma. *Int J Oncol.*, 36(5), pp.1309–1314.

Ookhtens, M. et al., 1984. Liver and adipose tissue contributions to newly formed fatty acids in an ascites tumor. *Am J Physiol.*, 247(1 Pt 2), pp.146–53.

Otto, O. et al., 2015. Real-time deformability cytometry: on-the-fly cell mechanical phenotyping. *Nature Methods*, 12, pp.199–202.

Plodinec, M. et al., 2012. The nanomechanical signature of breast cancer. *Nat Nanotechnol.*, 7(11), pp.757–65.

Press, M.F. et al., 1993. Disease Association of Overexpression with Increased Risk of Recurrent Tissue Quantitation by Computerized Image Analysis and Her-2/neu Expression in Node-negative Breast. *Cancer Res*, 53, pp.4960–4970.

Puhalla, S. & Brufsky, A., 2008. Ixabepilone: A new chemotherapeutic option for refractory metastatic breast cancer. *Biologics: Targets and Therapy*, 2(3), pp.505–515.

Rawicz, W. et al., 2000. Effect of chain length and unsaturation on elasticity of lipid bilayers. *Biophysical journal*, 79(1), pp.328–339.

Remmerbach, T.W. et al., 2009. Oral cancer diagnosis by mechanical phenotyping. *Cancer research*, 69(5), pp.1728–32.

Ridley, A. et al., 1999. Rho family proteins and cell migration. *Biochem Soc Symp.*, 65, pp.111–23.

Rui, L., 2014. Energy Metabolism in the Liver. *Compr Physiol.*, 4(1), pp.177–197.

Rysman, E. et al., 2010. De novo lipogenesis protects cancer cells from free radicals and chemotherapeutics by promoting membrane lipid saturation. *Cancer research*, 70(20), pp.8117–26.

Sabine, J.R., Abraham, S. & Chaikoff, I.L., 1967. Control of lipid metabolism in hepatomas: insensitivity of rate of fatty acid and cholesterol synthesis by mouse hepatoma BW7756 to fasting and to feedback control. *Cancer Research*, 27(4), pp.793–799.

Schneiker, S. et al., 2007. Complete genome sequence of the myxobacterium Sorangium cellulosum. *Nature biotechnology*, 25(11), pp.1281–9.

Scott, K.E.N. et al., 2012. Metabolic regulation of invadopodia and invasion by acetyl-CoA carboxylase 1 and de novo lipogenesis. *PloS One*, 7(1), p.e29761.

Selvendiran, K. et al., 2010. HO-3867, a synthetic compound, inhibits the migration and invasion of ovarian carcinoma cells through downregulation of fatty acid synthase and focal adhesion kinase. *Molecular cancer research: MCR*, 8(9), pp.1188–97.

Shen, Y. et al., 2004. A mechanism for the potent inhibition of eukaryotic acetyl-coenzyme A carboxylase by Soraphen A, a macrocyclic polyketide natural product. *Molecular cell*, 16(6), pp.881–91.

Shimkets, L.J., Dworkin, M. & Reichenbach, H., 2006. The Prokaryotes M. Dworkin et al., eds., pp.31-115.

Sieg, D.J., Hauck, C.R. & Schlaepfer, D.D., 1999. Required role of focal adhesion kinase (FAK) for integrin-stimulated cell migration. *J Cell Sci.*, 16, pp.2677–2691.

Simons, K. & Vaz, W.L.C., 2004. Model Systems, Lipid Rafts, and Cell Membranes. *Annual Review of Biophysics and Biomolecular Structure*, 33(1), pp.269–295.

Swaminathan, V. et al., 2011. Mechanical stiffness grades metastatic potential in patient tumor cells and in cancer cell lines. *Cancer research*, 71(15), pp.5075–80.

Swinnen, J., Brusselmans, K. & Verhoeven, G., 2006. Increased lipogenesis in cancer cells: new players, novel targets. *Curr Opin Clin Nutr Metab Care*, 9(4), pp.358–65.

Swinnen, J. V et al., 2000. Selective activation of the fatty acid synthesis pathway in human prostate cancer. *Int. J. Cancer*, 88(2), pp.176–179.

Tong, L., 2005. Acetyl-coenzyme A carboxylase: crucial metabolic enzyme and attractive target for drug discovery. *Cellular and molecular life sciences: CMLS*, 62(16), pp.1784–803.

Tong, L. & Harwood, J., 2006. Acetyl-coenzyme A carboxylases: versatile targets for drug discovery. *Journal of cellular biochemistry*, 99(6), pp.1476–88.

Vahlensieck, H.E., 1994. Identification of the yeast ACC1 gene product (acetyl-CoA carboxylase) as the target of the polyketide fungicide Soraphen A. *European Journal of Biochemistry*, (25), pp.95–100.

Webb, Y., Hermida-Matsumoto, L. & Resh, M.D., 2000. Inhibition of protein palmitoylation, raft localization, and T cell signaling by 2-bromopalmitate and polyunsaturated fatty acids. *Journal of Biological Chemistry*, 275(1), pp.261–270.

Wenzel, S. & Müller, R., 2009. The biosynthetic potential of myxobacteria and their impact in drug discovery. *Curr Opin Drug Discov Devel.*, 12(2), pp.220–30.

Yamaguchi, H. et al., 2009. Lipid rafts and caveolin-1 are required for invadopodia formation and extracellular matrix degradation by human breast cancer cells. *Cancer Research*, 69(22), pp.8594–8602.

Yamaguchi, H. & Condeelis, J., 2007. Regulation of the actin cytoskeleton in cancer cell migration and invasion. *Biochim Biophys Acta.*, 1773(5), pp.642–652.

Yamaguchi, H. & Oikawa, T., 2010. Membrane lipids in invadopodia and podosomes: Key structures for cancer invasion and metastasis. *Oncotarget.*, 1(5), pp.320–328.

Yoon et al., 2007. Up-regulation of acetyl-CoA carboxylase alpha and fatty acid synthase by human epidermal growth factor receptor 2 at the translational level in breast cancer cells. *The Journal of Biological Chemistry*, 282(36), pp.26122–26131.

7 Appendix

7.1 Abbreviations

ACC	acetyl-CoA carboxylase
ACLY	ATP-citrate lyase
APS	ammonium persulfate
ATCC	American Type Culture Collection
ATP	adenosine triphosphate
BC	biotin carboxylase
BCA	bicinchoninic acid
BCCP	biotin carboxyl-carrier protein
BSA	bovine serum albumin
CLS	Cell Line Services
co	control
Co-IP	co-immunoprecipitation
CPT-I	carnitine palmitoyltransferase I
CS	citrate synthase
CT	carboxyltransferase
DMEM	Dulbecco`s modified Eagle`s medium
DMSO	dimethyl sulfoxide
DNA	deoxyribonucleic acid
DSMZ	German Collection of Microorganisms and Cell Cultures
DSS	disuccinimidyl suberate
DTT	dithiothreitol
ECL	enhanced chemiluminescence
EDTA	ethylenediaminetetraacetic acid
EGF	epidermal growth factor
EGFR	epidermal growth factor receptor
EGTA	ethylene glycol tetraacetic acid

EtOH	ethanol
FACS	fluorescence activated cell sorting
FAK	focal adhesion kinase
FCS	fetal calf serum
fps	frames per second
FRAP	fluorescence recovery after photobleaching
HEPES	4-(2-hydroxyethyl)-1-piperazineethanesulfonic acid
HFS	hypotonic fluorochrome solution
JCRB	Japanese Collection of Research Bioresources
MP	milk powder
Myr	myristoylation
OXPHOS	oxidative phosphorylation
Palm	palmitoylation
PBS	phosphate-buffered saline
PDH	pyruvate dehydrogenase
PFA	paraformaldehyde
PI	propidium iodide
PIPES	piperazine-N,N'-bis(2-ethanesulfonic acid)
PLA	proximity ligation assay
PMSF	phenylmethanesulfonyl fluoride
RD	relative deformation
RNA	ribonucleic acid
ROI	region of interest
RT-DC	real-time deformability cytometry
S_A	Soraphen A
SDS	sodium dodecyl sulfate
SDS-PAGE	SDS polyacrylamide gel electrophoresis
siRNA	small interfering RNA
Sor.A	Soraphen A
TCA	tricarboxylic acid

TEMED	tetramethylethylenediamine
Tris	tris(hydroxymethyl)aminomethane
Tyr	tyrosine
VLDL	very low density lipoprotein

7.2 Publications

7.2.1 Articles

Simone Braig*, B. U. Sebastian Schmidt*, Katharina Stoiber*, Chris Händel*, Till Möhn, Oliver Werz, Rolf Müller, Stefan Zahler, Andreas Koeberle, Josef A. Käs and Angelika M. Vollmar (2015). **Pharmacological targeting of membrane rigidity: implications on cancer cell migration and invasion.** *New Journal of Physics,* 17 (083007). * These authors contributed equally to this work.

Stefan Wuttke, Andreas Zimpel, Thomas Bein, Simone Braig, Katharina Stoiber, Angelika Vollmar, Dominik Müller, Kirsten Haastert-Talini, Jörn Schaeske, Meike Stiesch, Gesa Zahn, Alexander Mohmeyer, Peter Behrens, Oliver Eickelberg, Deniz A Bölükbas, Silke Meiners. **Validating metal-organic framework nanoparticles for their nanosafety in diverse biomedical applications.** Submitted to *Biomaterials.*

Katharina Stoiber, Oliver Werz, Rolf Müller, Stefan Zahler, Andreas Koeberle, Maria Winzi, Jochen Guck, Melanie Ulrich, Angelika M. Vollmar and Simone Braig. **Targeting membrane characteristics by Soraphen A: A novel therapeutic option.** In preparation.

7.2.2 Oral presentations

Katharina Ferkaljuk, Simone Braig, Rolf Müller, Stefan Zahler, Josef A. Käs and Angelika M. Vollmar. **Effect of Soraphen A and E on cancer cells**, 4th FOR 1406 Meeting, July 16-18, 2013, Saarbrücken, Germany.

Katharina Ferkaljuk, Simone Braig, B. U. Sebastian Schmidt, Chris Händel, Till Möhn, Oliver Werz, Rolf Müller, Stefan Zahler, Andreas Koeberle, Josef A. Käs and Angelika M. Vollmar. **Biophysical characterization of the myxobacterial compound Soraphen A: an innovative option to fight invasive cancer.** GP-NIM Summer Retreat June, 25-27, 2014, Kreuth/Tegernsee, Germany.

Angelika M. Vollmar, Simone Braig, Katharina Ferkaljuk, B. U. Sebastian Schmidt, Chris Händel, Rolf Müller, Stefan Zahler, Oliver Werz, Andreas Koeberle and Josef A. Käs. **Biophysical characterization of the myxobacterial compound Soraphen A: an innovative option to fight**

invasive cancer. 5th annual symposium Physics of Cancer, October 2-5, 2014, Leipzig, Germany.

Katharina Ferkaljuk, Simone Braig, B. U. Sebastian Schmidt, Chris Händel, Till Möhn, Oliver Werz, Rolf Müller, Stefan Zahler, Andreas Koeberle, Josef A. Käs and Angelika M. Vollmar. **The effect of the myxobacterial compound Soraphen A on cancer cells.** 5th FOR 1406 Meeting, January 8 - 9, 2015, Munich, Germany.

Katharina Stoiber, Simone Braig, B. U. Sebastian Schmidt, Chris Händel, Till Möhn, Oliver Werz, Rolf Müller, Stefan Zahler, Andreas Koeberle, Josef A. Käs and Angelika M. Vollmar. **The effect of the myxobacterial compound Soraphen A on cancer cell proliferation**. 6th FOR 1406 Meeting, June 30 - July 2, 2015, Saarbrücken, Germany.

7.2.3 Poster presentations

Katharina Ferkaljuk, Simone Braig, Rolf Müller and Angelika M. Vollmar. **The myxobacterial compound SORAPHEN A: A potent inhibitor of migration and invasion in metastatic cancer.** 1st European Conference on Natural Products, September 22-25, 2013, Frankfurt, Germany.

B. U. Sebastian Schmidt, Katharina Ferkaljuk, Simone Braig, Chris Händel, Andreas Koeberle, Oliver Werz, Rolf Müller, Stefan Zahler, Josef A. Käs and Angelika M. Vollmar. **Modulation of membrane rigidity impacts cell migration and invasion.** 5th annual symposium Physics of Cancer, October 2-5, 2014, Leipzig, Germany.

K. Ferkaljuk, B. U. Sebastian Schmidt, Chris Händel, Oliver Werz, Rolf Müller, Stefan Zahler, Andreas Koeberle, Josef A. Käs, Angelika M. Vollmar and Simone Braig. **Modulation of membrane stiffness by the myxobacterial compound Soraphen A impacts migration and invasion.** 5th HIPS Symposium, July 2, 2015, Saarbrücken, Germany.

7.3 Danksagung

Nach etwas mehr als drei Jahren intensiver und spannender Arbeit ist es nun an der Zeit mich bei den Menschen zu bedanken, die mir die Erstellung meiner Doktorarbeit ermöglicht und mich während dieser Zeit geprägt und begleitet haben.

Ganz besonders möchte ich mich bei Frau Prof. Dr. Vollmar bedanken. Vielen Dank, dass Sie mir die Möglichkeit gegeben haben an Ihrem Lehrstuhl zu promovieren und mich während der gesamten Doktorarbeit durch eine hervorragende und zielgerichtete Betreuung begleitet haben. Die Zeit der Promotion hat mich sowohl wissenschaftlich als auch persönlich sehr geprägt und weitergebracht. Es war für mich eine große Bereicherung meine Arbeit im Rahmen der Forschergruppe FOR1406 anfertigen zu dürfen und Teil des Graduierten Programms der NIM sein zu dürfen.

Ein besonderes Wort des Dankes möchte ich an Herrn Prof. Dr. Zahler richten. Vielen Dank für viele hilfreiche Tipps und Ratschläge zu meinem Projekt. Danke, dass Sie sich so viel Zeit für gemeinsame Diskussionen genommen haben.

Den Mitgliedern meines Prüfungskomitees Prof. Dr. Wagner, PD Dr. Michalakis, Prof. Dr. Bracher sowie Prof. Dr. Wahl-Schott möchte ich sehr herzlich für Ihre Zeit und Mühe danken.

Ganz herzlich möchte ich mich bei meiner wissenschaftlichen Mentorin Dr. Simone Braig bedanken. Vielen Dank für deine Unterstützung, die zahlreichen Diskussionen und vor allem für deine Motivation. Zusammen haben wir schon so manche Soraphen A Probleme überwunden.

Ein großes Dankeschön geht auch an unsere Kooperationspartner:
Dr. Andreas Koeberle und Prof. Dr. Oliver Werz vom Institut für Pharmazie, Lehrstuhl für Pharmazeutische/Medizinische Chemie der Universität Jena für die Durchführung der Lipidomanalyse und die konstruktiven Diskussionen.
Chris Händel, Sebastian Schmidt und Prof. Josef A. Käs von der Fakultät für Physik und Geowissenschaften der Universität Leipzig für die Durchführung der Messungen der Zell- und Membransteifigkeit.

Dr. Maria Winzi und Prof. Jochen Guck von der Technischen Universität Dresden für die RT-DC-Messungen der Zelldeformation.

Danke auch an meine Masterstudentin Eva-Maria Baur für den experimentellen Beitrag.

Mein ganz besonderer Dank geht an die aktuellen und ehemaligen Mitglieder des AK Vollmar für ein tolles Arbeitsklima und eine großartige gegenseitige Unterstützung.
Tini, Lena, Flo, Julia, Michi, Verena, Siwei und Sandra vielen Dank dafür, dass ihr mich so herzlich in die Gruppe aufgenommen habt.
Liebe Lina und Henri wir haben zusammen angefangen und ich möchte mich bei euch für die tolle Freundschaft bedanken die in den drei Jahren gewachsen ist. Lina, danke fürs Zuhören, deine wertvollen und immer ehrlichen Ratschläge, die lustigen Stunden im Labor und dafür, dass du immer da warst. Henri danke für deine positive und mitreißende Art, die vielen Gespräche und vielen Dank dafür, dass man sich immer auf dich verlassen kann.
Liebe Chrissi, Meli, Fabi und Karin es hat mich sehr gefreut, dass wir uns durch die vielen gemeinsamen Stunden im PBIII und QPha-Praktikum, aber auch außerhalb des Labors richtig kennenlernen konnten. Es war eine schöne Zeit mit euch.

Der Nanosystems Initiative Munich (NIM) danke ich für die finanzielle Unterstützung.